

INFORMATION TO USERS

This manuscript has been reproduced from the microfilm master. UMI films the text directly from the original or copy submitted. Thus, some thesis and dissertation copies are in typewriter face, while others may be from any type of computer printer.

The quality of this reproduction is dependent upon the quality of the copy submitted. Broken or indistinct print, colored or poor quality illustrations and photographs, print bleedthrough, substandard margins, and improper alignment can adversely affect reproduction.

In the unlikely event that the author did not send UMI a complete manuscript and there are missing pages, these will be noted. Also, if unauthorized copyright material had to be removed, a note will indicate the deletion.

Oversize materials (e.g., maps, drawings, charts) are reproduced by sectioning the original, beginning at the upper left-hand corner and continuing from left to right in equal sections with small overlaps. Each original is also photographed in one exposure and is included in reduced form at the back of the book.

Photographs included in the original manuscript have been reproduced xerographically in this copy. Higher quality 6" x 9" black and white photographic prints are available for any photographs or illustrations appearing in this copy for an additional charge. Contact UMI directly to order.

UMI

A Bell & Howell Information Company
300 North Zeeb Road, Ann Arbor MI 48106-1346 USA
313/761-4700 800/521-0600

NOTE TO USERS

The original manuscript received by UMI contains pages with slanted print. Pages were microfilmed as received.

This reproduction is the best copy available

UMI



**A Study of Externally Reinforced
Fibre-Reinforced Concrete Bridge Decks on Steel Girders**

by


Lorna Jane Thorburn

A Thesis Submitted to the
Faculty of Engineering
in Partial Fulfilment of the Requirements
for the Degree of

DOCTOR OF PHILOSOPHY

Major Subject: Civil Engineering

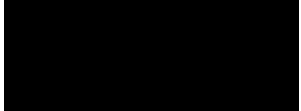
APPROVED:




Dr. A. A. Mufti, Supervisor



Dr. F. Taheri



Dr. G. Lee



Dr. A. Watson, University of Sheffield, External Examiner

DALHOUSIE UNIVERSITY - DalTech

Halifax, Nova Scotia

1998



National Library
of Canada

Acquisitions and
Bibliographic Services

395 Wellington Street
Ottawa ON K1A 0N4
Canada

Bibliothèque nationale
du Canada

Acquisitions et
services bibliographiques

395, rue Wellington
Ottawa ON K1A 0N4
Canada

Your file Votre référence

Our file Notre référence

The author has granted a non-exclusive licence allowing the National Library of Canada to reproduce, loan, distribute or sell copies of this thesis in microform, paper or electronic formats.

The author retains ownership of the copyright in this thesis. Neither the thesis nor substantial extracts from it may be printed or otherwise reproduced without the author's permission.

L'auteur a accordé une licence non exclusive permettant à la Bibliothèque nationale du Canada de reproduire, prêter, distribuer ou vendre des copies de cette thèse sous la forme de microfiche/film, de reproduction sur papier ou sur format électronique.

L'auteur conserve la propriété du droit d'auteur qui protège cette thèse. Ni la thèse ni des extraits substantiels de celle-ci ne doivent être imprimés ou autrement reproduits sans son autorisation.

0-612-31536-3

Canada

DALHOUSIE UNIVERSITY - DalTech LIBRARY

"AUTHORITY TO DISTRIBUTE MANUSCRIPT THESIS"

TITLE:

**A Study of Externally Reinforced
Fibre-Reinforced Concrete Bridge Decks on Steel Girders**

The above library may make available or authorize another library to make available individual photo/microfilm copies of this thesis without restrictions.

Lorna Jane Thorburn

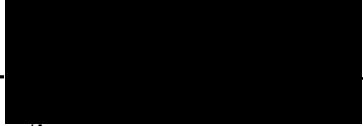

03/30/1998

TABLE OF CONTENTS

LIST OF TABLES	viii
LIST OF FIGURES.	ix
LIST OF SYMBOLS	xii
ACKNOWLEDGEMENTS	xvii
ABSTRACT	xviii
1.0 INTRODUCTION	1
1.1 Background to Current Study	1
1.1.1 Definition of a Slab-on-Girder Bridge.	1
1.1.2. Proportioning the Slab of a Slab-on-Girder Bridge	2
1.1.2.1. Traditional Approach to Deck Transverse Bending	2
1.1.2.2. Slab Design Recognizing Internal Arching	4
1.2 Previous Experimental Studies of Externally Reinforced FRC Systems	6
1.3 Advantages of an Externally Reinforced FRC Slab	9
1.3.1. External Slab Reinforcing.	9
1.3.2 Polypropylene Fibre-Reinforced Concrete, FRC	10
2.0 ANALYTICAL METHOD TO PREDICT SLAB PUNCHING LOAD	14
2.1 Prediction of Floor Slab Punching Capacity	14

2.2	Refined Model for a Steel Reinforced Bridge Slab	15
2.3	Analysis of an Externally Reinforced Deck Slab	17
2.3.1	Rigid Body Behaviour.	18
2.3.1.1	Idealized System Behaviour	18
2.3.1.1.1	Crack Pattern Development.	19
2.3.1.1.2	Assumptions	20
2.3.1.2	Wedge Geometry	24
2.3.1.3	Forces Acting on the Wedge.	26
2.3.2	Equilibrium Considerations	32
2.3.3	Potential Limits to the Slab Arching Behaviour.	36
2.3.3.1	Concrete Compressive Stress Limit	36
2.3.3.2	Yielding of External Restraint	40
2.3.3.3	Geometric Instability of Rigid Body	40
2.3.4	Iterative Solution to Predict Load Response	41
3.0	OPTIMIZATION OF AN EXTERNALLY RESTRAINED FRC SLAB.	43
3.1	Scope of Optimization	43
3.1.1	Variables Considered.	43
3.1.2	Structural System Constraints	43
3.1.3	Slab Span-to-Depth Ratio	46
3.1.4	Experimental Study	47
3.2	System Design	49
3.2.1	Recommended Design Load	49
3.2.1.1	Strength Requirements	49
3.2.1.2	Serviceability Considerations	56
3.2.2	External Restraint Requirements	63
3.2.3	Procedure to Establish a Minimum Weight System	65

3.3	System Cost Considerations.	67
3.3.1	Material Costs	70
3.3.2	Construction Costs	71
3.3.3	Life Cycle Costs	73
4.0	DESIGN DETAILS OF FULL-SCALE TEST BRIDGE.	75
4.1	General	75
4.2	Design of Full-Scale PFRC Bridge	75
4.2.1	Steel Girders	75
4.2.2	Slab External Reinforcing.	77
4.2.3	Concrete Deck Slab	79
4.2.3.1	Description of the PFRC	79
4.2.3.2	Material Testing	82
4.2.4	Cross Bracing.	83
4.3	Construction of Experimental Bridge	85
4.3.1	Summary of Deck Placing for Full-scale Deck	85
4.3.2	Placement of Repair Concrete	87
4.4	Description of Experimental Program	88
4.4.1	Loading Arrangement	88
4.4.2	Experimental Procedure	93
4.4.3	Structural Modifications Made During the Experimental Program.	94
5.0	RESULTS OF EXPERIMENTAL PROGRAM	
5.1	Material Testing	95
5.1.1	Material Tests Performed on Fresh Concrete	95
5.1.2	Core Sampling of Cured FRC Deck	97

5.1.3	Air Content Analysis	98
5.2	Monitoring the Behaviour During Load Tests	102
5.3	Observed Cracking Behaviour During Testing	103
5.4	Deflection Results	108
5.5	Strain Results	110
6.0	DISCUSSION	113
6.1	Comparison of Theoretical and Experimental Results.	113
6.1.1	Comparison of Calculated Punching Load with Experimental Results	113
6.1.2	Load Deformation Behaviour	114
6.1.3.	Behaviour of External Restraints	120
6.1.3.1	Strain Behaviour.	120
6.1.3.2	Yielding of the External Restraints.	129
6.2	Polypropylene Fibre-Reinforce Concrete Properties	130
6.2.1	Compressive Strength.	130
6.2.2	Air Content	133
6.2.3	Slump	137
6.2.4	Fibre Dispersion.	137
6.2.5	Steps to Improve the FRC Properties	138
6.3	Quantifying the Slab Restraint Stiffness	140

7.0	CONCLUSIONS AND RECOMMENDATIONS	143
7.1	Conclusions	143
7.2	Recommendations for Further Study	145
7.2.1	Strap attachment detail	145
7.2.2	FRC Mix Proportions	145
7.2.3	Material Resistance Factors	145
	REFERENCES	147
APPENDIX A:	FORTRAN Program to calculate slab load/deformation history	152
APPENDIX B:	Results of Microscopic Air Content Testing	156

LIST OF TABLES

Table 1.1:	Mechanical properties of polypropylene fibres	11
Table 3.1:	Strap areas used in the experimental model, mm ²	49
Table 3.2:	Ultimate Limit State wheel loads.	51
Table 3.3:	Serviceability Limit State wheel loads	52
Table 3.4:	Serviceability deflections and ultimate capacities for 175 mm slabs, maintaining a constant external restraint stiffness.	60
Table 3.5:	Fatigue Limit State wheel loads	61
Table 3.6:	Structural parameters for the two systems on which the cost comparison is based	69
Table 3.7:	Material cost comparison (\$ / m length)	70
Table 3.8:	Construction cost comparison (\$ / m length).	72
Table 3.9:	Life cycle cost comparison (\$ / m length)	74
Table 4.1:	Variation in transverse strap area (given in mm ²)	78
Table 4.2:	Concrete specification	79
Table 4.3:	Concrete mix designs	81
Table 5.1:	Concrete compressive strength results	96
Table 5.2:	Compressive strength results of deck core samples.	98
Table 5.3:	Summary of the results of the microscopic air testing	100
Table 6.1:	Comparison of calculated punching load with experimental capacity	114
Table 6.2:	Measured strap strains	121
Table 6.3:	Summary of air test results for plain concrete and FRC	133
Table 6.4:	Comparison of punching capacity for variations in restraint stiffness	142

LIST OF FIGURES

Figure 1.1:	Plan view of experimental bridge deck	8
Figure 2.1:	Section through a conventionally reinforced slab-on-girder bridge	15
Figure 2.2:	Section of an externally reinforced slab-on-girder bridge with an FRC deck slab	18
Figure 2.3:	Crack development for an externally reinforced slab subjected to a vertical concentrated load	19
Figure 2.4:	Plan view of idealized crack pattern for rigid body model assumed to represent arching behaviour	20
Figure 2.5:	Geometry of the rigid body during rotation	22
Figure 2.6:	Beam model used in the calculation of the lateral stiffness of the system	23
Figure 2.7:	Freebody diagram of a wedge	24
Figure 2.8:	Geometry of the rigid body wedge	24
Figure 2.9:	Plan of wedge showing forces acting during rotation	27
Figure 2.10:	Influence of the concrete confinement constant on the load/deflection behaviour	39
Figure 2.11:	Steps in iterative analysis to describe slab load deflection history during internal arching.	42
Figure 3.1:	Influence of slab thickness on girder design moment	44
Figure 3.2:	Plan view of experimental deck giving location of external restraints	48
Figure 3.3:	Maximum serviceability deflections for slabs designed for a punching capacity of 500 kN	58
Figure 3.4:	Influence of restraint stiffness on the calculated ultimate load	64

LIST OF FIGURES, cont'd

Figure 3.5: Minimum restraint requirements for a 500 kN ultimate capacity . 65

Figure 4.1: Plan view showing layout of experimental bridge structure . . . 76

Figure 4.2: Typical section of experimental bridge 77

Figure 4.3: Layout of transverse diaphragm typical at the vertical supports 84

Figure 4.4: Details of the transverse diaphragm located at center span. . . 84

Figure 4.5: Photograph of testing arrangement 89

Figure 4.6: Plan of deck showing test locations 90

Figure 4.7: Photograph of load application setup 91

Figure 4.8: Photograph of deflection dial gauge layout 92

Figure 5.1: Samples of FRC and plain concrete showing visible difference in air content 101

Figure 5.2: Idealized crack pattern observed during load test. 104

Figure 5.3 (a): Underside of slab showing formation of radial cracks . . 105

(b): Topside cracking; flexural cracks along the girder and circumferential shear cracks 106

(c): Slab from below, showing radial crack development during rigid body rotation 107

(d): Crack pattern on top surface after punching 108

Figure 5.4: Load / deflection history measured during first test series. . . 109

Figure 5.5: Applied load vs strap strain, Test # 4 111

Figure 5.6: Typical stress strain relationship for structural steel. 112

Figure 6.1: Load deformation results, Test # 1 116

Figure 6.2: Load deformation results, Test # 2 116

Figure 6.3: Load deformation results, Test # 3 117

LIST OF FIGURES, cont'd

Figure 6.4: Load deformation results, Test # 4	117
Figure 6.5: Load deformation results, Test # 5	118
Figure 6.6: Load deformation results, Test # 6	118
Figure 6.7: Load deformation results, Test # 7	119
Figure 6.8: Load deformation results, Test # 8	119
Figure 6.9: Load position for series 1 tests	123
Figure 6.10: Strain in external restraints, Test # 1	124
Figure 6.11: Strain in external restraints, Test # 2	124
Figure 6.12: Strain in external restraints, Test # 3	125
Figure 6.13: Strain in external restraints, Test # 4	125
Figure 6.14: Strain in external restraints, Test # 5	126
Figure 6.15: Strain in external restraints, Test # 6	126
Figure 6.16: Strain in external restraints, Test # 7	127
Figure 6.17: Strain in external restraints, Test # 8	127
Figure 6.18: Variation in strap strain with a change in distance from the applied load	128
Figure 6.19: Influence of concrete compressive strength on the predicted punching load	131
Figure 6.20: Relationship between concrete compressive strength and air content	136
Figure 6.21: Continuous beam model used to determine the system restraint stiffness	140

LIST OF SYMBOLS

- A_s area of external restraint, mm^2
- B diameter of equivalent circular loaded area; inner diameter of the wedge, mm
- C diameter of "equivalent" circular slab; outer diameter of the wedge; for the slab-on-girder deck system, C is the clear spacing between adjacent girder top flanges, mm
- c_1 depth of conical compression zone (rectangular stress block) from the top surface of the slab, measured perpendicular to force, T , mm
- c_2 depth of the compressive stress block developed at the outer edge of the wedge due to the lateral restraint, F_w , measured from the underside of the slab, mm
- d slab thickness, mm
- E_c Modulus of elasticity of concrete, MPa
- E_s Modulus of elasticity of steel, MPa
- F slab lateral restraint force per unit length, kN/m

- F_w total lateral restraint force acting on a wedge and proportional to the slab radial deflection, kN
- F_{wr} lateral restraint force acting on a wedge in a direction parallel to the central plane, kN
- f'_c concrete compressive strength, MPa
- k_s axial stiffness of external restraint per unit length, assumed axisymmetric about the centre of the loaded area, N/mm/mm
- K_l system lateral restraint, N/mm/mm
- K_c concrete confinement constant
- I dynamic load factor for vehicle loading
- P vertical load applied to the slab, kN
- P_{ult} ultimate load capacity of the deck slab, kN
- R circumferential compressive slab force which develops above the C.R. as the wedge rotates, kN
- R_w resultant circumferential force developed on a wedge during arching, kN
- R_{wr} radial component of R through the centre of the wedge, kN

- r** radial dimension from C.R., mm
- S_g** girder spacing, mm
- S_s** spacing of external restraint, mm
- T** oblique compressive force acting through the imaginary conical shell; T transfers the applied load from the loaded portion of the slab to the unloaded wedge of slab. T is assumed to act parallel to the direction of the shear crack; i.e. at an angle ($\alpha-\psi$) measured from the horizontal. To satisfy equilibrium, the sum of the vertical components of T for all wedges axisymmetric to the load must be equal in magnitude to the applied vertical force, P, kN.
- T_w** oblique compression force which acts on a wedge, kN.
- T_{wr}** component of the oblique compression force acting on a wedge in a direction parallel to the central plane, kN.
- T_{wrh}** horizontal component of T_{wr}, kN.
- T_{wrv}** vertical component of T_{wr}, kN.
- V** vertical reaction force acting at outer boundary of wedge, mm.
- y** vertical distance from the upper surface of the slab to centre of rotation of the wedge. Note that y is analogous to the depth of the assumed

rectangular compression block, "c" in a reinforced concrete beam. The depth y is dependent on the size of compression block required to transfer the applied load to the wedge and will be determined from equilibrium requirements, mm.

C.R. centre of rotation of slab portion outside the shear crack, this slab portion is also referred to as "the wedge" , the C.R. is located on a vertical axis below the point of load

α angle of inclination of shear crack that forms inner boundary of wedge

α_L load factor for live loads

β sector length (of wedge)

Δ vertical deflection of the wedge under load, mm

δ radial slab deflection during arching, mm

ϵ_{ct} concrete circumferential strain at the top surface of the slab, mm/mm

ϵ_s steel strain, mm/mm

ϵ_y yield strain of steel, mm/mm

ϵ_{cu} concrete crushing strain, mm/mm

- ψ angle of rotation about the C.R., in a vertical plane, of a slab wedge outside the shear crack as it deflects under load
- $\Delta\phi$ angle subtended between radial cracks
- σ_{α} concrete tangential compressive stress, MPa
- σ_1 minor principal stress; due to the applied vertical load, MPa
- σ_2 intermediate principal stress in the slab; due to the radial confining force in the slab, MPa
- σ_3 major principal stress in slab; due to the circumferential confining force in the slab, MPa
- ϕ_{FRC} material resistance factor for fibre-reinforced concrete
- ϕ_{Punch} partial resistance factor representing the variability in the analytical prediction of the punching capacity

ACKNOWLEDGEMENTS

This project was made possible through the financial support provided the author through the Teaching Internship Program offered by the Faculty of Engineering at DalTech.

Experimental work was supported through research funding contributed by the Natural Sciences and Engineering Research Council of Canada, Vaughan Engineering Ltd. and the Nova Scotia Department of Industry, Trade and Technology to my supervisor, Dr. A.A.Mufti.

The support and encouragement maintained through my program by my supervisor, Dr. A.A. Mufti, as well as the continued intellectual support offered by Dr. L. Jaeger, Professor Emeritus, DalTech and Dr. B. Bakht, Ministry of Transportation of Ontario, is gratefully acknowledged.

Also recognized is the valuable technical support contributed in the laboratory by Messrs. R. Sarty and B. Nickerson.

The thesis is dedicated to those who have prepared me and to those who have sustained me.

ABSTRACT

A concrete slab acting compositely with steel girders is commonly an economical solution for short and medium span highway bridges. A severe maintenance penalty exists for such a system in areas where the use of de-icing chemicals is prevalent, largely due to the corrosion of embedded steel reinforcing bars and the attendant concrete degradation. Transverse steel straps, placed below the concrete slab, eliminate the deleterious effects of corrosion on the concrete and allow improved access for routine maintenance. Further, the straps can be designed to provide the restraint necessary to promote the development of internal arching in the concrete slab in response to a concentrated load. Inert fibres are incorporated in the concrete slab to control shrinkage and temperature effects.

A static testing program, initiated in 1994, has been undertaken at DalTech on a full-scale externally restrained fibre reinforced concrete (FRC) bridge slab. This program includes three series of destructive tests. The first test series was performed on an intact FRC deck, and was designed to study the influence of varying external restraint. A second and a third series of tests were performed; the second series on deteriorated sections of the deck in the vicinity of the local punchout and the third on repaired sections of the deck. The latter two series were performed to investigate the influence of adjacent cracked concrete and to study the usefulness of a deck repair procedure.

The failure pattern observed at the ultimate load in each test can be characterized as a punching shear mechanism, with localized damage. The

results of static tests obtained from a full-scale laboratory model of an externally reinforced FRC deck supported on longitudinal steel girders are presented. The load-deformation results of these tests were compared with the behaviour predicted analytically, modelling the slab as an arching mechanism.

The major contributions of the work are summarized as:

1. Design of a full-scale externally reinforced FRC bridge superstructure to be used for experimental testing to establish the relationship between the degree of external restraint and the system ultimate capacity. Results obtained from this model led to the design criteria for the steel free bridge decks that have been constructed in Canada.
2. Refinement of an analytical model that can be used to predict the load-deformation response and the ultimate punching load of a restrained FRC deck slab acted upon by a concentrated load. In particular, the external transverse restraint is represented in the analytical model and the failure criterion for concrete in a triaxial stress field was revised.
3. Comparison of the measured response of an intact externally restrained FRC slab with the predicted behaviour based on the refined analytical model was made for varying degrees of external restraint. The comparison of the predicted ultimate load to that measured experimentally showed their means to be within 11.2 %, with a standard deviation of 5.3%.
4. The degree of external restraint that is required to assure a punching

failure mechanism in an externally restrained FRC acted upon by a concentrated load was optimized on the basis of system weight and safety.

5. The residual system capacity inherent in a deteriorated section of an externally restrained FRC bridge slab was also investigated. The measured capacities for two deteriorated sections are presented and compared with analytical predictions.
6. Deck repairs were undertaken to locally restore the deck capacity at punched locations. From this work, a recommended repair procedure is presented that was demonstrated to restore 75% of the system capacity of a "punched" concrete slab.

1.0 INTRODUCTION

1.1 Background to Current Study

1.1.1 Definition of a Slab-on-Girder Bridge

One of the most common structural forms used for North American highway bridges is the slab-on-girder superstructure. This system consists of a number of parallel longitudinal girders topped by a concrete slab. The girders, typically either steel or concrete, span in the direction of traffic flow and are supported at the ends, and often at intermediate interior points, by foundations that transfer the girder reactions to the supporting ground.

The concrete slab performs two primary functions in the slab-on-girder superstructure. Firstly, the concrete deck provides the continuous wearing surface for the bridge; the interface between the vehicular loads and the main distributing support structure, the girders. Secondly, the concrete slab transfers the concentrated vehicle loads imposed on it directly as reactions to the supporting girders. The girders then respond to these slab reactions primarily in a longitudinal flexural mode. And, it is through this longitudinal girder bending that the vehicle loads are ultimately transferred to the supports.

The concrete slab is used in many bridges to perform a further tertiary function.

The slab can contribute significantly to the longitudinal flexural stiffness of the girders provided that certain design considerations are met to ensure that the slab and girder act integrally. Such a system is referred to as a composite slab-on-girder superstructure. In such a system, a positive connection is introduced between the slab and girder to ensure strain continuity at their interface. This shear connection between the concrete slab and the longitudinal girder will be a factor in the system restraint which will be discussed in more detail later.

Such a system of longitudinal steel girders acting compositely with a concrete deck slab is often an economical solution for short and medium span highway bridges. Maintenance of such a system is proving costly in many regions of North America given the harsh winter environment, coupled with the prevailing use of deicing chemicals and the advanced age of the bridge infrastructure. The maintenance concerns stem largely from corrosion of the steel reinforcing bars in a conventionally reinforced concrete deck. Elimination of the reinforcing steel bars in the concrete would thus greatly improve the bridge deck durability,

1.1.2 Proportioning the Slab of a Slab-on-Girder Bridge

1.1.2.1 Traditional Approach to Deck Transverse Bending

Conventional bridge slab design techniques rely on elastic plate bending analysis to establish the transverse moments in a deck slab acted upon by live loads. This approach assumes that the slab reacts in pure flexure and is based on Westergaard's solution of the Lagrangian fourth order differential equation of plate bending for a concentrated load distributed over a circular area on a simple span. AASHTO represents this solution in an empirical form for one-way slabs, considering a strip of unit width perpendicular to the girder as a rectangular

beam subjected to a standard truck load. This approach also uses an effective slab width, this width has been calibrated such that the single wheel solution will be safe for the case of multiple wheels on the span. A further 20% reduction to the simple span moment is introduced for slabs continuous over three or more supports for the calculation of the maximum positive and negative moments. While it is commonly accepted that the transverse moments thus calculated are an overestimation of the true effects, the method is easy to apply and has prevailed with bridge designers for many years.

The resulting envelope of transverse design moments has maximum positive amplitude at the midpoint between girders and a maximum negative amplitude in the slab over the girders. To reinforce for the tensile effects caused by these moments transverse steel is typically provided near the top face of the slab over the girders and in the bottom of the slab in the positive moment region between the girders. To simplify construction, detailing this reinforcing as continuous transverse bars top and bottom is the norm.

Typically, slabs designed to the AASHTO requirements have between 3.2% and 4.0% steel reinforcing distributed orthotropically in four layers. The longitudinal steel is provided to control shrinkage and temperature cracks, as well as to satisfy the longitudinal bending effects known to exist in such a monolithic structure. This reinforcing, in bridge code terms, is referred to as "distribution steel". The end result of the traditional elastic method for proportioning slabs based on plate bending analyses is heavy orthogonal steel reinforcing in the concrete deck.

1.1.2.2 Slab Design Recognizing Internal Arching

In the mid-1960's the maximum legal axle weights on Ontario highways were almost twice the AASHTO recommended weight, [Dorton (1976)]. It was observed that the Ontario highway bridges were performing well despite this "overloading". This led bridge engineers to question the conventional AASHTO deck design recommendations. An extensive research program was undertaken by the Ministry of Transportation in Ontario to determine the capacity of an "AASHTO-designed" deck and to account for the apparent excess capacity. This research program had four complementary components; field testing of existing AASHTO-designed bridges, laboratory testing to study the ultimate behaviour of scaled structures, an analytical study to model the behaviour observed in the physical tests, and finally, the construction of a full-scale prototype bridge incorporating the knowledge gained from the preceding research.

Field test results of 40 Ontario structures showed that concrete deck slabs of slab-on-girder bridge systems were inherently stronger than predicted by the conventional design methods used at that time, [Csagoly and Lybas(1989)]. Consider; the structures were load-tested to 445 kN, over 6 times the AASHTO service load of 71 kN. Experimental load-displacement measurements showed 39 of the bridges to perform very well during the test, with negligible plastic deformation upon unloading. Furthermore, strain readings showed that stresses in the top transverse steel over the longitudinal girders were insignificant.

The second part of this research program was a series of destructive laboratory tests conducted at Queen's University on 1/8 scale models of slab-on-girder superstructures. These models included isotropically and orthotropically reinforced decks, having varying reinforcement ratios, as well as unreinforced

decks. Both static and fatigue tests were performed. From the results, reported by [Batchelor et al., (1978)], it was observed that the concrete slabs were capable of withstanding ultimate concentrated loads much greater than those predicted by the traditional bridge slab design methods and that the mode of failure was that of a local punch in the vicinity of the load. The measured ultimate strengths in static load tests showed a deck capacity in the order of 15 to 21 times the strength predicted by the AASHTO design method. The fatigue limit was measured at 40% of the ultimate static capacity for decks with a total of 0.8% isotropic reinforcement.

In conjunction with the model testing, analytical work was performed at Queen's University to study the load-response behaviour of a concrete bridge slab. [Hewitt (1972)] adapted a mechanical failure model for simply supported slabs, first proposed by [Kinnunen and Nylander (1960)], to represent the punching of a concrete deck slab. He modified their earlier representation by introducing boundary restraint effects attributable to the slab tensile reinforcing as well as the system restraint of the slab-on-girder structure. By calibrating the magnitude of these boundary effects using the physical test results, it was concluded that the ultimate punching capacity of the slab was most influenced by the degree of boundary restraint. A further comparison was made analytically to determine the restraint factors appropriate for the 40 field-tested bridges. The work showed that lower bound predictions of the load/deflection response could be made assuming a restraint factor of 0.25 for non-composite slab-on-girder bridges and a factor of 0.50 for composite structures.

A prototype test bridge was constructed in Ontario in 1975, to verify the previous research test results, [Dorton et al., (1977)]. Variations in slab thickness and reinforcing ratios were incorporated in the slab of this bridge to study their influence on the deck behaviour under concentrated test loads and in-service

loading. From this structure, it was established that a total reinforcing ratio of 1.2%, distributed isotropically in 4 layers provided an acceptable safety margin for both the ultimate and serviceability conditions. This work provided the basis for the OHBDC empirical design method for reinforced concrete deck slabs.

1.2 Previous Experimental Studies of Externally Reinforced FRC Systems

Following is a summary of the research to-date on externally reinforced FRC slab-on-girder superstructures. Although the concept is felt to be readily adaptable to other slab-on-girder bridge types, the experimental work has been focused on a bridge with longitudinal steel girders, designed compositely with a polypropylene fibre reinforced concrete slab.

A series of half-scale slab-on-girder bridge models have been tested at the Technical University of Nova Scotia, as reported by [Mufti et al., (1993)]. Single span 2 and 3 girder bridges were tested, constructed of longitudinal steel girders topped with a cast-in-place FRC composite concrete deck. The slabs were reinforced with fibrillated polypropylene fibres with a fibre volume ratio of 0.88% and had a span-to-depth ratio of 10.5. The primary variable studied was the influence of lateral restraint provided to the concrete slab by alternate arrangements of supporting steel. The layout of the supporting steel was varied to establish an arrangement which would exhibit punching shear failures at ultimate in response to an applied static concentrated load. This testing program demonstrated that FRC deck slabs with no internal reinforcing steel will fail by local shear punching provided that the steel girders are adequately restrained. The recommended method of providing this restraint was a series of

transverse steel flat bars welded to the underside of the girder flanges. This system provides an ultimate capacity much greater than that of the current code recommended highway design live loads.

The fibre reinforced deck has also been subjected to cyclic loading at Carleton University to examine its fatigue behaviour. The results, reported by [Selvadurai and Bakht, (1995)], show the deck to be virtually undamaged after being subjected to 4×10^6 passes of a 98 kN load.

Previous experimental programs have shown that a concrete deck reinforced only with polypropylene fibres and without internal steel reinforcing can be designed to fulfil the deck design requirements for a highway bridge. The fibre reinforcing provides crack control to the slab. Elimination of the steel reinforcing in the slab will significantly reduce the maintenance concerns. Half-scale laboratory testing has shown that the capacity of such a fibre-reinforced concrete (FRC) slab would be limited by the formation of a punching failure mechanism providing that sufficient lateral restraint is provided to anchor the slab arching forces, [Mufti et al. (1993)]. This lateral restraint can be provided externally to the slab in the form of transverse steel bars welded to the underside of the steel girder top flange. In subsequent research, an analytical representation was developed to predict the load-deflection behaviour and the load-capacity of such a system, [Wegner and Mufti (1994b)]. This technique was used to predict the optimum combination of slab span-to-depth ratio and the size of external reinforcing to be investigated in the current study.

The full-scale testing program described herein uses an PFRC deck incorporating external reinforcing steel. The configuration of the experimental model is shown in Figure 1.1. The test results were used to validate the analytical procedure for predicting the behaviour of such a deck when subjected

to a concentrated load. Additionally, the load-deflection behaviour and failure mechanism exhibited by the full-scale model was monitored. The behaviour results were used to refine the rational model to better predict the capacity of an externally reinforced FRC deck subjected to concentrated loads.

The analytical model was then used to optimize the quantity of external reinforcing steel.

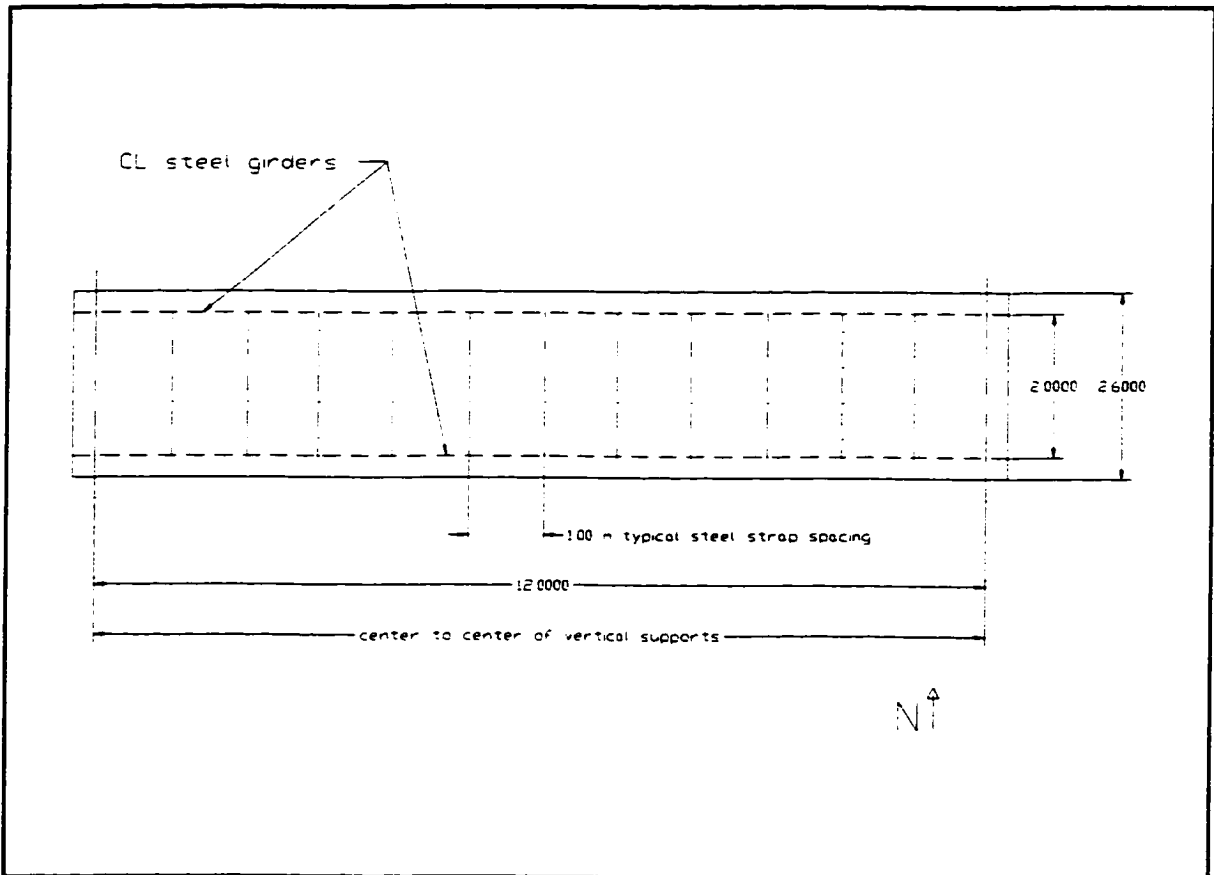


Figure 1.1: Plan view of experimental bridge deck

1.3 Advantages of an Externally Reinforced FRC Slab

1.3.1 External Slab Reinforcing

Removing the reinforcing steel from a concrete bridge deck is attractive from the standpoint of through-life system maintenance, as the steel reinforcing bars in conventional concrete decks contribute significantly to deterioration of the slab. Consider a typical North American environment; a series of severe freeze thaw cycles with numerous applications of de-icing chemicals. Small cracks form in the concrete under these service conditions. These cracks are not a limit to the structural integrity of the system, but are a concern due to their potential to limit the deck serviceability. Penetration of the corrosive agents to the level of the steel bars is aided by the cracks. The chemicals in contact with the steel bars create a highly corrosive environment. Corrosion of the steel ensues, accompanied by expansion of the bars, this in turn causing more extensive cracking of the surrounding concrete. The amount of expansion can be characterized though the Pilling Bedworth ratio; the ratio of the oxide to metal volume. In the extreme this process results in spalling of the concrete deck necessitating costly repairs. Removing the reinforcing steel from the concrete would eliminate many deleterious effects.

The earlier Ontario tests, [Hewitt and Batchelor (1975)], showed that slabs with only minimal reinforcing were capable of developing the arching action, with the ultimate behaviour characterized by the formation of a localized punching mechanism. Would it then be possible to extend this concept to a concrete slab having no internal reinforcing steel? Two concerns would have to be addressed at the outset to make such a system feasible; an alternate means of restricting the shrinkage and temperature effects must be provided and the system must have "sufficient lateral restraint" necessary to allow the arching mechanism to

develop. The study of what constitutes a system of "sufficient" restraint for the concrete deck slab of a conventional slab-on-girder bridge has been the subject of ongoing research at the Technical University of Nova Scotia in collaboration with the Ministry of Transportation of Ontario (MTO), [Mufti et al., 1993].

1.3.2 Polypropylene Fibre-Reinforced Concrete, FRC

What is meant by the term FIBRE REINFORCED CONCRETE? For the current study FRC has been taken to mean a fibre reinforced composite material consisting of a Portland cement concrete and randomly distributed, discontinuous polypropylene fibre reinforcing.

It is well documented in the literature, [Portland Cement Association, (1991)], that the polypropylene fibres do not increase the concrete's tensile strength. The sole purpose for inclusion of the fibres in the system was to prevent plastic shrinkage cracks from occurring. Such cracks, although of no consequence to the structural capacity of the bridge deck system, could detract from the durability required for a field application. So, although consideration was given early on to using a plain concrete deck for the experimental program, the concrete was reinforced with polypropylene fibres to gain further experience with a material showing promise for field applications.

Polypropylene is a hydrocarbon polymer man-made using an extrusion process in which the material is hot-drawn through a die. Fibrillated polypropylene fibres, (produced by the FORTA Co.), were used in the FRC concrete. Such fibres are produced by first extruding the polypropylene into a thin film, the film is then slit longitudinally into tapes and the tapes are further slit internally into thin "fibrils" of polypropylene, resembling a shallow honeycomb structure. These fibrillated tapes are then twisted about their longitudinal axis and finally chopped

to length. The chopped fibrillated fibres are manufactured by FORTA in lengths ranging from 20 to 64 mm. Upon incorporation of the fibres into the fresh concrete the twisted fibrils expand and disperse through the concrete (with 7 minutes mix time). The cement matrix penetrates the fibre structure during mixing. Such penetration later results in the strong mechanical bond developed between these fibres and the hardened concrete.

Physical properties of the polypropylene fibres are given in Table 1.1.

Table 1.1: Mechanical properties of polypropylene fibres

Modulus of elasticity	4826 MPa
Minimum tensile strength	483 MPa
Elongation	8%
Density	897 kg/m ³

The polypropylene fibrous mix is being studied as a means to address the temperature and shrinkage effects in the concrete slab. Low-modulus polypropylene fibres are currently being used in the experimental program, at concentrations 8 times the industry norm. Such concentrations were felt to be necessary to restrict the cracking arising from both plastic shrinkage of the fresh concrete and the drying shrinkage of the hardened matrix, whereas the low fibre volumes (typically in the order of 0.8%) are effective in controlling only the former, [Carmichael, (1988)].

The polypropylene fibres were chosen primarily due to their cost effectiveness. When comparing the cost of the polypropylene fibres to other nonferrous

alternatives, the low fibre cost of the former is the main advantage. Additionally the fibres are lightweight, inert and hydrophobic. Some of the disadvantages of the polypropylene fibres include their relatively low modulus of elasticity, a decreased workability, thereby necessitating an increased use of superplasticizers, and a poor chemical bond with the cement matrix. The modulus of elasticity (E) of the polypropylene fibres is, by comparison, typically eleven times less than that of glass and thirty times smaller than that of steel. This means that for the same stress, assuming E is constant characterizing elastic behaviour, the polypropylene strain will be in the order of 8.5 times the strain of the concrete. The behaviour of the polypropylene fibres remains elastic up to failure, which is a sudden.

To help offset the poor bond between fibres and matrix, a chopped fibrillated fibre was used. The fibrillated fibre is produced by slitting a polypropylene film, thus making it expandable into an open network of fibres. This open mesh develops an improved mechanical bond between the fibres and matrix by allowing the cement paste to penetrate the fibre mesh. Thus, the fibrillated fibres become mechanically well bonded in the mix as a result of their open net structure, although their hydrophobic surface does not contribute chemically to the bond.

Polypropylene fibres were used to resist shrinkage and temperature effects. Polypropylene fibres bridge the micro cracks that begin to form during the hardening phase. It is not the drying shrinkage itself that is responsible for the crack formation, rather, it is the restraint to such shrinkage that causes tensile stresses to arise and the tensile stresses cause cracking to provide stress relief. In a plain concrete mix micro cracks also begin as very fine fissures which appear as the mix begins to dry. And, in the plain mix there is nothing to prevent such micro cracks to consolidate and form a shrinkage crack. The formation of

these shrinkage cracks would occur over a period of weeks or months as the drying and the attendant cycle of tensile stress creation, stress relief by micro-cracking and coalescence of the fine fissures into visible shrinkage cracks takes place. Mixes with high water contents are most susceptible cracks associated with shrinkage.

Reports on the early use of the fibres by the U.S. Army Corps of Engineers show that small quantities of polypropylene fibres substantially increase impact resistance and durability, [Goldfein (1965)].

2.0 ANALYTICAL METHOD TO PREDICT SLAB PUNCHING LOAD

2.1 Prediction of Floor Slab Punching Capacity

Kinnunen and Nylander, (1960), performed research on a series of simply supported slabs having steel flexural reinforcement subjected to concentrated loading. Their research included an experimental program accompanied by a theoretical study to predict the ultimate punching load. The authors studied circular slabs having span-to-depth ratios between 4 and 17 that were simply supported at the boundary and loaded through supporting columns. The test slabs were reinforced with steel flexural reinforcement in two directions, radial and circumferential.

The theoretical study was based on describing the equilibrium relations which characterized the rigid body behaviour of the collapse mechanism inherent in a punching failure. The authors found their analysis gave a lower bound solution that was able to predict the punching shear capacity of simply supported slabs within 20%. Evidence of the rigid body behaviour of the slab wedges was found in the deflection and strain measurements recorded in their experiments. The strains measured in the circumferential reinforcement outside the shear crack appear very close to inversely proportional to the radius, approximately the strain relationship of a rigid body subjected to the angular rotation in a radial vertical plane. The concrete strain measured in a radial direction was negligible, supporting the concept of rigid body behaviour. Furthermore, the calculated and measured values for the slope of the shear crack and the angle of rotation at failure showed close correlation.

2.2 Refined Model for a Steel Reinforced Bridge Slab

The research of Kinnunen and Nylander was extended to study loading and support configurations representative of slab-on-girder composite bridges, [Hewitt And Batchelor, (1975)]. They extended the model, developed for a circular slab with radial and circumferential reinforcing and a circular loaded area, using it to represent a concrete slab bridge deck supported on longitudinal girders having conventional orthogonal reinforcing. Fig. 2.1 represents a section from such a bridge superstructure. Their idealization expanded the

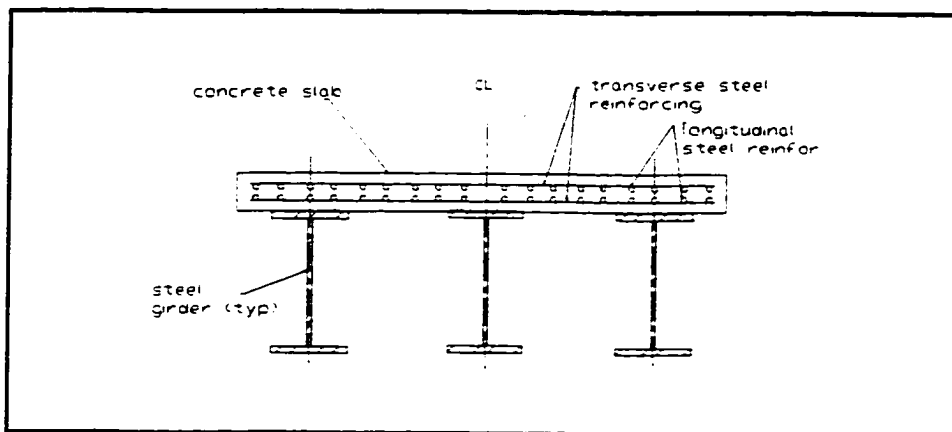


Figure 2.1: Section through a conventionally reinforced slab-on-girder bridge

model to include boundary restraining forces and moments acting through the tensile reinforcement at the extremity. These restraints arise from the efforts of the slab tensile reinforcing and the system restraint of the slab-on-girder structure. They showed that by varying these boundary effects empirically using a factor to represent the two extremes of simple and rigid conditions, the load capacity of such a system could be predicted.

By calibrating the magnitude of these boundary effects using the physical test results, it was concluded that the ultimate punching capacity of the slab was

most influenced by the degree of boundary restraint. A further analytical comparison was made by these authors to determine the restraint factors appropriate for 40 field-tested bridges. The work showed that lower bound predictions of the load/deflection response could be made assuming a restraint factor of 0.25 for non-composite slab-on-girder bridges and a factor of 0.50 for composite structures. For a slab-on-girder bridge superstructure the variables which influence the restraint include the girder spacing and stiffness, the characteristics of the transverse diaphragms, the number and spacing of shear connectors, as well as the restraint provided by the inertia of the surrounding slab itself.

The authors concluded that very high factors of safety against punching are inherent in isotropically reinforced composite slab on girder systems and, in fact, the reinforcement necessary for temperature and shrinkage alone provide an adequate factor of safety against punching.

The results of this research program pointed to additional strength inherent in the system over that predicted by conventional plate bending analyses. This additional strength is attributed to the load-carrying mechanism referred to as internal arching. The internal arching mechanism stems from the difference in tensile and compressive capabilities of concrete. Consider a concrete slab spanning continuously over several intermediate supports and acted upon by a concentrated load at midspan. Such a slab will bend in response to the load, initially producing compressive bending stresses in the top fibres of the slab and corresponding tensile bending stresses through its lower portion at midspan. The opposite stress field will develop over the adjacent intermediate support. Radial cracking will initiate in the tensile zones under the application of a small load. The resulting crack pattern causes a shift in the net compressive force toward the compressive slab surfaces, i.e. toward the top and midspan and

toward the bottom of the slab over the support. This system of compressive force is representative of that of an internal arch; a compressive membrane force field capable of significant load transfer. It should be noted that the establishment of this internal arch does further depend on the structure's ability to balance the net compressive effect at the boundary. Typically this boundary restraint is provided by the combined resistance of any tensile reinforcement, the adjacent concrete slab, and any lateral restraint provided by the slab support structure, (i.e. girder lateral stiffness, transverse diaphragms, shear connectors, etc.).

2.3 Analysis of an Externally Reinforced Deck Slab

The rational model in the form presented by Batchelor and Hewitt was not directly applicable to the study of externally restrained FRC bridge slab for several reasons. Firstly, the proposed slab system did not contain internal steel reinforcing. Secondly, it was desirable that the refined model would be able to account for the system lateral restraint directly rather than through the use of a restraint factor as recommended by the previous researchers. Another limitation of the previous work was its inability to predict the load deformation history of the slab. The limitations of the rational model were addressed to enable prediction of the load/response behaviour of an externally reinforced slab-on-girder system acted upon by a static concentrated load. Such a system is shown in Fig. 2.2.

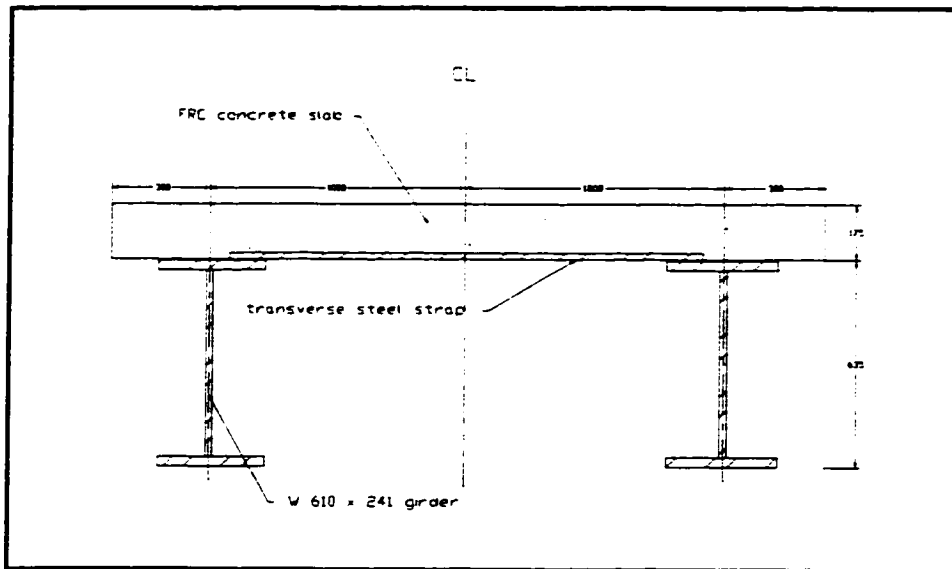


Figure 2.2: Section of an externally reinforced slab-on-girder bridge with an FRC deck slab

2.3.1 Rigid Body Behaviour

At low values of load, the applied load is transferred to the supports, i.e. the longitudinal girders, through flexure. The tensile capacity of such a slab is limited to the tensile strength of the concrete. Cracking of the slab at small magnitudes of load is evidence that the tensile strength, and consequently the flexural capacity, has been exceeded. The fact that the system develops significant capacity subsequent to the formation of cracks points to the existence of an alternate load transfer mechanism. This alternate load transfer is believed to be that of internal arching and it is a model to represent this post-cracking capacity that will be described in the following sections.

2.3.1.1 Idealized System Behaviour

As the vertical load was increased a predictable crack pattern developed that

transformed the intact slab, spanning from girder to girder, into a system of radial sectors that behaved independently as rigid bodies under increasing load. The system for which the pattern of crack development will be described is shown in Fig. 2.3.

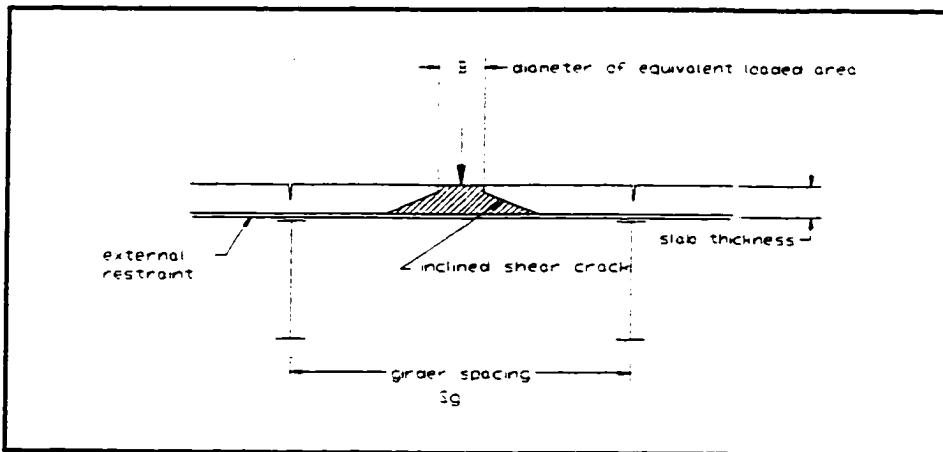


Figure 2.3: Crack development for an externally reinforced slab subjected to a vertical concentrated load

2.3.1.1.1 Crack Pattern Development

Consider a vertical load applied to the slab centrally between the longitudinal girders and the external restraints. At low magnitudes of load the first cracks appeared on the underside of the slab oriented radially below the load point. As the load was increased the radial cracks extended through the slab toward its top surface. Simultaneously cracks began to develop on the top surface, originating in the vicinity of the girder which supports the initial flexural behaviour of the slab. These circumferential cracks extended progressively around the load, approximating a circle, as the load was increased. As the radial and circumferential cracks developed, a shear crack was established. The shear crack also originated on the bottom slab surface, at a radius somewhat larger

than the load area, and progressed toward the top of the slab. The angle of inclination of the shear crack has been shown in a later section of this chapter to be a function of the system geometry and the assumptions made regarding concrete capability.

When the shear and radial cracks had penetrated to the top surface, the crack pattern approaches the idealized axisymmetric systems shown in Fig. 2.4. It was the circular area inside the shear crack that formed the top of the concrete plug that was ultimately punched through the slab.

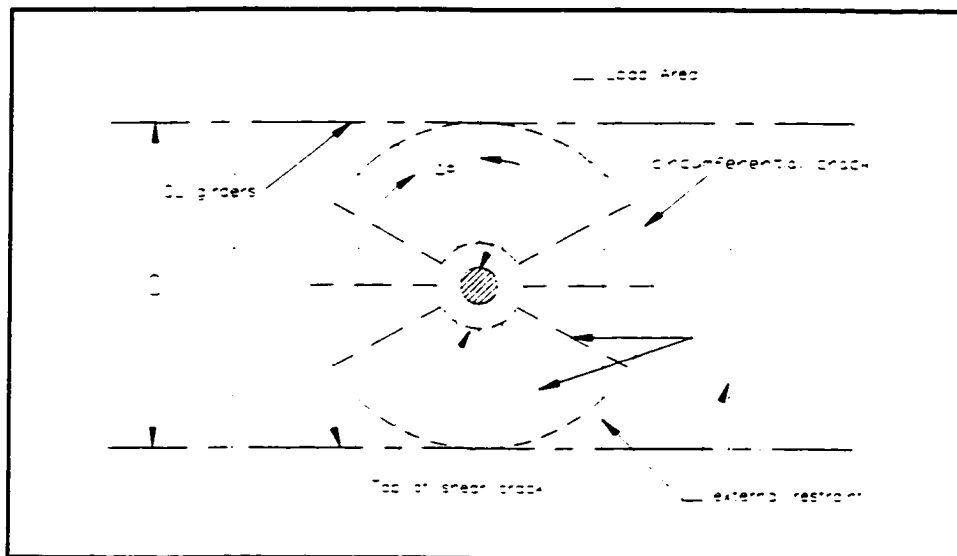


Figure 2.4: Plan view of idealized crack pattern for rigid body model assumed to represent arching behaviour

2.3.1.1.2 Assumptions

Several idealizations were necessary in order to facilitate use of a rigid body model to represent internal arching. Those assumptions are discussed below.

Firstly, the problem has been assumed axisymmetric about the load point. This

implies that the structure, the loading and the system restraint to rotation are axisymmetric. This is an idealization, as, for example, the external restraints are orientated transversely at finite spacing along the girder length. In the model two forces have been used to characterize the system restraint; a radial restraining force representing the transverse restraint and a circumferential compressive force to account for the longitudinal restraint to rotation due to the mass of concrete.

Secondly, in developing an expression for the lateral stiffness of the system, the elastic shortening of the compressed concrete has been ignored. As the concrete is stiffer by an order of magnitude than the axial stiffness of the external restraint, this omission would not be expected to change the response measurably.

The applied vertical load has been assumed to be transferred to the rigid body through a localized zone that can be described as a highly compressed state of triaxial stress. Through this zone the compressive membrane forces, necessary for the internal arch, develop.

As the internal arching, and thus the rigid body rotation, occurs, the center of rotation progresses from the root of the shear crack toward the center of the load. At the completion of the cracking phase establishing the rigid body, the center of rotation (C.R.) is located below the centre of the applied load. To simplify the analysis, recognizing intuitively that the load carrying capacity of the system during crack development is insignificant when compared to that attributable to internal arching, the C.R. was assumed stationary below the load.

The total lateral restraint force, F , represents the total lateral restraint offered to

the slab during rigid body rotation. Previous researchers, [Wegner and Mufti, (1994b)], quantified this force as that due to the axial stiffness of the external restraint as;

$$F = k_s \delta = k_s \psi (d - y) , \quad (1)$$

where δ is the lateral deflection of the rotated wedge, as shown in Fig. 2.5

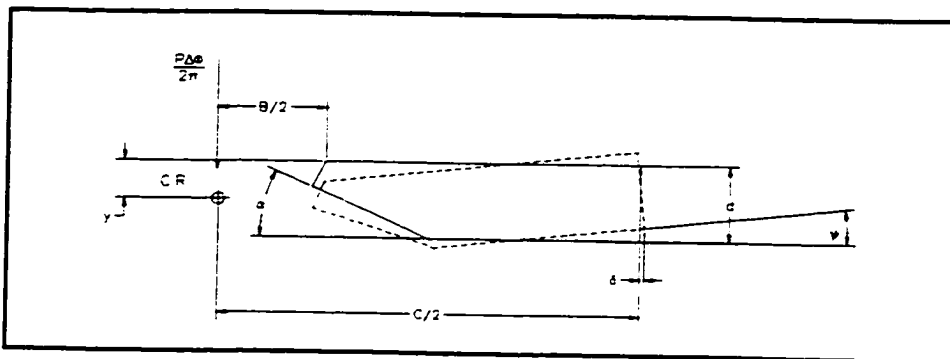


Figure 2.5: Geometry of the rigid body during rotation

and k_s is the axial stiffness of the external restraint as calculated from the following:

$$k_s = \frac{A_s E_s}{S_s + 0.5 * S_g} \quad (2)$$

However, it is recognized that the "system" restraint also contributes to the slab lateral restraint during arching. Inherent in the system restraint are both the lateral and torsional stiffness of the composite steel plate girder as well as the inertia of the intact concrete beyond the cracked region. To quantify the total lateral restraint a beam analysis was performed. For this, the model consisted of a continuous beam supported on springs and acted upon by a unit lateral load,

as depicted in Fig. 2.6.

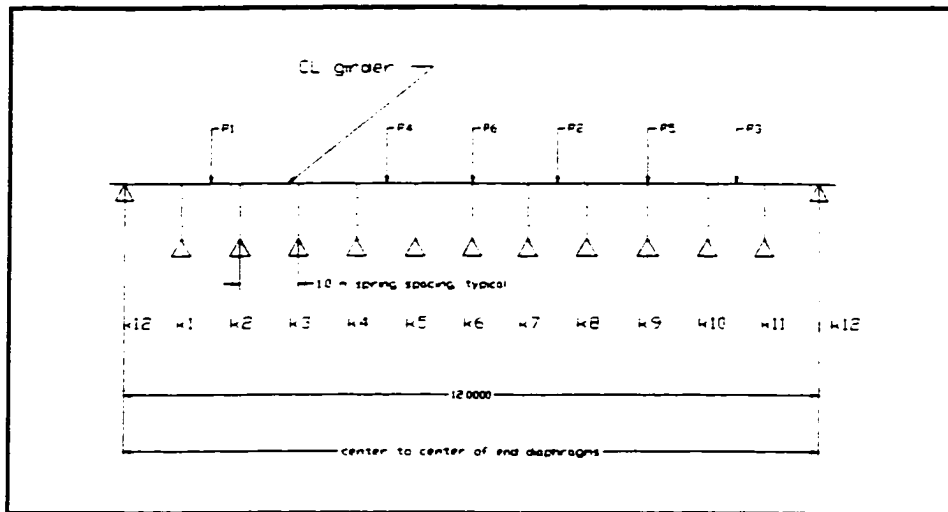


Figure 2.6: Beam model used in the calculation of the lateral stiffness of the system

The spring stiffnesses, k_1 through k_{12} in the figure, represented the axial stiffness of the external steel restraints and the transverse diaphragms. The girder properties used were the lateral bending stiffness and the torsional stiffness of the composite steel girder. A unit load was applied and the deflection at the load point calculated. The system lateral stiffness was calculated based on the results of such an analysis from:

$$K_l = \frac{P_n}{\Delta * S_s} \quad (3)$$

where P_n is the applied unit load, N , Δ is the deflection calculated from the model, mm , and S_s is the spacing of the external restraints, mm . The stiffness thus calculated represents the lateral stiffness of the system in MPa . This will be illustrated using the experimental parameters of the current work later, in Ch.6.

2.3.1.2 Wedge Geometry

The portions of the slab that rotate as rigid bodies will be referred to as wedges. A freebody diagram of one such wedge subtending an arc $\Delta\phi$ is shown in Fig. 2.7, with a dimensioned section through such a wedge given in Fig. 2.8. This section will describe its geometry and the following section will quantify the forces.

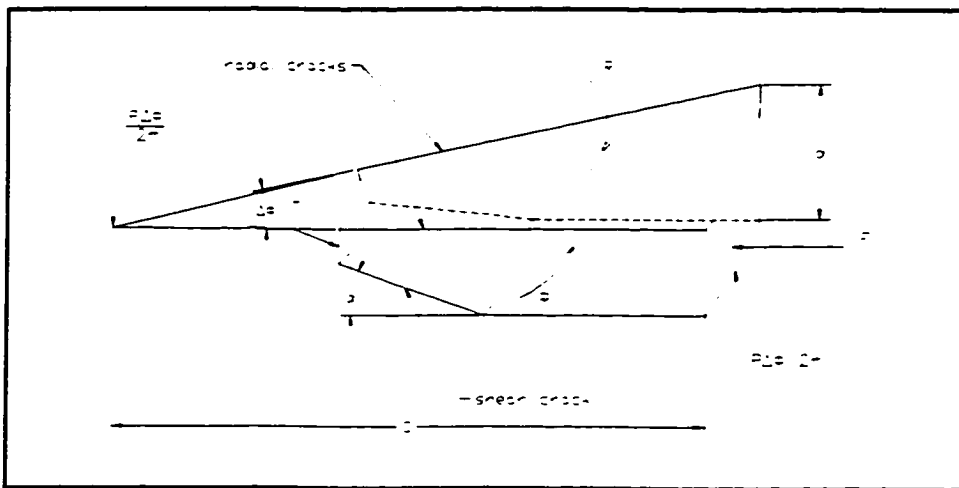


Figure 2.7: Freebody diagram of a wedge

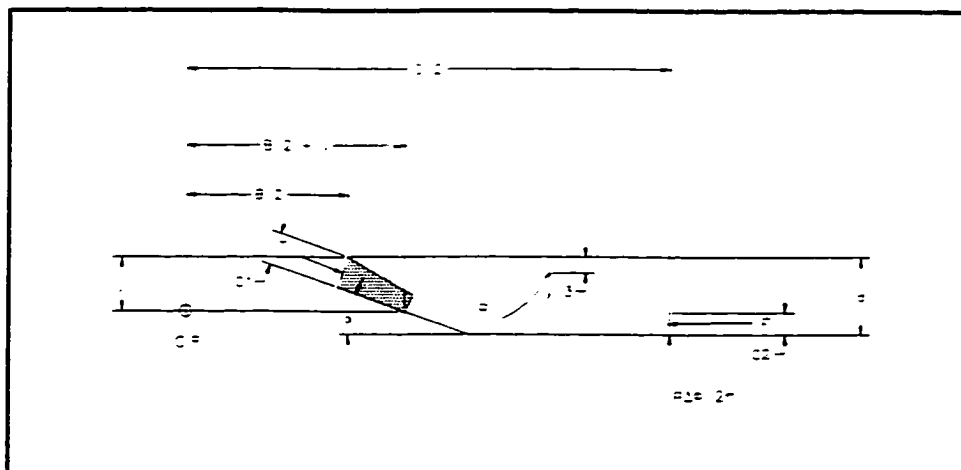


Figure 2.8: Geometry of the rigid body wedge

The vertical load applied to the slab is assumed to be transferred to the wedge uniformly over an inclined compression block oriented perpendicularly to the angled shear crack with a depth c_1 . The depth c_1 can be defined in terms of the wedge geometry, the concrete cylinder strength and the applied load. Consider the maximum force that can be transferred as the product of the maximum concrete stress and the effective area on which it acts.

$$\frac{P}{\sin(\alpha-\psi)} = 0.85 \sigma_{3c} * c_1 * 2\pi * \frac{B}{2} \quad (4)$$

rearranging and writing in terms of c_1 gives,

$$c_1 = \frac{P}{\sin(\alpha-\psi) 0.85 \sigma_{3c} * \pi * B} \quad (5)$$

Note that in these two expressions, as the equilibrium equation is written to describe the failure condition, σ_{3c} is the maximum value of the major principal stress and is based on the adopted failure criterion for the assumed state of triaxial stress.

The resultant oblique force acts on the wedge at mid-depth of the compression block, or $(c_1 \cos \alpha)$ below the top of the slab. The depth to the center of rotation, y , can be expressed using an analogy to the ultimate strength considerations for an ordinary reinforced concrete beam, for which a constant rectangular stress is assumed over a block having a depth $\beta_1 c$. In this expression, β_1 is an empirical factor which is a function only of the concrete cylinder strength and c is the distance to the point of zero stress, i.e. the neutral axis. In the slab arching problem the point of zero stress is the centre of rotation of the wedge.

Considering the geometry of the wedge, y is expressed in terms of the depth of

the stress block as:

$$y = \frac{c_1 \cos \alpha}{\beta_1} \quad (6)$$

2.3.1.3 Forces Acting on the Wedge

Four forces act on the wedge isolated as a free body, as shown in Fig. 2.9. The forces are described below, expressed as a force per unit length of wedge:

- T_w oblique compressive force acting on the wedge, through which the applied vertical load is transferred to the rigid body during arching
- R_w circumferential compressive force developed in the concrete above the center of rotation due to confinement as the rigid body rotation occurs
- F_w lateral restraining force acting on the wedge due to system constraints
- V vertical support reaction at the boundary of the wedge

An expression for each of the forces acting on a vertical plane that is central to a wedge that extends between radial cracks at $-\Delta\phi/2$ and $+\Delta\phi/2$ will be developed, as shown in plan in Fig. 2.9:

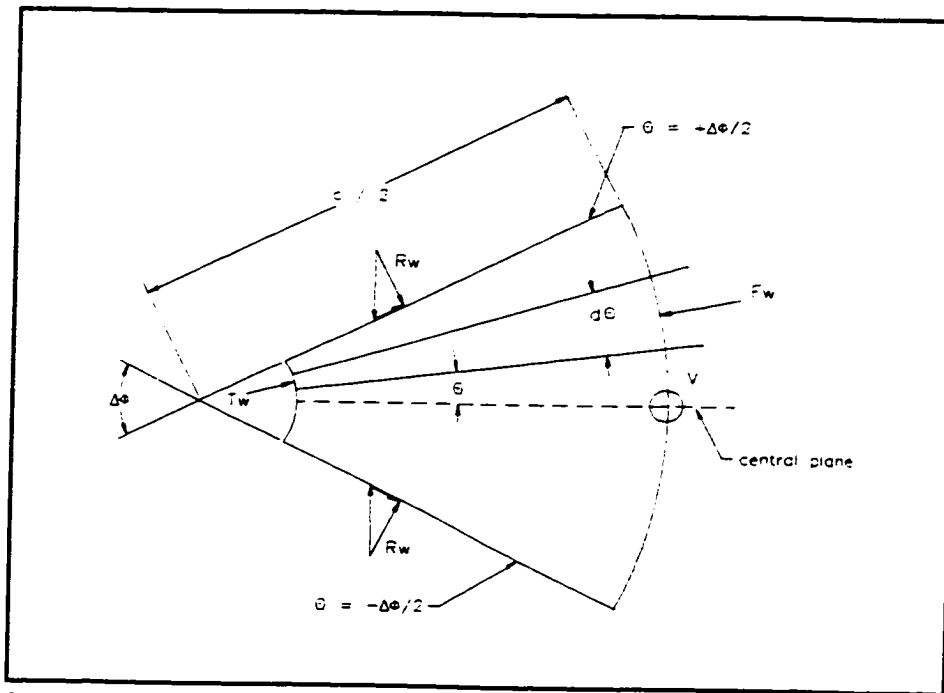


Figure 2.9: Plan of wedge showing forces acting during rotation

The vertical component of the of the total inclined compressive force must be equal to the applied vertical load.

$$T = P \frac{1}{\sin(\alpha - \psi)} \quad (7)$$

Representing the inclined force acting on a wedge $\Delta\phi$,

$$T_w = \frac{P\Delta\phi}{2\pi} \left[\frac{1}{\sin(\alpha - \psi)} \right] \quad (8)$$

The force dT_w that acts on the segmental sector $d\theta$ is therefore

$$dT_w = \frac{P d\theta}{2\pi} \left[\frac{1}{\sin(\alpha - \psi)} \right] \quad (9)$$

of which the component acting in the central plane, T_{wr} , must be $dT_{wr} = dT_w \cdot \cos \theta$, giving:

$$dT_{wr} = \frac{P \cos \theta d\theta}{2\pi} \left[\frac{1}{\sin(\alpha - \psi)} \right] \quad (10)$$

Then by integrating this over the limits of the wedge, one can obtain:

$$T_{wr} = \int_{-\Delta\phi/2}^{+\Delta\phi/2} \frac{P \cos \theta}{2\pi} \left[\frac{1}{\sin(\alpha - \psi)} \right] d\theta \quad (11)$$

$$T_{wr} = \frac{P}{2\pi \sin(\alpha - \psi)} * 2 \sin \frac{\Delta\phi}{2} \quad (12)$$

This radial force acting on the central plane is inclined at an angle ($\alpha - \psi$) to the horizontal, and therefore, can also be represented as two orthogonal components:

$$T_{wrV} = \frac{P}{2\pi} * 2 \sin \frac{\Delta\phi}{2} \quad (13a)$$

$$T_{wrH} = \frac{P}{2\pi} \cot(\alpha - \psi) * 2 \sin \frac{\Delta\phi}{2} \quad (13b)$$

Consider now the lateral restraint force acting on the wedge boundary. The lateral force acting on the wedge can be proportioned from the total restraint

force F considering the angular fraction and the circumference of the wedge as:

$$F_w = F \left[\frac{\Delta\phi}{2\pi} \right] \left[2\pi \frac{C}{2} \right] = F * \frac{C}{2} * \Delta\phi \quad (14)$$

and the incremental force is:

$$dF_w = F * \frac{C}{2} d\theta \quad (15)$$

The radial component of the restraint force is integrated over the limits, similarly to the development for T_{wr} , giving:

$$F_{wr} = \int_{-\Delta\phi/2}^{+\Delta\phi/2} dF_{wr} d\theta = \int_{-\Delta\phi/2}^{+\Delta\phi/2} F \frac{C}{2} \cos \theta d\theta = F * \frac{C}{2} * 2 \sin \frac{\Delta\phi}{2} \quad (16)$$

When the element outside the shear crack rotates, compressive stresses arise tangentially in the concrete above the center of rotation. The circumferential compressive body forces acting on the radial wedge boundaries are R_w , having two radial components acting parallel to the central plane, as shown in Fig. 2.9, is:

$$R_{wr} = R_w * 2 \sin \frac{\Delta\phi}{2} \quad (17)$$

From first principles, the compressive force in the concrete during rotation can

be calculated by integrating the concrete stress as follows:

$$R_w = \int_0^y \int_{B/2-y}^{C/2} \sigma_{ct} dr dz = \int_0^y \int_{B/2-y}^{C/2} E_c \epsilon_{ct} dr dz \quad (18)$$

where ϵ_{ct} is the concrete tangential strain and can be expressed as the change in circumference for a point at a given radius. Considering the change in circumference at a radius r as the wedge rotates in a vertical plane through an angle ψ to be approximately a linear function of the distance above the center of rotation, in the elastic range, ie. $\Delta r = \psi z$. The strain then can be written:

$$\epsilon_{ct} = \frac{2\pi\Delta r}{2\pi r} = \frac{\psi z 2\pi}{2\pi r} = \frac{\psi z}{r} \quad (19)$$

And the force can be expressed in terms of this strain as:

$$R_w = \int_0^y \int_{B/2-y}^{C/2} E_c \frac{\psi z}{r} dr dz \quad (20)$$

Performing the integration, the following relation is obtained:

$$R_w = E_c \psi \frac{y^2}{2} \ln \left[\frac{\frac{C}{2}}{\frac{B}{2} + y} \right] \quad (21)$$

Referring to Fig. 2.8, it should be noted that the force acting on a small triangular section above the inclined shear crack, between the edge of the load, at $r = B$,

and $r = B/2 + y$ has been omitted. This omission was made to simplify the calculation, as the shear crack inclination, α , will be shown later to be a function of the magnitude of the tangential force.

The expression developed above represents the circumferential force assuming a linear elastic material. It is well accepted that behaviour of the confined concrete near the compressive limit is nonlinear. Empirically Kinnunen and Nylander, (1960) have developed a relationship for the tangential forces in terms of a concrete stress that they were able to measure experimentally and which gave more accurate predictions. An empirical form of Eqn.(21) is given below:

$$R_w = \frac{y^2}{2} \left[\frac{B}{2y} + 1 \right] \sigma_{cty} \ln \left[\frac{\frac{C}{2}}{\frac{B}{2} + y} \right] \quad (22)$$

In this relationship, σ_{cty} is the tangential concrete stress at the slab surface adjacent to the shear crack, just prior to crushing. These researchers were able then to relate this measured stress to the concrete cube and cylinder strengths using the following relations, quoted here in imperial units, (psi).

$$\sigma_{cty} = 1007 + 0.392 \sigma_{cube} \quad (23)$$

$$\sigma_{cube} = \frac{f'_c}{0.75 + 0.000025 f'_c} \quad (24)$$

The final freebody force to be considered is the vertical reaction at the boundary. This reaction acts in a direction parallel to the central plane and is directly

proportional to the total vertical force applied:

$$V = \frac{P\Delta\phi}{2\pi} \quad (25)$$

2.3.2 Equilibrium Considerations

In term of the wedge geometry and the freebody forces just developed, force and moment equilibrium considerations for the wedge were used to develop relationships to express the ultimate load, P , and the angle of inclination of the shear crack, α . The equilibrium relationships have been used to describe the external forces acting on a wedge during the rigid body rotation that occurs subsequent to cracking. During this stage the load carrying capacity of the system has been shown to increase. Equilibrium will be satisfied for a given radial sector of the cracked slab, subtending an angle $\Delta\phi$, as was shown in Fig. 2.9.

The six possible static equilibrium equations for a three-dimensional system, expressed using polar coordinates are:

$$\begin{array}{ll} \sum F_r = 0 & \sum M_r = 0 \\ \sum F_\theta = 0 & \sum M_\theta = 0 \\ \sum F_z = 0 & \sum M_z = 0 \end{array}$$

As the problem being studied is one in which the deformation is axisymmetric, it follows that the stress components are independent of the angle θ , measured in the horizontal or z plane. All derivatives with respect to $\partial\theta$ also vanish. The stress components in such a system, described as a state of axisymmetric stress, are functions only of r and z , and three of the equilibrium equations are

satisfied as a priori. The three remaining equations are thus:

1. Vertical Force Equilibrium, $\sum F_z = 0$
2. Radial Force Equilibrium, $\sum F_r = 0$
3. Radial Moment Equilibrium, $\sum M_r = 0$

Using the first equilibrium equation, the vertical force acting on each sector can be expressed in terms of the total vertical load applied to the slab as was given in Eqn. 25.

Force equilibrium on a radial plane can be used next to describe P in terms of the restraining forces, F and R_w , and the angle that the rotated wedge makes with the horizontal plane, $(\alpha - \psi)$. The three forces acting on the wedge subtending an arc $\Delta\phi$ are shown in plan in Fig. 2.9; the radial forces, T_w and F_w , and the circumferential force R_w . The force equilibrium has been described on a vertical plane central to this wedge, shown as the dashed line in the figure. Radial components of the three forces acting on the central plane of the wedge were described by equations (16) and (17) as:

$$F_{wr} = \frac{C}{2} F * 2 \sin \frac{\Delta\phi}{2} \quad (16)$$

$$R_{wr} = R_w * 2 \sin \frac{\Delta\phi}{2} \quad (17)$$

$$T_{wr} = \frac{P}{2\pi} \cot(\alpha - \psi) * 2 \sin \frac{\Delta\phi}{2} \quad (13b)$$

The summation of the radial forces on the central radial plane then gives:

$$T_{wrh} + R_{wr} - F_{wr} = 0 \quad (26)$$

Substituting from equations above and dividing through by $2 \sin \Delta\phi/2$ gives:

$$\frac{P}{2\pi} \cot(\alpha - \psi) = F \frac{C}{2} - R_w \quad (27)$$

and in terms of P , $P = 2\pi \left[F \frac{C}{2} - R_w \right] \tan(\alpha - \psi)$ (28)

The final equilibrium consideration is that of moment equilibrium in the radial plane. The moments causing vertical rotation of the central plane (dashed line of Fig. 2.9) were summed the point of intersection of the horizontal and vertical boundary reactions, F_w and $P\Delta\phi/2\pi$, respectively.

$$\sum M = 0 \quad (+ \text{Clockwise})$$

$$0 = R_{wr} \left[d - \frac{y}{3} - \frac{c_2}{2} - \psi \left(\frac{C}{4} - \frac{B}{4} \right) \right] + T_{wrh} \left[d - \frac{y\beta_1}{2} - \frac{c_2}{2} - \psi \left(\frac{C}{2} - \frac{B}{2} \right) \right] - T_{wrv} \left[\frac{C}{2} - \frac{B}{2} + \psi \left(d - \frac{c_2}{2} - \frac{y\beta_1}{2} \right) \right] \quad (29)$$

Rearranging, substituting for R_w from (17), T_{wrh} from (13b) and T_{wrv} from (13a) and eliminating the common term $2\sin\Delta\phi/2$

gives:

$$R_w \left[d - \frac{y}{3} - \frac{c_2}{2} - \psi \left(\frac{C}{4} - \frac{B}{4} \right) \right] + \frac{P}{2\pi} \cot(\alpha - \psi) \left[d - \frac{y\beta_1}{2} - \frac{c_2}{2} - \psi \left(\frac{C}{2} - \frac{B}{2} \right) \right] = \frac{P}{2\pi} \left[\frac{C}{2} - \frac{B}{2} + \psi \left(d - \frac{c_2}{2} - \frac{y\beta_1}{2} \right) \right]$$

(30)

and multiplying through by $2\pi/P$ and rearranging gives:

$$\frac{R_w 2\pi}{P} = \frac{\left[\frac{C}{2} - \frac{B}{2} + \psi \left(d - \frac{c_2}{2} - \frac{y\beta_1}{2} \right) \right] - \left[\cot(\alpha - \psi) \left[d - \frac{y\beta_1}{2} - \frac{c_2}{2} - \psi \left(\frac{C}{2} - \frac{B}{2} \right) \right] \right]}{\left[d - \frac{y}{3} - \frac{c_2}{2} - \psi \left(\frac{C}{4} - \frac{B}{4} \right) \right]}$$

(31)

Substituting for P from Eqn. 28, calling $W = [(F * C/2) - R_w]$, and simplifying the equation gives the following relation for the angle of inclination of the shear crack:

$$\alpha = \tan^{-1} \left[\frac{\frac{R_w}{W} \left[d - \frac{y}{3} - \frac{c_2}{2} - \psi \left(\frac{C}{4} - \frac{B}{4} \right) \right] + \left[d - \frac{y\beta_1}{2} - \frac{c_2}{2} - \psi \left(\frac{C}{2} - \frac{B}{2} \right) \right]}{\left[\frac{C}{2} - \frac{B}{2} + \psi \left(d - \frac{c_2}{2} - \frac{y\beta_1}{2} \right) \right]} \right] + \psi$$

(32)

2.3.3. Potential Limits to the Slab Arching Behaviour

Three potential limits are recognized to describe the extent of load-carrying potential of the wedge undergoing rigid body rotation. Two of the limiting conditions are strength limits and the third is an instability condition. The strength limits are crushing of the concrete in compression or yielding of the external restraint in tension. Satisfying either of these limits will result in a slab punch through. Occurrence of a wedge instability, on the other hand, precludes a punching failure. These three limits will now be considered in more detail.

2.3.3.1 Concrete Compressive Stress Limit

Concrete in the vicinity of the concentrated load exists in a state of triaxial compressive stress. This state of stress can be described in terms of three principal stresses; $\sigma_1 \leq \sigma_2 \leq \sigma_3$, termed the minor, the intermediate and the major principal stress, respectively. The minor principal stress is the vertical stress arising from the concentrated applied load, P. The intermediate and major principal stresses are the radial and circumferential stresses that arise due to restraint inherent in the structural system. The system restraint accrues from several sources; the surrounding concrete slab, the axial stiffness of the external reinforcing, the lateral bending stiffness of the composite longitudinal steel girder and the torsional stiffness of the girder. The degree of composite action, as a function of the shear connection between the steel girder and the concrete slab will also influence the last two girder stiffnesses. These restraining influences have been idealized as two principal stresses, σ_2 and σ_3 , in the radial and the circumferential directions, to allow an albeit idealized axisymmetric model.

When the concrete is prevented from expanding laterally the orthogonal compressive stress that it can carry can exceed the uniaxial compressive

strength by a substantial margin. Many researchers have validated the finding that in such a stress state, the maximum principal stress is independent of the magnitude of the intermediate principal stress. The fact will enable the expression of the radial confining stress in the concrete slab as a function of the stress due to the applied vertical load. When the maximum principal stress reaches the concrete crushing strength the transfer from the loaded portion to the wedge can no longer be made and the load is said "to punch through" the concrete slab.

Previous researchers, [Wegner and Mufti, (1994b)], represented the limiting triaxial stresses in the load area using the failure criterion as used in the finite element software, ADINA, [Bathe, (1982)]. Assuming the state of stress to be approximated by the condition that the minor and intermediate stresses are equal, the major principle stress becomes:

$$\sigma_{3c} = f'_c \left(1.0 + 1.5 \frac{\sigma_1}{f'_c} \right) \quad (33)$$

Several researchers have attempted to model the influence of concrete confinement on the maximum attainable concrete stress. A summary of the more relevant models was made as part of a study of the use of advanced composite sheets to rehabilitate concrete columns, (Demers and Neale, 1994). There was consensus among the researchers that the maximum principal stress attainable was not directly affected by the magnitude of the intermediate principal stress and the relationships they recommended to predict the major principal stress were all of the form:

$$\sigma_{3c} = f'_c \left(1 + K_c \frac{\sigma_1}{f'_c} \right) \quad (34)$$

The term K_c in Eqn.34 is a confinement constant which gives an empirical representation of the confinement inherent in the system. This constant can be expected to vary from system to system depending on the nature and magnitude of the confinement. For example, for a concrete cylinder loaded axially to failure while subjected to a constant confining fluid pressure [Richart et al., (1929)] recommended a value of 4.1. The same research showed the value of 4.1 to hold true for concrete confined by circular spirals.

For the current study the confinement afforded the concrete as the internal arching mechanism responds to increasing vertical load arises from two sources; circumferential stress and radial stress. The former is due to the circumferential concrete force, R , and the latter is due to the restraining force, F . As arching proceeds and the slab rotation increases, the magnitude of the circumferential confinement increases. To establish K_c to be used as part of the algorithm to predict punching failure of the arching mechanism, a parametric analysis was made. The value of the constant was varied from 4 to 12, for a given set of system parameters. The influence of the concrete confinement constant on the load deflection prediction is illustrated graphically in Fig. 2.10. The results of this study show that the predicted stiffness and ultimate punching capacity of the slab increased as K_c increased. The best correlation with experimental behaviour was found setting K_c equal to 10, which will be presented in Ch. 6.

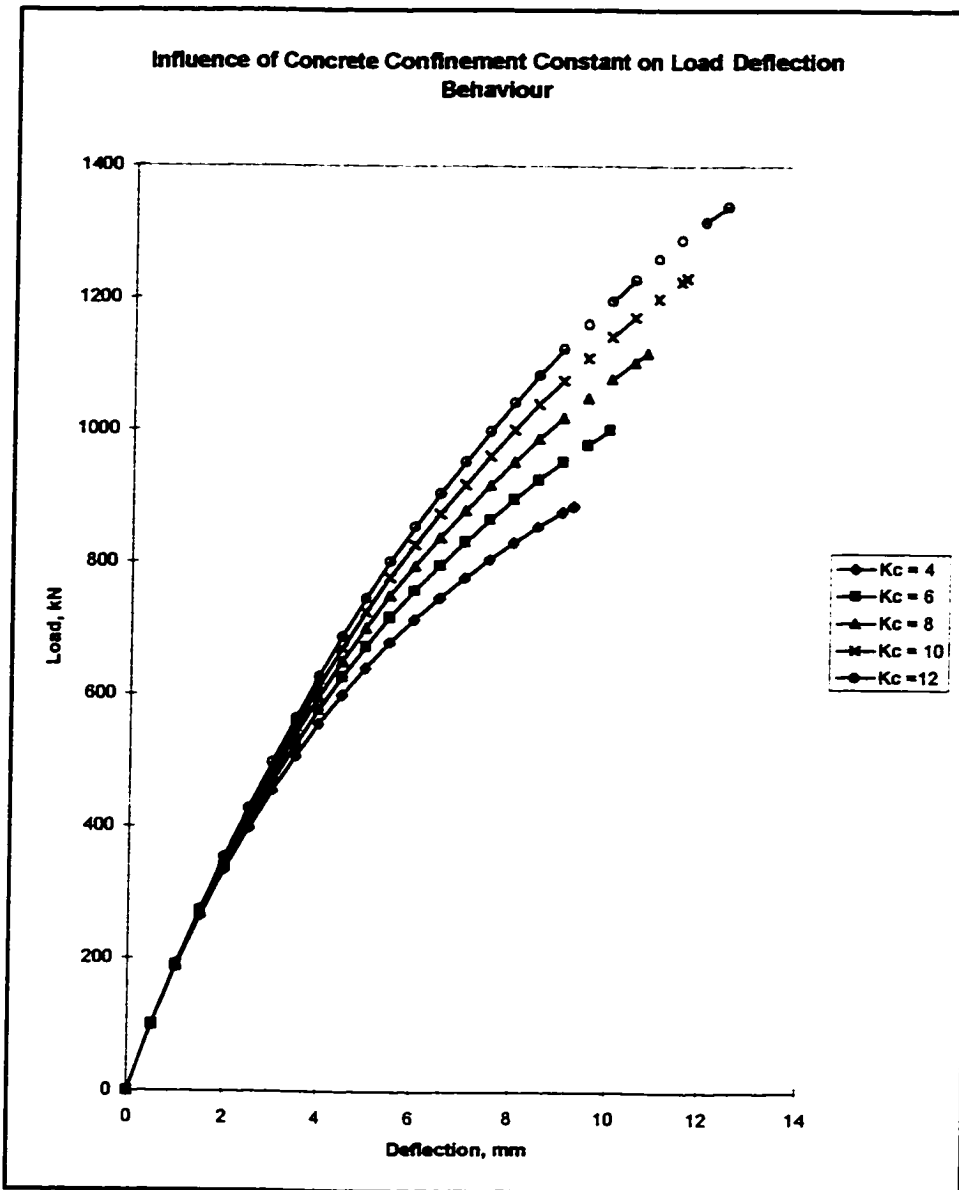


Figure 2.10: Influence of concrete confinement constant on the load/deflection behaviour

The criterion for a concrete punching is that described by a compression failure in the concrete at the surface of the slab near the top extent of the shear crack when the tangential strain in the concrete reaches the accepted limit for

maximum uniaxial compression, i.e. a limiting strain ϵ_{cu} of 0.002 mm/mm. The uniaxial strain limit was used to ensure a lower bound solution, recognizing that crushing failure of the concrete adjacent to the load transfer area would result in a sudden collapse, accompanied by a high release of energy. Physically, this limit represents the loss of confinement in the transfer area, the compressed conical shell. Without such confinement the capacity of the internal arch in compression is degraded and punching failure follows.

2.3.3.2 Yielding of External Restraint

Tensile yielding of the external restraint imposes a serviceability constraint to the system. Consistent with the stress/strain characteristics of a structural grade steel, after the axial stress in the strap has reached the yield stress an elongation in the order of 20% can be expected without a further increase in the applied load. Such deflection, if allowed to proceed, would give a ductile indication of distress in the system, prior to a tensile failure of the external restraint. A tensile failure of the external restraint would also effectively represent a limit to internal arching, as the external restraint supplies the tensile force necessary to complete the internal arch. Thus, rupture of the tie in tension destroys the integrity of the internal arch and leads to a concrete punch through. Thus a calculated strain in excess of the steel yield strain of $\epsilon_y = 0.0015$ mm/mm was recognized as a system limit for the analytical model.

2.3.3.3 Geometric Instability of Rigid Body

A third type of limiting behaviour was that marked by a geometric instability of the load area; termed a snap-through failure mode. This failure mode was evident in scale testing and can be predicted by analysis. Evidence of this limit occurs analytically when, for a given formulation of equilibrium for the rigid body,

an additional deflection results in a decreased value of vertical load to maintain equilibrium. Mathematically this behaviour is described as a point of zero slope on the load/deflection curve, i.e. $dP/d\Delta = 0$. Practically this instability failure mode can be expected to occur at loads less than that to cause punching only at very low values of external restraint.

2.3.4 Iterative Solution to Predict Load Response

An iterative approach was required to solve for the maximum punching load as well as the deflection and strain history of a loaded slab using the relationships derived from the equilibrium equations, as the geometry of the rigid body was not independent of the magnitude of the freebody forces.

A FORTRAN program was developed, [Newhook and Mufti, (1995b)], to facilitate the calculation and is presented in a Appendix A. A summary of the iterative technique is presented in Fig. 2.11.

1. Assume a slab central deflection of 0.
2. Calculate the angle of wedge rotation, $\psi = 2\Delta/c$.
3. Estimate the depth to the center of rotation, $y_{ass} = d/100$.
4. Calculate the resultant of circumferential compressive stress in the concrete above the center of rotation as the wedge rotates, R_w .
5. Calculate $W = [(F * C/2) - R_w]$.
6. Calculate α , the angle of inclination of the shear crack.
7. Calculate the vertical load to cause the assumed deflection, P .
8. Back calculate to find the calculated distance to the center of rotation, y_{cal} , for the calculated vertical load.
9. Calculate the difference between y_{cal} and y_{ass} .
10. If the difference is greater than .0001 reiterate the calculation using y_{cal} as the starting point.
11. If the difference is less than .0001, the calculated values of P and Δ define a point on the load/deflection history for the slab.
12. If the calculation process does not converge ($y_{cal} - y_{ass} \leq 0.0001$) in 1000 iterations the procedure is stopped.
13. If ($y_{cal} - y_{ass} \leq 0.0001$) calculate the concrete tangential strain in the top of the compressed conical shell.
14. Compare the concrete compression strain to the crushing limit, set at 0.002 mm/mm.
15. If $\epsilon_{ct} = 0.002$ and ($y_{cal} - y_{ass} \leq 0.0001$) the wedge is in equilibrium and the concrete compressive strain has reached the limit..this defines the ultimate punching capacity of the slab

Figure 2.11: Steps in iterative analysis to describe slab load deflection history during internal arching

3.0 OPTIMIZATION OF AN EXTERNALLY RESTRAINED FRC SLAB

3.1 Scope of Optimization

3.1.1 Variables Considered

The structural system to be optimized is that of an externally restrained FRC bridge slab which is acting compositely with supporting longitudinal steel girders. Specifically, the aim was to recommend a procedure to establish minimum requirements for the two principal slab design variables; namely, the area of external restraint and the slab span-to-depth ratio. Thus establishing a minimum weight system. The influence of varying the former was considered both analytically and experimentally, while the variations in the span-to-depth ratio was only studied analytically due to the financial constraints imposed by physical tests. The costs were then considered in order to compare the system as optimized to a conventional bridge slab having internal reinforcing steel.

3.1.2 Structural System Constraints

The selection of the optimum layout for an externally restrained slab-on-girder superstructure is influenced by a number of factors relating to the slab support structure. In the bridge superstructure being studied that slab support is the composite steel girder. Size and spacing of the steel girders have been considered beyond the scope of the current optimization study. It has been assumed that the optimum girder proportions as well as the girder spacing have been established based on the strength and serviceability criteria, considering the girder's role of longitudinal load transfer. The optimization of the composite girder itself hinges on an attempt to balance the contribution of the concrete slab resisting compression induced by longitudinal bending with the tensile capacity

of the steel section below the neutral axis. In order to justify this assumption, the influence of slab thickness on the composite girder's effectiveness was considered.

Figure 3.1 illustrates the sensitivity of the girder design moment to changes in the slab thickness. From this graph, it can be seen that doubling the slab thickness from 125 mm to 250 mm, changes the design moment by the following percentages:

Maximum positive moment (single span)	10.4%
Maximum positive moment (continuous)	6.4%
Maximum negative moment (continuous)	7.1%

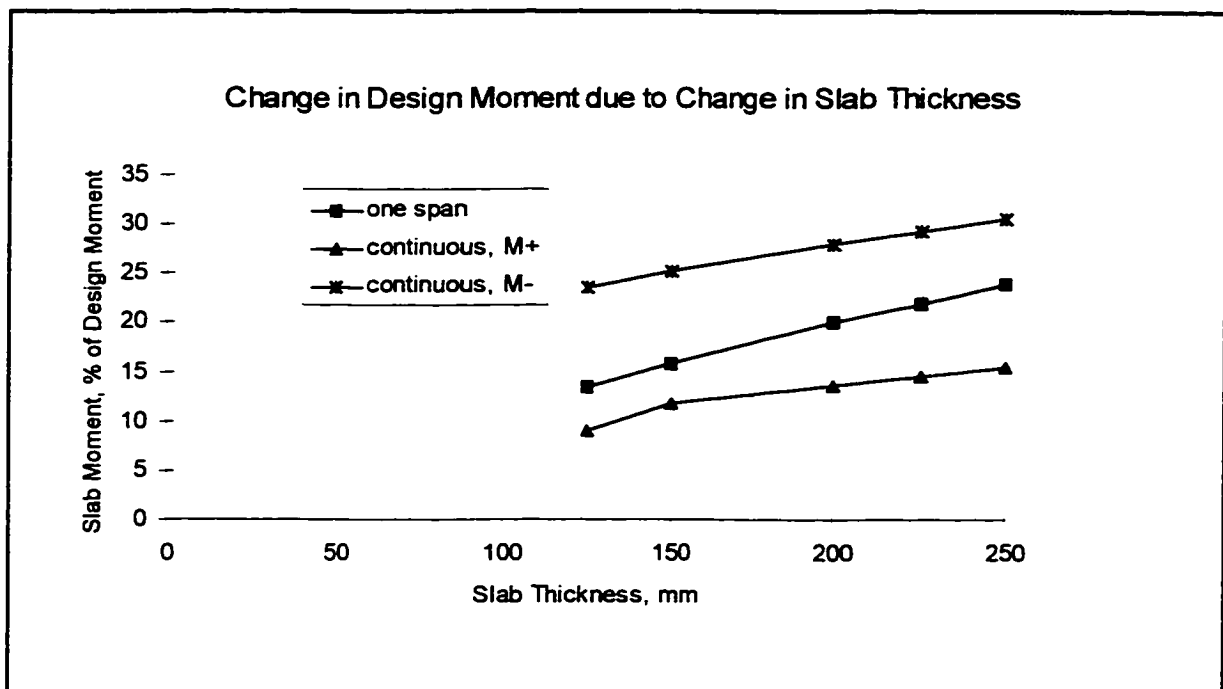


Figure 3.1: Influence of slab thickness on girder design moment

A reduction in the slab thickness decreases the system dead load, which benefits the girder effectiveness by causing a small reduction in design moment, as demonstrated above. Offsetting this benefit, however, is a reduction in composite girder capacity. In positive moment regions the capacity reduction is a direct result of the reduction in deck thickness. In negative moment regions, although the concrete is assumed to be cracked and to make no contribution to the composite section, there is a more significant loss of composite girder capacity due to loss of composite action provided through the longitudinal steel reinforcing of a conventionally reinforced deck.

In the positive moment regions, considering the two effects simultaneously, reducing the slab thickness will cause a nominal decrease in the maximum girder tensile stress. Typically, for a 50 mm reduction in slab thickness, the girder tensile stress would increase 1% due to the reduced section, offset by a 2 to 4% decrease in design moment caused by the reduced dead weight. Considering these two counteracting effects on the compressive stress in the girder top flange, the result would be a net stress increase of approximately 11 to 13%. This stress increase, although significant, would not alter the fact that the compressive stresses in the top flange do not drive the design, [AISC, (1986)]. The top flange size in regions of positive bending is kept to a minimum as its primary role is to provide strength and stability during the construction phase. The girder size and spacing would still be controlled by tensile stresses, which have been shown insensitive to changes in slab thickness. Thus, for single span or noncontinuous composite systems, a significant change in slab thickness would not influence either the weight nor the spacing of the longitudinal girders. The current study will then focus on the optimization of the slab thickness and the external restraint stiffness independent of the girder size.

It is worth noting that, although this study does not address the system capacity in negative bending, for the same 50 mm change in slab thickness in a negative moment region there would be more severe consequences. Here, the loss of section is more significant as the elimination of the traditional internal steel reinforcing in the deck eliminates the benefit of composite design. Hence, the plate girder stresses in the negative moment region must be calculated assuming that the steel girder is non-composite. As such, the resultant stress increases can be in the order of 26% for the tensile flange and 4% for the compression flange. A 2 to 4% moment decrease due to the 50 mm loss of concrete dead weight can be expected. This translates into an increase in girder top flange stress in the order of 25%, accompanied by a nominal increase in the bottom flange stress. Contrary to the case of positive bending then, for negative bending regions the slab thickness can be expected to directly influence both the girder proportions and the girder layout.

3.1.3 Slab Span-to-Depth Ratio

Current Canadian composite bridge design practice is governed by slab minimum thickness requirements of 225 mm and 200 mm, specified by the OHBDC('91) and CSA S6-M88, respectively. These are empirical limits that have been fixed primarily to satisfy deck durability concerns that arise from the minimum cover and spacing requirements for the traditional 4 layers of internal steel reinforcing. Thus, the industry norm is very much a function of durability rather than either strength or serviceability. Being a durability concern related to protection of the internal steel reinforcing, the empirical limit on slab thickness is irrelevant to an externally reinforced bridge slab.

For the optimization, the maximum span length to thickness ratio considered was 16. For comparison, the maximum permissible span-to-depth ratio for use of

the OHBDC empirical design method is 15. Within this range the minimum slab thickness was limited to 125, associated with a girder spacing of 2000 mm, and the maximum slab thickness considered was 250 mm, associated with a 4000 mm girder spacing.

Having thus established the minimum recommended slab thickness, based on a given girder spacing and a maximum span to thickness ratio of 16, the optimization was furthered to produce a system design using minimum external restraint. The aim being to maximize the external restraint spacing for a given girder spacing. This maximum spacing will be established as a function of the minimum restraint stiffness required in order to induce a punching limit for the slab.

3.1.4 Experimental Study

In the full-scale testing program an FRC bridge deck supported on longitudinal steel girders provided with regularly spaced transverse steel straps was considered. These steel straps provided the slab external restraint used to prevent lateral separation of the girder flanges in response to a concentrated load acting on the slab between the girders. The straps would develop the tensile force necessary to support the internal arch as the slab rotates as a rigid body, as was described mathematically in Ch. 2.

A 175 mm thick slab was selected for the experimental model for two reasons. At this thickness the deck has a span-to-depth ratio of 11.4, which is within the range of ratios for a conventionally reinforced bridge deck. The 175 mm thickness does represent a marginal reduction in slab thickness from the 200 mm to 225 mm thicknesses that currently dominate Canadian practice. The 175 mm slab thickness was also made recognizing the prediction of a minimum cost

system for a 180 mm thick slab made by the preliminary analytical work, [Wegner and Mufti, (1994b)].

For the experiment, the stiffness of the external restraint was varied along the length of the test bridge. The stiffness was changed by varying the area of the transverse steel straps. The strap layout is shown in Figure 3.2 and the strap sizes are given in Table 3.1.

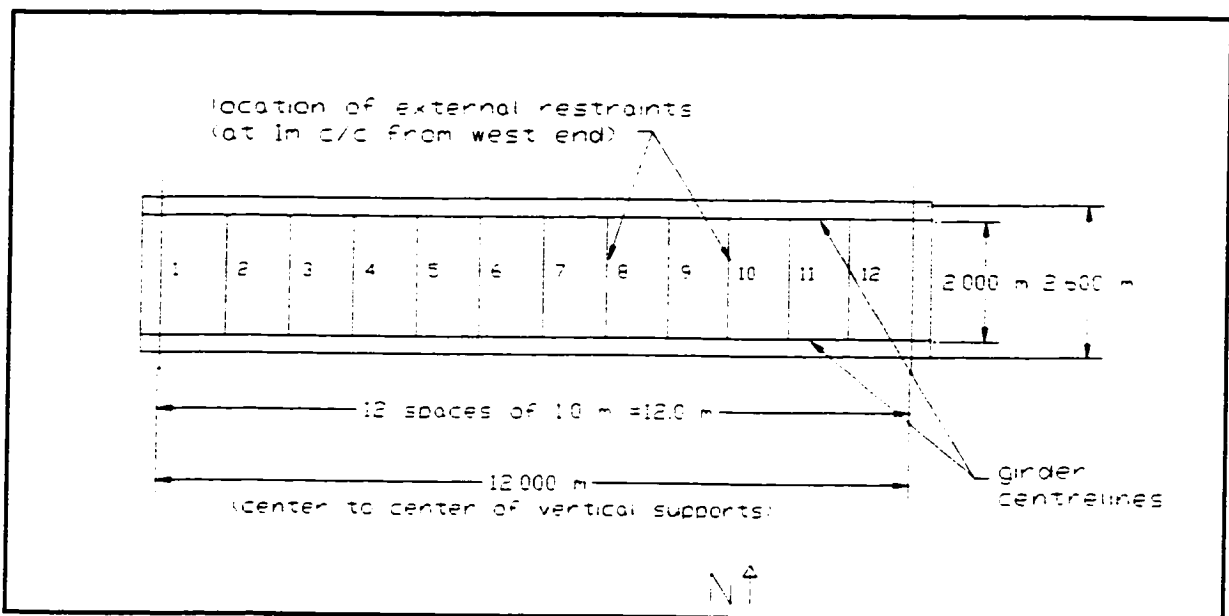


Figure 3.2: Plan view of experimental slab giving location of external restraints

The width of the strap was maintained and the thickness varied. Details of the steel strap thickness, area and axial stiffness are also summarized in Table 3.1 and a further description of the experimental model can be found in Ch. 4. This testing program was designed to empirically establish the minimum degree of external restraint required to produce a punching shear failure in a concrete slab while providing an adequate reserve on the service capacity requirements for a highway bridge deck.

Table 3.1: Strap areas used in experimental model, mm²

Strap No.	1	2	3	4	5	6	7	8	9	10	11
Tests 1,2,3	2500	2500	2500	1900	1900	1900	1250	1250	1250	950	950
Test 4	2500	2500	2500	635	635	635	1250	1250	1250	950	950
Tests 5,6,7,8	2500	2500	635	635	635	635	635	635	635	635	950

3.2 System Design

3.2.1 Recommended Design Load

3.2.1.1 Strength Requirements

The focus of the FRC slab system optimization was to define the minimum parameters of the structure required to provide a "safe" and "serviceable" externally reinforced highway bridge deck for Canadian interprovincial use. The first step of this optimization process was to define the design load. To establish this load, which would appropriately define the minimum load capacity of an externally restrained FRC slab, a review of the vehicle loads currently used to design Canadian highway bridges was made. The results of the review are

presented below in terms of vehicle wheel loads, recognizing that the critical vehicle loading for short span structural components, which include most highway bridge decks, is a single wheel load or an axle group load. This is in contrast to the importance of single heavy vehicles on intermediate length components and the extreme effects of the simultaneous action of multiple vehicles on a long span structure.

Canadian highway bridges are currently designed using the Limit States Design criteria of either the OHBDC(91) or the CSA S6-M88. At the time of writing, technical development of a national bridge code for Canada is well underway and it is expected that this code will be invoked by the appropriate provincial regulatory authorities upon its expected publication in 1998. The Canadian Highway Bridge Design Code, or CHBDC as it has become known, is being developed based on the OHBDC model by a nationally based technical committee. All three bridge design codes reflect the philosophy that a structure should perform without collapse when subjected to overload conditions and also remain functional under normal working loads. These qualitative design goals are interpreted mathematically in the codes using probabilistic methods. The probability of exceeding the extreme event or working load behaviour is reduced to a very low percentage based on statistical knowledge of materials, loads and member resistances. It is the aim of the limit states method of design that a uniform probability of failure exist irrespective of the variability of each of these design effects. For conditions related to safety, considered under overload conditions, the national bridge code will provide a probability of approximately 1% chance of being exceeded in a 75 year life cycle, [CSA, (1994)].

For the three prevailing Canadian bridge codes, the maximum design wheel loads for the overload and working conditions are compared in Tables 3.2 and

3.3, which follow. The tables show the appropriate load factors and an allowance for dynamic effects experienced by highway structures.

Table 3.2: Ultimate Limit State wheel loads

CODE	OHBDC	CSA-S6	CHBDC
Max'm wheel load P	100 kN	90 kN*	87.5 kN*
Max'm load factor α_L	1.4	1.6	1.75
Max'm impact factor I	1.4	1.4	1.4
ULS wheel load $= P \times \alpha_L \times I$	196 kN	202 kN	214 kN

*the maximum wheel load is 0.15 times the gross vehicle load, and the standard design vehicle has a gross vehicle load of 600 kN, however the code recognizes the authority of a jurisdiction to specify a lesser or greater gross vehicle load.

Table 3.3: Serviceability Limit State wheel loads

CODE	OHBDC	CSA-S6	CHBDC
Max'm wheel load P	100 kN	90 kN*	87.5 kN*
Max'm load factor α_L	0.75	1.0	0.9
Max'm impact factor I	1.40	1.40	1.40
SLS design load $= P \times \alpha_L \times I$	140 kN	126 kN	110 kN

*the maximum wheel load is 0.15 times the gross vehicle load, and the standard design vehicle has a gross vehicle load of 600 kN, however the code recognizes the authority of a jurisdiction to specify a lesser or greater gross vehicle load.

Modern highway loadings include several variations in commercial vehicle types ranging from the shorter two axle trucks to long truck trains of up to 9 axles. Additionally there exists a wide range of combinations of interaxle spacing and axle weights. In Canada legal axle limits are imposed through provincial acts, which also invoke the relevant bridge design code in which the minimum structural standards for new bridge construction are specified. In 1991, as a step toward eliminating variations in legal loads at the interprovincial boundaries, the provincial and territorial authorities signed a document which established national standards for truck sizes and weight limits for structures on routes intended for interprovincial trucking, [Transportation Association of

Canada, (1994)]. As a result of this agreement, the maximum wheel load on highways designated for interprovincial use was set nationally at 45 kN. It is noted, however, that each province will allow some exceptional loads in excess of those established by the agreement for certain roads, or for specific goods being transported in a controlled fashion.

Comparing the maximum design wheel loads at the ultimate and serviceability limit states from the tables given above to the maximum regulated wheel load of 45 kN, the inherent reserve implicit in the current bridge design codes is evident. For example, the serviceability factored design load of 110 kN for the CHBDC represents a load that is 2.4 times the legislated maximum wheel load. The ultimate design load for the same code is 4.8 times the legislated maximum wheel load.

For consistency with the Canadian Limit States Design approach, load and resistance factors were incorporated in the expression developed for the design punching load. These factors quantify the degree of variability inherent in the prediction of the resistance and the load. A resistance factor less than unity is incorporated in the resistance expression and a load factor, a multiple greater than 1, is used to describe the load effect. That is, the resistance is underestimated and the loads overestimated. The safety factor, expressed as the ratio of the resistance provided to the load effect is an expression of the probability of failure of the given component.

Considering first the resistance factor appropriate for the FRC punching resistance. The material resistance factors for concrete vary from 0.75 for normal density concrete to 0.57 for low density concrete, [Calibration Committee, OHBDC, (1990)]. For FRC, due to a higher variability in the resulting material, it seems reasonable to assume that the material resistance

factor should be set lower than 0.75. Further studies focusing on the material properties and producibility of fibrous mixes are required to verify this assumption and to quantify an appropriate factor, however to illustrate the system optimization, a recommended design load for FRC slabs subjected to a concentrated load was desired. To this end, the following assumptions were made to set a hypothetical resistance factor, in order to proceed with the optimization. The material resistance factor for FRC concrete has been assumed to be 0.5.

First it was desirable to set a resistance factor for punching of FRC slabs that will account for two distinct variations; that of the material and that of the analytical technique used to predict the capacity. Expressed mathematically in terms of partial resistance factors, this can be represented as:

$$\phi_{FRC\ Punch} = \phi_{FRC} * \phi_{Punch} \quad (35)$$

The value of the partial resistance factor, ϕ_{Punch} , which represents variability inherent in the analysis to predict the ultimate punching load, was calculated based on a comparison of the results of analyses and the results of the experimental study that was carried out as a part of this work. This comparison, to be presented in more detail in Ch.6, shows that the mean of the ratio of the calculated punch load to that measured experimentally, is 0.88, i.e.:

$$\frac{P_{Analysis}}{P_{Experimental}} = 0.88 \quad (36)$$

If it is assumed that ϕ_{FRC} is 0.5, then:

$$\phi_{FRC\ Punch} = 0.5 \times 0.88 = 0.44. \quad (37)$$

For comparison, it is noted that the section of the OHBDC intended for

evaluating existing bridge structures, OHBDC, 1991, section 11, sets the material resistance factor for a concrete slab, ϕ_{md} , at 0.5. The requirements further specify that this material resistance factor be used to factor the resistance, i.e. $R_r = \phi_{md} R_n$, recognizing that the resistance factor is more conservative than the concrete resistance factor to be used for design of a new structure to ensure an adequate level of safety against a punching shear failure of the concrete slab.

The design load on which the system optimization will be developed can be represented in the following form:

$$\mathit{PunchingLoad}_{ULS} = \frac{\alpha_L * P_{wheel} * I}{\phi_{FRC\ Punch}} \quad (38)$$

This form incorporates terms from the ULS vehicle live load formulation of the CHBDC; α_L the live load factor, the maximum wheel load, P , and an allowance for dynamic effects, I .

Substituting the maximum ULS values from the code, as given in Table 3.2, the punching load can be expressed as:

$$\mathit{Punching\ Load}_{ULS} = \frac{1.75 \times 87.5 \text{ kN} \times 1.4}{\phi_{FRC\ Punch}} = \frac{214 \text{ kN}}{\phi_{FRC\ Punch}} \quad (39)$$

And, incorporating the assumed resistance factor to modify the FRC slab punching resistance, gives:

$$\mathit{Punching\ Load}_{ULS} = \frac{214 \text{ kN}}{0.44} = 486 \text{ kN} \quad (40)$$

Based on the above, the optimization was progressed using 500 kN as a

reasonable definition of the minimum structural requirement for an externally restrained concrete bridge slab. While it is expected that further work to quantify the variation in the material and the analysis to predict the system behaviour will alter this formulation, the method to define the load is consistent with both the maximum highway loading and the probabilistic approach, resulting in a design load of the correct order of magnitude.

3.2.1.2 Serviceability Considerations

Two serviceability concerns were examined as part of the process to establish the design load appropriate for slab punching; slab deflection and fatigue. This was necessary to ensure that an externally reinforced slab designed at ultimate for 500 kN would remain serviceable under working loads. The following discussion will show the effect of applying the current code deflection limits to an externally reinforced bridge slab. Additionally, a brief review will be included of current bridge code fatigue design requirements and their application to an externally reinforced FRC slab.

The bridge deflection limits imposed by the three Canadian codes are identical and relate to pedestrian comfort in response to vehicle-induced bridge vibrations. The bridge codes define the maximum acceptable static deflection for only the main longitudinal components when subjected to the factored serviceability load. This limit is expressed as a function of the level of pedestrian use and the natural frequency of that element. For a slab-on-girder bridge, the main longitudinal components to which the deflection limit applies are the composite girders. There is no explicit deflection limit for the concrete slab. For practical considerations, such as proper adherence and performance of the deck wearing surface and to prevent local ponding of water, slab deflections require examination for the externally restrained slab that is being studied.

Limitations on the live load deflection as a function of span, the form commonly adopted by building codes, are included in only one section of the CHBDC; that applicable to timber components. Here the maximum static deflection due to the serviceability limit state loading, without a dynamic load factor, is limited to 1 in 400 of the span.

Using an approach consistent with that described above for the ultimate design load, the service load appropriate for punching was established. Equations 41 and 42 illustrate the process:

$$\mathit{Punching\ Load}_{SLS} = \frac{0.9 \times 87.5 \text{ kN}}{\phi_{\text{Punch}}} = \frac{79 \text{ kN}}{\phi_{\text{Punch}}} \quad (41)$$

$$\mathit{Punching\ Load}_{SLS} = \frac{79 \text{ kN}}{0.88} = 90 \text{ kN} \quad (42)$$

Note that the resistance factor considered for the service load level differs from that used to express the ultimate load. Here, the material resistance factor, ϕ_{FRC} , was not been included in the definition of the serviceability load level, in order to be consistent with the existing Canadian limit state design philosophy for working load conditions. The factor of 0.88 has been included, however, to adjust the service load level to account for the variability between the punching behaviour predicted by analysis and that observed experimentally. On this basis, it was found that a service load of 90 kN would correspond to the 500 kN wheel load considered for the ultimate limit state.

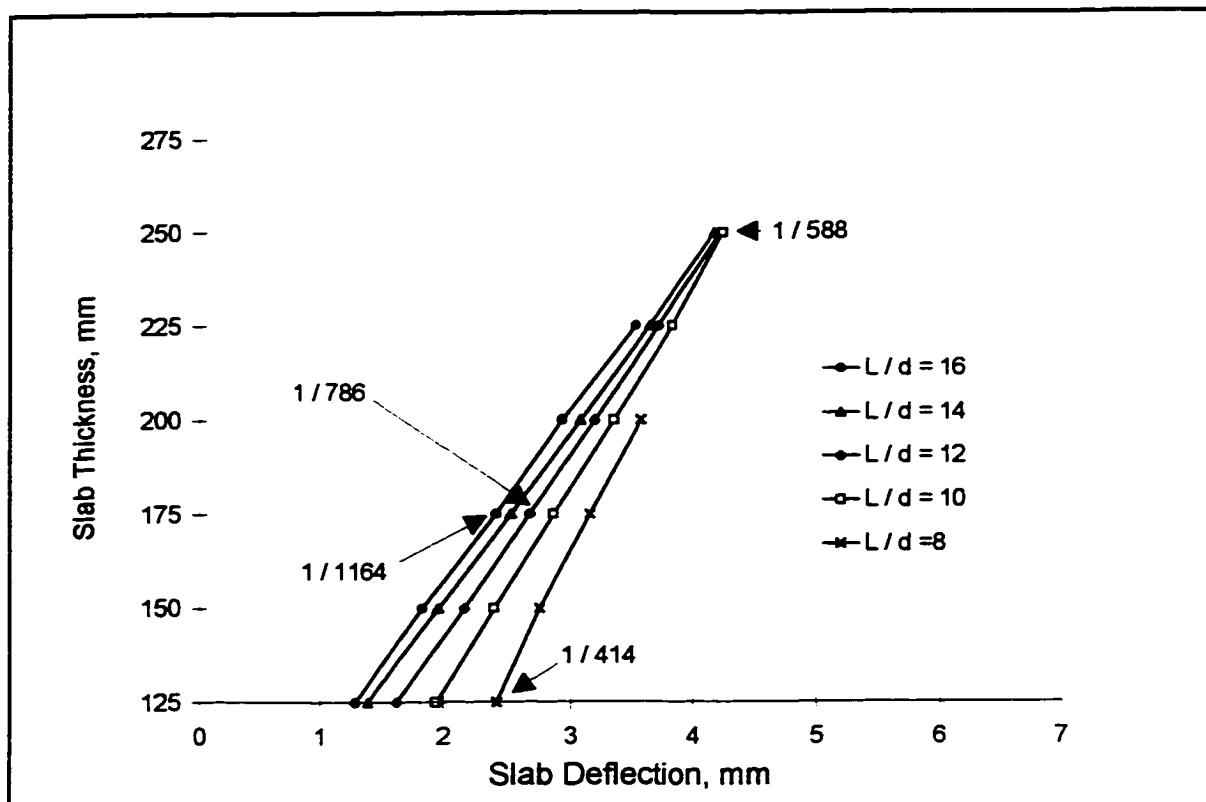


Figure 3.3: Maximum serviceability deflections for slabs designed for a punching capacity of 500 kN

For slabs configured for a 500 kN ultimate design load, i.e. slabs designed to fail by punching when subjected to a 500 kN load, analyses were performed to predict service load deflections. Using the analytical approach described in the last chapter, a parametric study was performed, considering slabs varying in thickness from 125 to 250 mm, with span-to-depth ratios between 8 and 16. The following figure plots the maximum predicted deflection calculated for the slabs when subjected to a 90 kN service load. Figure 3.3 shows that the maximum deflection of externally reinforced slabs that have been designed for a minimum restraint stiffness to provide an ultimate punching capacity of 500 kN, based on concrete having a 28 day strength of 30 MPa. From the graph it can be seen that, for the range considered, the maximum absolute slab deflection is 4.25 mm. Also given on the figure are three examples of the live load deflection as a

function of span. The maximum deflection rate is 1 in 414, shown for a 125 mm thick slab, with a span of 1000 mm, i.e. an L / d of 8. Also illustrated are the deflection rates of 1 in 786 and 1 in 1164, for 175 mm thick slabs having spans of 2100 mm and 2800 mm, respectively. Other rates for the various slab thicknesses and spans can readily be calculated from the information provided. The deflection rates vary from 1 in 414 to less than 1 in 1500, with the larger deflection rates typically occurring for the smaller span-to-depth ratios.

The results of this study of serviceability deflections shows that the deflections will not impose limitations over and above the ultimate strength requirements for the system. In other words, a slab designed for an ultimate capacity of 500 kN can be expected to deflect minimally under service load conditions. These service load deflections are less than 1 in 400, which is considered to be a reasonable practical limit for serviceability concerns.

It should be noted that, for the analyses represented by the above graph, the minimum external restraint stiffness necessary to give an ultimate punching capacity of 500 kN has been used. This explains the apparent anomaly that the deflection increases with decreasing span to depth ratios. Had the restraint stiffness been maintained constant, the deflection would decrease with decreasing span to depth ratios, as expected. Of course, serviceability deflections calculated for systems having equal stiffness could not form the basis of a relevant comparison, as the ultimate capacities would not be the same. An example of the deflections and the expected ultimate punching capacities that can be expected if the restraint stiffness is kept constant (at 149 MPa) is given in Table 3.4 which follows. This information shows that for decreasing span-to-depth ratios, if one kept the external restraint stiffness constant, the ultimate capacity tends to increase and the central deflection decreases.

Table 3.4: Serviceability deflections and ultimate capacities for 175 mm slabs, maintaining a constant external restraint stiffness

L / d ratio	Span, m	Deflection, mm	Ultimate Load, kN
16	3.20	3.65	448
14	2.80	3.07	500
12	2.40	2.51	574
10	2.00	1.97	688
8	1.60	1.43	887

The current study addresses the static load capacity of an externally reinforced system, however, some comments on fatigue are considered necessary in the context of establishing the design load requirements. Table 3.5 summarizes the fatigue design criteria given in the three Canadian bridge codes. These criteria apply directly to issues of fatigue in structural steel, aluminum and steel reinforcing. The provisions for the CHBDC are based on satisfactory performance under two million cycles of the specified FLS design load. Although the CHBDC code does not impose fatigue restrictions directly to concrete structures, it does prescribe a limiting stress of 125 MPa for reinforcing steel at load levels appropriate for fatigue. Of course, this requirement will also provide an indirect control on the maximum stress level in the concrete. At load levels required to stress the steel reinforcing to 125 MPa, concrete adjacent to the bars would typically be subjected to tension cracks. Nonetheless, the imposed limit on the steel reinforcing is an indirect control on the level of acceptable cracking.

Comparing the design wheel load of 126 kN to be considered for fatigue to the design wheel load of 214 kN specified for the ultimate limit state, it is seen that fatigue concerns deal with a much lower magnitude loading; one that is expected to have a much higher frequency of occurrence during the design life of the structure.

Table 3.5: Fatigue Limit State wheel loads

CODE	OHBDC	CSA-S6	CHBDC
Max'm wheel load P	100 kN	90 kN*	87.5 kN*
Max'm load factor α_L	0.8	0.9	0.9
Max'm impact factor I	1.40	1.40	1.60
FLS design load $= P \times \alpha_L \times I$	112 kN	113 kN	126 kN

Experimental work to assess the fatigue resistance of a steel free deck under rolling wheel loads has been reported elsewhere, Bakht and Selvadurai, 1996. Testing undertaken by these authors confirmed that an externally reinforced FRC slab performed favourably when subjected to 16 million cycles of a 98 kN rolling load. Cracking was observed during this series of tests, but the authors report that the crack growth was stable and that the same slab's static performance subsequent to the cyclic loading exceeded the bridge code requirements.

Although beyond the scope of the current study, it is worth mentioning that if a steel free deck with external reinforcement is to be considered for regions of longitudinal negative bending, the fatigue characteristics of the strap attachment detail will become important. In such areas the top flange of the girder is loaded in tension and the detail of attaching the external restraint to the longitudinal girder may alter the fatigue life of the girder. In the current study steel flat bars were fillet welded to the girder top flange. The CHBDC fatigue design criteria precludes the use of plates attached to girder flanges using only fillet welds that are transversely located. Using longitudinal fillet welds has the potential to reduce the fatigue design category to a category E. For composite girders, having welded shear studs, the top flange would be classified as a category C. Degrading the fatigue design category from C to E reduces the fatigue resistance from 34.5 MPa to 15.5 MPa at this location. To satisfy the fatigue design requirements, this fatigue resistance must exceed the 56% of the stress calculated in the girder flange using the design fatigue load. (The factor 0.56 represents the difference between the code "design" truck and the trucks that are expected to occur with sufficient regularity to cause fatigue damage.) On this basis, the attachment detail will be significant when the top flange is subjected to longitudinal tensile bending stresses. One alternative to the welded flat bars would be to bolt the flat bar to the girder flange. A bolted detail would be classified as a Category B detail for fatigue, which represents an improved fatigue behaviour as compared to a welded stud connector, which, as discussed above, is classified as a category C detail. Further examination of restraint attachment details and the fatigue consequences has been made elsewhere, [Bakht et al., (1996)].

3.2.2 External Restraint Requirements

The variation of the ultimate load capacity of a restrained FRC bridge deck as a function of the lateral stiffness of the external steel restraint is shown in Figure 3.4. This graph shows that the calculated punching load, based on the refined rigid body model, increases as the stiffness of the external restraint is increased. This means that an increased deck capacity can be realized by providing a stiffer transverse restraint below the concrete slab. The increase in ultimate load is very rapid for low values of restraint, but the rate of increase decreases appreciably as the restraint stiffness is increased. Beyond a strap stiffness in the range of 1500 MPa, a very large increase in restraint stiffness must be provided to realize a significant increase in the ultimate capacity of the slab. The figure also illustrates that for punching loads less than about 1000 kN a change in the compressive strength of the concrete does not significantly influence the restraint stiffness requirement.

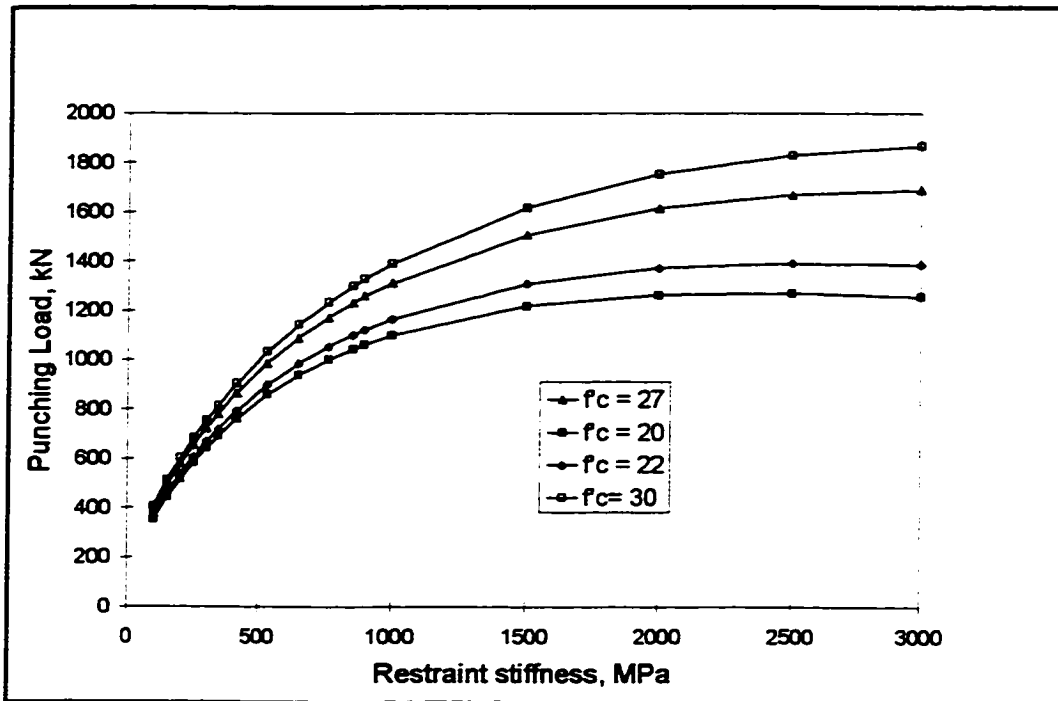


Figure 3.4: Influence of restraint stiffness on the calculated ultimate load

Using the analytical model that has been presented in Ch. 2, parametric studies were undertaken to study the external restraint requirements. A parametric study was performed to investigate the restraint stiffness requirement to cause slab punching failure at a load of 500 kN. For slab thicknesses between 150 and 250 mm the restraint stiffness required to cause punching for increasing girder spacing is shown in Fig. 3.5.

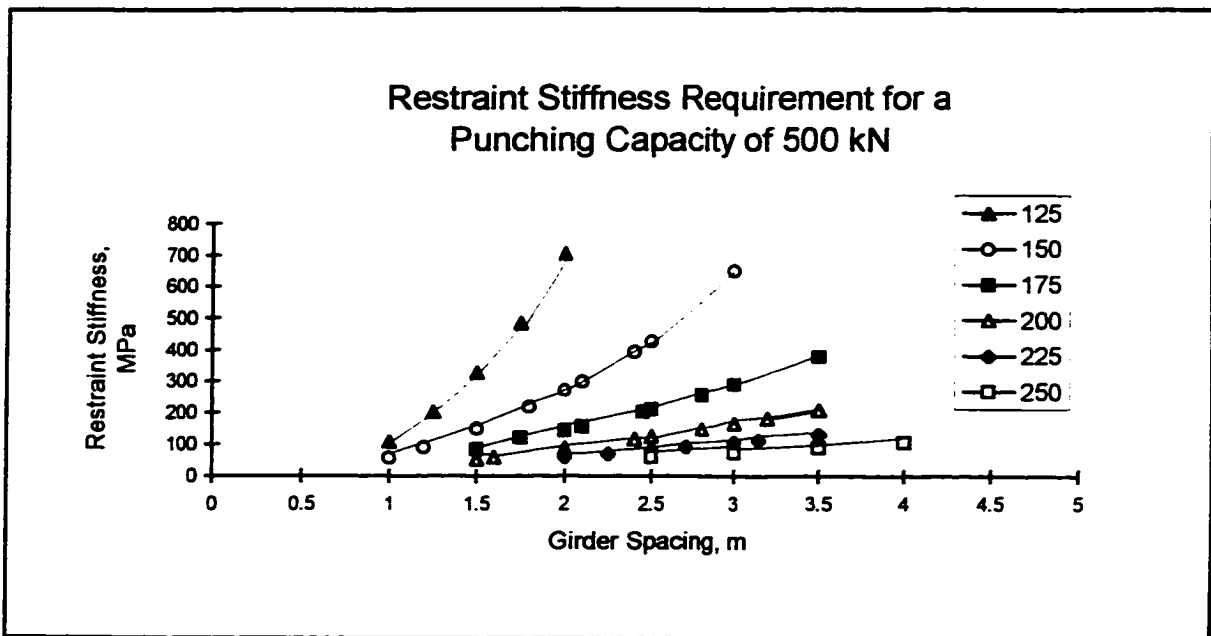


Figure 3.5: Minimum restraint requirements for a 500 kN ultimate capacity

As discussed above, an externally reinforced slab that is designed for satisfactory performance at the overload condition will perform adequately at service load levels.

3.2.3 Procedure to Establish a Minimum Weight System

To illustrate how such information could be utilized in design, the following design sequence is offered:

1. Establish "design load" requirement; e.g. 500 kN
2. Establish economical girder spacing considering functional width requirements for the structure. The practical range of girder spacings is not large; between 2 m and 4 m spacing are usually the most economical, [Ritchie et al., (1991)].

3. **Select minimum slab design thickness based on a maximum slab span to depth ratio of 16. (For girder spacing between 2000 and 4000 mm and a maximum L / d ratio of 16, the minimum slab thickness would be 125 mm and the maximum would be 250 mm.)**

4. **Use a figure such as Figure 3.5, for $P = 500$ kN, to establish the minimum restraint stiffness requirement. It is noted that this figure will provide the minimum "system" restraint requirements and the designer must evaluate the system restraint considering the size and spacing of external restraints, as well as the lateral restraint provided by the composite steel girder and the surrounding concrete. It would be conservative in all cases to size the external restraints to provide the total stiffness as determined from Fig. 3.5. The total system restraint may be quantified, for example, by considering an analogous continuous beam supported on springs, having stiffness derived from the axial stiffness of the external restraints. This concept was introduced in Ch. 2 and will be discussed further in relation to the experimental model in Ch.6.**

6. **Recommend an area and spacing of external restraint based on the restraint stiffness requirement established above, considering the external restraint stiffness as a component of the overall system restraint.**

Consider a slab system for which it has been determined that the optimum longitudinal girder spacing is 2 m. If a slab thickness of 175 mm is desired, using Fig. 3.5 one could determine that the restraint stiffness required to cause a

punching capacity of 500 kN is 145 MPa. Rearranging Eqn. 2 in terms of the restraint area:

$$A_s = \frac{k_s * S_s * 0.5 S_g}{E_s} \quad (43)$$

With a strap spacing of 1000 mm and Young's Modulus of steel taken as 200 000 MPa, the required steel area is calculated:

$$A_s = \frac{145 \text{ MPa} * 1000 \text{ mm} * 0.5 * 2000 \text{ mm}}{200000 \text{ MPa}} = 725 \text{ mm}^2 \quad (44)$$

A further reduction in the required steel area can be achieved if one considers the lateral restraint offered by the girder lateral bending stiffness. For example, if the superstructure being designed has steel composite longitudinal girders, having a lateral bending inertia of $185.2 \times 10^6 \text{ mm}^4$, and the girders span 12 m between very stiff end transverse diaphragms, the required strap area reduces to 250 mm².

3.3 System Cost Considerations

Two features were considered worthy of attention at the outset of the optimization procedure: system cost and system weight. The issue of weight has been addressed in the above discussion which focused on maximizing the span depth to thickness ratio while minimizing the size of the external restraint required to ensure development of an internal arching mechanism. In the context of a slab system for which the external restraint requirements have been

established, system costs will next be examined to compare the externally reinforced slab to a conventionally reinforced system. Material costs, construction costs, and life cycle costs will be discussed for each of the two systems. The comparison will be limited to a qualitative assessment, as there can be expected to be significant subjective variations in costs due to such influences as regional transportation and labour costs and variations in fabricator's equipment and construction practices. The material and construction cost estimates were developed using information provided by a steel fabrication company located in Dartmouth, Nova Scotia, having experience in the industry, [Pook, (1997)]. Also, it is assumed that costs associated with the design, construction and maintenance of the deck supporting members and the substructure of the bridge remains unchanged and it is only the bridge deck slab and its reinforcing that will differ between the two systems.

The basis of the cost comparison provided in the following sections is a composite slab-on-girder bridge system using an FRC externally reinforced deck slab, for which the required external restraint was determined in the previous section. This FRC system is compared to a conventional bridge slab having internal steel reinforcing. The latter has been designed empirically to the OHBDC utilizing two orthogonal meshes of steel reinforcing in each direction; with a reinforcing ratio of each mesh of 0.3%, for a total of 1.2% internal steel reinforcing.

The parameters for each of the two structural systems are summarized in Table 3.6.

Table 3.6: Structural parameters for the two systems on which the cost comparison is based

Item	Conventional slab	Externally reinforced FRC slab
Longitudinal girder spacing	2000 mm	2000 mm
Slab thickness	225 mm	175 mm
Concrete		
Type	plain	FRC @ 0.8%
28 day strength	30 MPa	30 MPa
Slab reinforcing	4 layers 0.3% isotropic steel rebar	external restraints spaced at 1000 mm c/c

Costs will be compared in the sections which follow for an interior slab section, typical of that spanning between two longitudinal girders, and will be presented as unit costs per meter length of deck. It is to be noted that the externally restrained system as studied in this work is not considered suitable for slab overhangs which commonly protrude beyond the exterior longitudinal girder on a conventional slab-on-girder superstructure. Slabs in the overhanging region develop negative bending, typified by compression stresses on the slab bottom surface and tension in its top surface, for which the externally reinforced system

is of no benefit. As such, the costs that are presented do not address the overhang portion of the superstructure, and it should be recognized that the costs differences for an entire superstructure would be calculated based on the number of girders in a given system.

3.3.1 Material Costs

A summary of the material costs associated with the externally reinforced FRC bridge slab and those of a conventionally reinforced slab are presented in Table 3.7. Based only on material costs, this comparison shows the FRC system to have a slight cost advantage, (-8.2% per meter), over the conventional deck.

Table 3.7: Material cost comparison (\$ / m length)

Item	Conventional slab	Externally reinforced FRC slab
30 MPa concrete	55.80	43.40
Internal steel reinforcing	44.00	Nil
External steel reinforcing	Nil	16.50
Polypropylene fibres	Nil	44.00
Superplasticizer	Nil	6.00
Deck waterproofing	20.00	Nil
Total	119.80	109.90

3.3.2 Construction Costs

Estimated construction costs are itemized for the two systems in Table 3.8, which shows the increased construction costs that can be expected for the externally reinforced FRC system. Here it is shown that the construction cost penalty for using the FRC option is \$106.00 per meter, i.e. an 88% increase in construction costs. As the comparison shows, this increase is mainly due to the costs of fitting the external restraint. It is noted that the information provided here is for a field welded restraint and alternative means of restraint and connections are being investigated elsewhere to reduce the associated construction cost disadvantage [Bakht et al., (1996)].

Table 3.8: Construction cost comparison (\$ / m length)

Item	Conventional slab	FRC slab
external restraint		
fitting flat bar	Nil	35.00
field welding	Nil	105.00
concrete		
formwork	52.50	63.00
placing internal reinforcing	8.75	Nil
placing and finishing	22.50	22.50
finishing		
installation of waterproofing system	36.00	Nil
Total	119.75	225.50

3.3.3 Life Cycle Costs

For the externally reinforced system the through life repair and maintenance costs are predicted to be much reduced due to the elimination of the internal steel reinforcing bars from the concrete slab and the resultant increase in concrete durability.

A report investigating the life cycle costs of a conventional reinforced concrete deck for comparison with costs of alternative materials, [Ehlen and Marshall, (1996)], reports that an exposed, unreinforced slab can be expected to experience a maintenance-free life of the slab to 28 years. The authors also quantify, based on a 40 year design life, that the projected cost of operation, maintenance and repair for the steel reinforced deck is \$74 per meter. Experience gained from deck rehabilitation projects have shown that after removal of a badly deteriorated concrete bridge deck, the steel support structure can be expected to be in good condition, [Dubas, (1991)]. For the externally reinforced alternative, the only remaining significant maintenance requirement is that of maintaining the external steel restraint. And, as it is common in Canadian bridge design practice to specify a weathering grade of structural steel, often in conjunction with an auxiliary paint protection layer, these maintenance costs are expected to be minimal.

A summary of the total life cycle costs for the conventional system and the externally reinforced FRC slab are given in Table 3.9. The comparison shows that the life cycle costs for the two systems are comparable, with a nominal increase, (7% or \$21.85 per meter), for the FRC system.

Table 3.9: Life cycle cost summary (\$ / m length)

Deck Type	Material Costs	Construction Costs	Maintenance Costs	Life Cycle Costs
Conventional	119.80	119.75	74.00	313.55
Externally Reinforced	109.90	225.50	Nil	335.40

4.0 DESIGN DETAILS OF FULL-SCALE TEST BRIDGE

4.1 General

The prototype bridge form chosen for experimental investigation was a short span highway bridge framed longitudinally with composite steel girders. The experimental section consisted of a typical two-girder interior longitudinal slice of the prototype structure. A 175 mm thick cast-in-place concrete deck is supported on W610x240, G40.21 300W steel girders spaced 2000 mm centre-to-centre, as represented in Figures 4.1 and 4.2. The span-to-depth ratio for the slab is 11.4, within the range of 10 to 16 typically used for composite steel girder bridges.

4.2 Design of Full-Scale FRC Bridge

4.2.1 Steel Girders

The slab test loadings were the governing design load for the steel girders of the test bridge. A W610 x 241 girder was selected to ensure that the maximum stress that the girder would experience during the testing program would be less than the steel yield stress. The structure was also validated for the design loadings prescribed by the Ontario Highway Bridge Design Code, OHBDC, 1991. The structural capacity of the test bridge at the ultimate, fatigue and serviceability limits states was adequate for the OHBDC requirements. (For comparison, it is noted that a W610 x 140 girder would fully satisfy the design requirements of the OHBDC, but the loads applied during the experimental program would have resulted in flange stresses exceeding the material yield

stress.) Use of a fabricated steel girder was also investigated. A singly symmetric fabricated I-section had a potential weight saving in the order of 32%, however high fabrication costs precluded use of such a girder for the small quantities required for the experimental program.

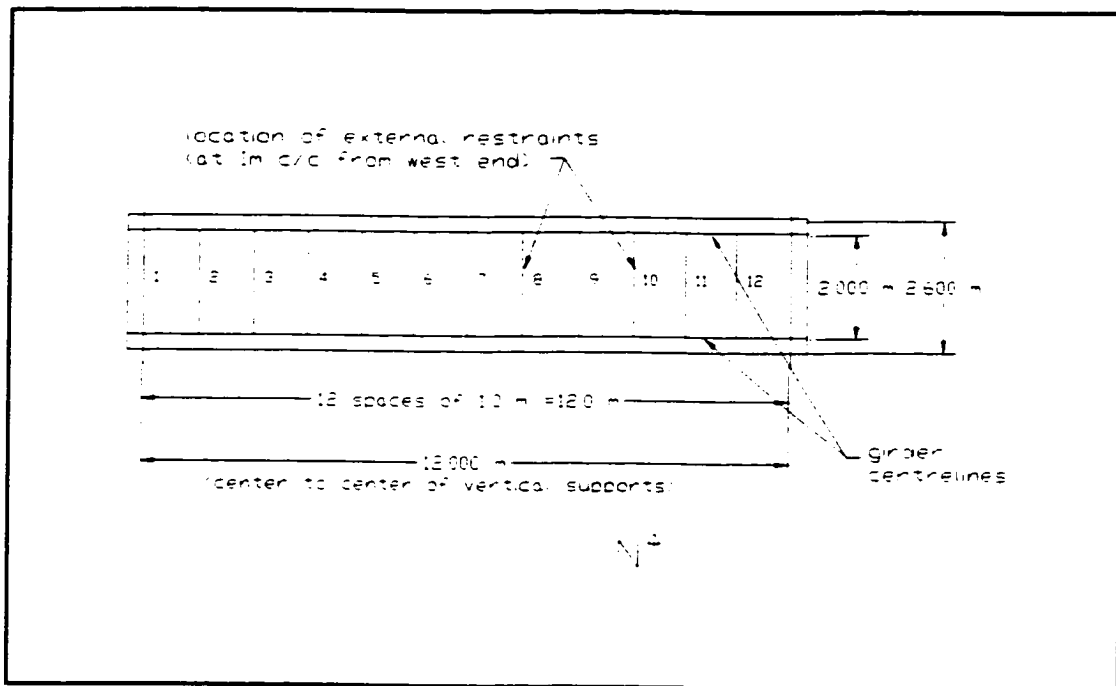


Figure 4.1: Plan view showing layout of experimental bridge structure

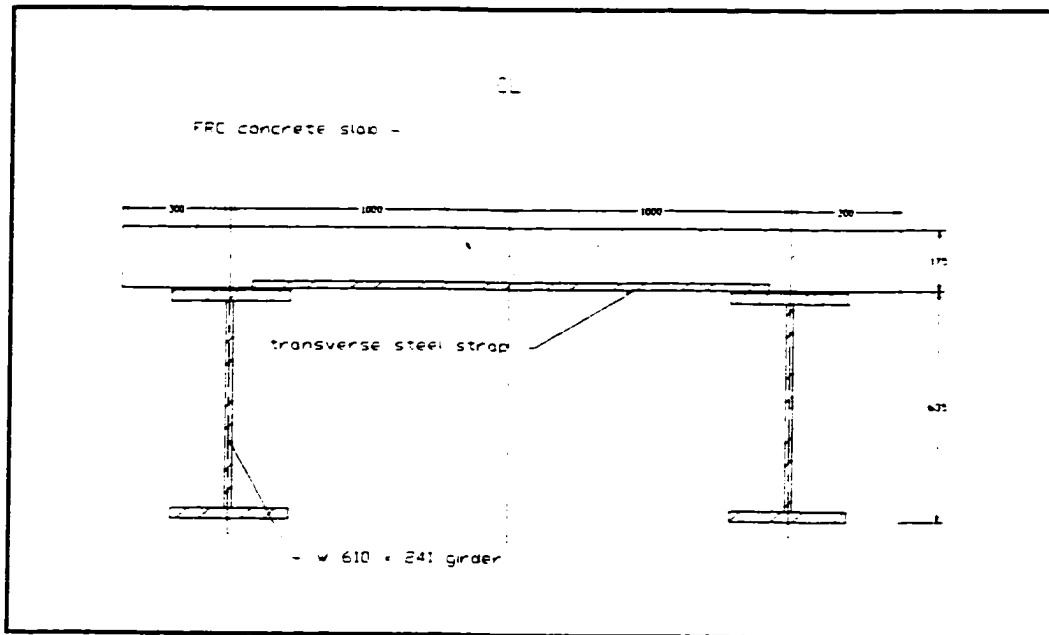


Figure 4.2: Typical section of experimental bridge

The steel girder spans 12 m, for a span-to-depth ratio of 20, which is at the lower end of the practical range; the practical upper limit for span-to-depth being in the order of 27. Shear connection between the steel and concrete was ensured through the use of stud-type steel shear connectors. The studs were 22 mm in diameter and were welded in groups of three to the top flange of the girder at 300 mm centres along the length.

4.2.2 Slab External Reinforcing

The 175 mm deck slab spanning 2000 mm between the steel girders is expected to resist the applied concentrated loads through arching action. Resistance to the horizontal thrust generated by the arching in the concrete was provided

A fatigue analysis of the connection of the transverse steel strap to the underside of the flange of the longitudinal girder was not warranted for the current study. The system studied herein is a single span composite bridge and, as such, the girder top flange would be subjected only to longitudinal compressive stress; not a fatigue-critical detail. Before the concept is expanded to a multi-span steel girder further study will be required.

Research is progressing with other configurations of external restraint and varying attachment details, [Bakht and Selvadurai, (1996)].

4.2.3 Concrete Deck Slab

4.2.3.1 Description of the FRC

"Conventional" 34.4 MPa concrete was specified for construction of the cast-in-place deck slab for the test bridge. In this context "conventional" is used to describe concrete that was ordered from a local ready-mix concrete supplier, who was asked to supply normal strength concrete to the specification given in Table 4.2.

Table 4.2: Concrete specification

Compressive strength	34.5 MPa
Maximum aggregate size	19 mm
Slump	50 to 75 mm
Air Content	0.06

Responsibility for the concrete mix design was deliberately left with the ready-mix supplier, to represent as closely as possible usual bridge construction practice. It was felt that any additional steps taken in the laboratory to control the concrete mix or quality would make the structural system being validated unduly restrictive. Indeed, as will be discussed more fully in Section 6, the inclusion of the high concentration of polypropylene fibres in the concrete mix did result in some deleterious effects, from the point of view of the material alone. However these material concerns did not impose limits on the capacity of the structural system under investigation. And, the focus of the current study was not the material performance of the FRC, rather the emphasis was on the structural behaviour and capacity performance of the system overall.

The deck so-constructed was used for the first two series of tests for the experimental phase. The third series of tests was performed on deck sections that had been repaired using a high early strength concrete mix. The concrete mix design was that of a local ready-mix supplier and was the same mix design employed for previous scale tests, [Wegner, (1993)]. The two mix designs are presented below in Table 4.3.

Table 4.3: Concrete mix designs

Component	Normal Strength Concrete	High Early Strength Concrete
Type 10 Portland cement	398 kg / m ³	Nil
Type 30 Portland cement	Nil	398 kg / m ³
Fine Aggregate	718 kg / m ³	718 kg / m ³
Coarse Aggregate	1032 kg / m ³	1032 kg / m ³
Water	155 kg / m ³	155 kg / m ³
Air Entraining agent	112 L / m ³	112 L / m ³
Water Reducer	1 L / m ³	1 L / m ³
Superplasticizer	5 L / m ³	7.8 L / m ³
Polypropylene Fibres	7.6 kg / m ³	7.6 kg / m ³

The concrete structures section, section 8 of the CHBDC, [CSA, (1994)], specifies a minimum concrete 28 day compressive strength as a function of the expected exposure conditions of the structure. The strength requirements vary from 30 to 45 MPa. This requirement expands on the current Canadian bridge code requirements which limit the 28 day strength of structural concrete to 30 MPa and has been included in the code to improve the bridge durability, recognizing that concrete durability increases as the strength increases. It is worthy of mention that the high quality of deck concrete that is typically specified is needed to achieve durability and usually results in much higher strength

concrete than is needed for the structural capacity of the deck.

Polypropylene fibres were the sole means of reinforcing the 175 mm deck internally. These fibres were 38 mm long fibrillated polypropylene, and were added to the ready-mixed concrete in the ratio of 0.834% by volume, or 0.34% by weight. Workability of the concrete mix was achieved through the addition of sufficient superplasticizer to give a slump of 75 mm. The polypropylene fibres were intended to provide crack control only, while the external reinforcing provided the restraint required to develop arching forces in the concrete. In comparison, for conventionally reinforced bridge decks, the codes limit the minimum slab reinforcement ratio to 0.002, to control shrinkage and temperature cracks. This is a serviceability rather than a strength requirement. Generally, reinforced concrete bridge slabs are designed to crack at service load levels, i.e. cracking is not considered a limiting state for deck behaviour.

The FORTA fibres were added directly to the ready-mixed concrete in the drum of the agitator truck. The fibre volume of 0.834% is approximately 8 times higher than the industry standard application rate of 0.1% by weight. The fibre volume of 0.84% by volume was maintained from the half-scale bridge slab tests performed at TUNS. This fibre volume was based on the results of a study of the fracture toughness of various fibrous concrete mixes, [Carmichael, (1993)]. This work established that the post-cracking resistance of polypropylene reinforced concrete of a 1.0% mix exceeded that of a 0.5% or a 2% mix.

4.2.3.2 Material Testing

As a check of the concrete quality as-supplied, limited material tests for

workability and strength were performed on the concrete as delivered by the local ready-mix concrete supplier. the concrete slump was measured and cylinders were prepared for testing the compressive strength. After the addition of the polypropylene fibres and the superplasticizer in the laboratory, the slump test was repeated and additional cylinders were prepared for compression testing of the fibrous concrete. Compressive strength of the plain concrete mix and the fibrous concrete mix were determined by means of standard tests for compressive strength, CSA Standard A23.2-9C, [CSA , (1994)]. An additional air content analysis was performed on samples of the freshly mixed fibrous concrete by the pressure method, as prescribed by CSA Standard A23.2-4C, [CSA, (1994)]. The results of the material testing is presented in Ch. 5.

An air content analysis was performed on samples of both the plain concrete and the fibrous concrete to ASTM C 457-82a: Standard Practice for Microscopical Determination of Air-Void Content and Parameters of the Air-Void System in Hardened Concrete, [ASTM, (1993)].

4.2.4 Cross Bracing

Cross frames were provided at the ends and at midspan of the test bridge, as illustrated in Figures 4.3 and 4.4. These cross frames were designed to resist the service wind loading which would occur normal to the length of the bridge. Construction wind loads (1 in 10 year return) and in-service wind loads (1 in 50 year return) were considered. Additionally, the end cross frames were detailed to accept a typical bridge expansion joint, and were designed compositely with the slab to withstand wheel loads that would occur in service, because of this detailing.

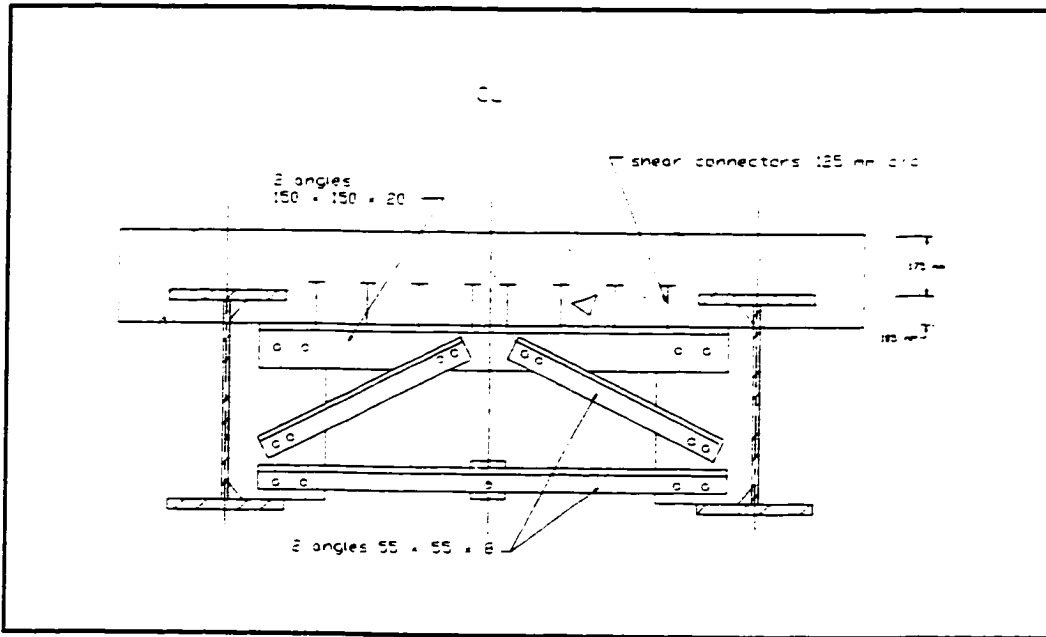


Figure 4.3: Layout of transverse diaphragm typical at the vertical supports

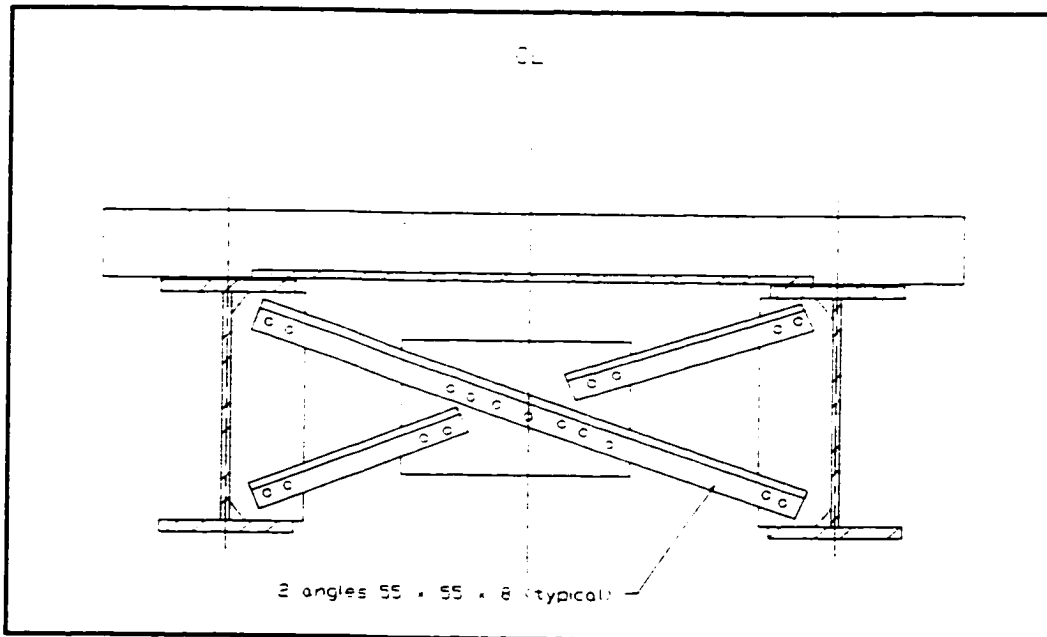


Figure 4.4: Details of the transverse diaphragm located at center span

These intermediate diaphragms aid in the transverse distribution of load between the longitudinal bending member, i.e. the composite steel girders. The support diaphragms have been included in the test bridge in order that the experimental structural form deviate as little as possible from slab-on-girder bridges in practice. The support diaphragms in practical bridge designs provide stability to the steel girder system during erection, form part of a system of horizontal wind bracing, local transfer of vehicle loads from the deck expansion joint to the girder and, ultimately to the support. Additionally, the diaphragm stabilizes the slender web of the steel girder at the support. The overall distribution characteristics of the bridge are not influenced by these end diaphragms, [Jaeger et al., (1989)].

4.3 Construction of Experimental Bridge

4.3.1 Summary of Deck Placing for Full-scale Deck

A description of the construction of the fibrous concrete slab in the formwork atop the steel framework of longitudinal girders and transverse steel straps is provided below.

A volume of 6.12 m³ of concrete, to the specification provided in Table 4.2, was delivered to the laboratory in rotary drum concrete mixing truck. The concrete, as-delivered was normal strength concrete, batched at the ready-mix plant using the supplier's mix design that was provided in Table 4.3. The drum had a

capacity of 6.88 m³ and was approximately 90% full before the addition of the fibres and the superplasticizer.

After testing of the plain concrete, fibre reinforced concrete was produced by the addition of superplasticizer and polypropylene fibres directly into a hopper that fed the rotary drum of the concrete mixer. The superplasticizer was added to the mix in two stages: before and after the addition of the fibres. Fifteen liters of superplasticizer were added to the concrete in the mixer before any fibres were added, (or 2.45 L/m³ of concrete). The polypropylene fibres were then added to the mix, also directly into the hopper of the rotary drum. A total of 64 bags of polypropylene fibres were added; i.e. 46.4 kg of fibre giving a fibre volume of 0.32% by weight or 0.834% by volume. After the fibre addition, an additional 16 liters of superplasticizer, (or 2.55 L/m³ of concrete), were added to the fibrous concrete in the mixer to achieve the required workability for concrete placing. The concrete was mixed approximately 15-20 min. in the drum of the rotary mixer before material testing of the fibrous concrete commenced. In total, 31 liters of superplasticizer, tradename Rheobuild 1000, (5.0 L/m³ of concrete) and 7.6 kg / m³ of polypropylene fibres were added.

A 0.573 cu m. bucket was used to move the concrete from the drum to the slab formwork. A flexible shaft vibrator was used internally to consolidate the concrete in the deck form. The deck was hand finished and floated initially. Placing of the deck concrete took approximately 1 1/2 hrs. Upon completion of this phase of construction, air bubbles were obvious on the surface of the fresh concrete at the east end of the deck and near the middle of the deck.

After several hours of partial curing, the deck surface was finished by a power

float. The deck was then moist cured under plastic for 14 days.

4.3.2 Placement of Repair Concrete

A similar fibrous concrete mix was used to make repairs to the slab in two regions that had been punched through during the first series of tests. The concrete for this repair was prepared in the same way as was the concrete for the original deck. The mix was obtained from a ready-mix plant and was delivered to the laboratory in a rotary drum concrete mixer, where superplasticizer and polypropylene fibres were added. The concrete was batched at the read-mix plant, using the high early strength design of Table 4.3. The primary difference between this mix and the original mix was the substitution of Type 30 Portland cement for the type 10 of the earlier mix. An enhanced hydration rate was desirable for the repair concrete to provide a higher compressive strength in less time for two reasons. First, the high early strength mix would allow testing of the repaired deck to begin in a reduced time and secondly, in practice it would be desirable to shorten the time between such a repair to a deteriorated bridge slab and the reintroduction of traffic to the structure.

Referring to Table 4.3, it is seen that slightly more superplasticizer was used to achieve the desired workability for the high early strength concrete; $7.8 \text{ L} / \text{m}^3$, as opposed to $5 \text{ L} / \text{m}^3$ used for the normal strength mix.

The repair required only 0.76 m^3 of concrete, but it was delivered in a standard 6.8 m^3 mixer. A flexible shaft vibrator was used internally to consolidate the concrete in the deck form, ensuring that the fluid concrete was exposed to all

surfaces of the hardened concrete that surrounded the punched out area that was being repaired. The deck was then hand finished and floated. Repairing the deck took approximately 1 1/2 hrs. After partial curing, the deck surfacepatches were finished by a power float. Initial curing included moist curing under plastic a plastic sheet for 14 days. Retesting of the repaired areas proceeded 16 days after casting. Seven day compression testing of the high early strength mix showed the strength to exceed that specified for the repair.

4.4 Description of Experimental Program

4.4.1 Loading Arrangement

The experimental program was carried out in the Structures Laboratory of the Technical University of Nova Scotia. A photograph of a typical loading arrangement is included as Figure 4.5. For each test a concentrated load was applied to the slab using a single acting hydraulic jack reacting through a steel loading frame which was attached to the universal testing floor of the laboratory. This load was applied to the top surface of the concrete slab through a 500 x 250 mm steel plate, having a minimum thickness of 50 mm, atop a 6 mm rubber pad. The concentrated load simulated the dual tire footprint of a heavy highway vehicle. The loads were applied centrally to the deck slab between the longitudinal girders. The sequence and location of the tests is represented in Figure 4.6.

The steel loading frame consisted of two horizontal beams, W610x241's, that were interconnected at midspan such that each beam resisted one half of the

total applied load. These beams were end supported by four vertical W460 x 82 steel sections. The beam-to-column connections were bolted double angle web connections, designed to transfer the beam shear to the column. The columns were connected through the laboratory strong floor using four anchor bolts.

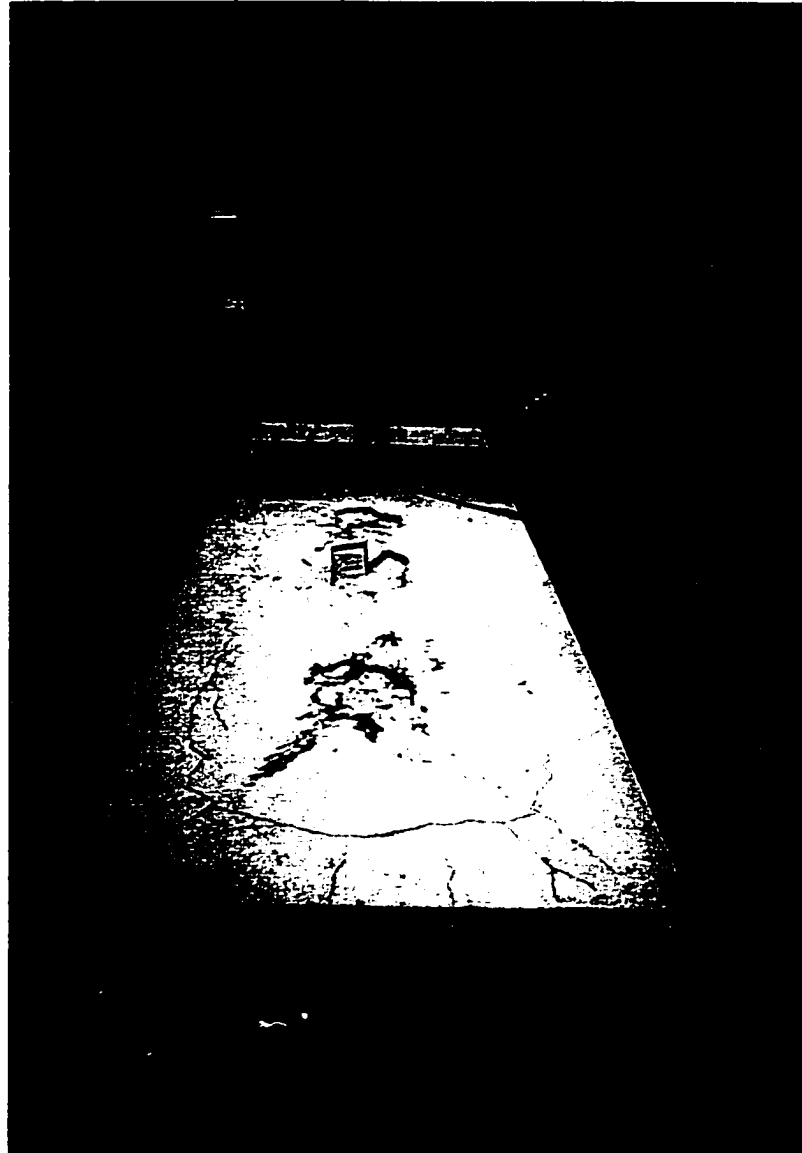


Figure 4.5: Photograph of testing arrangement

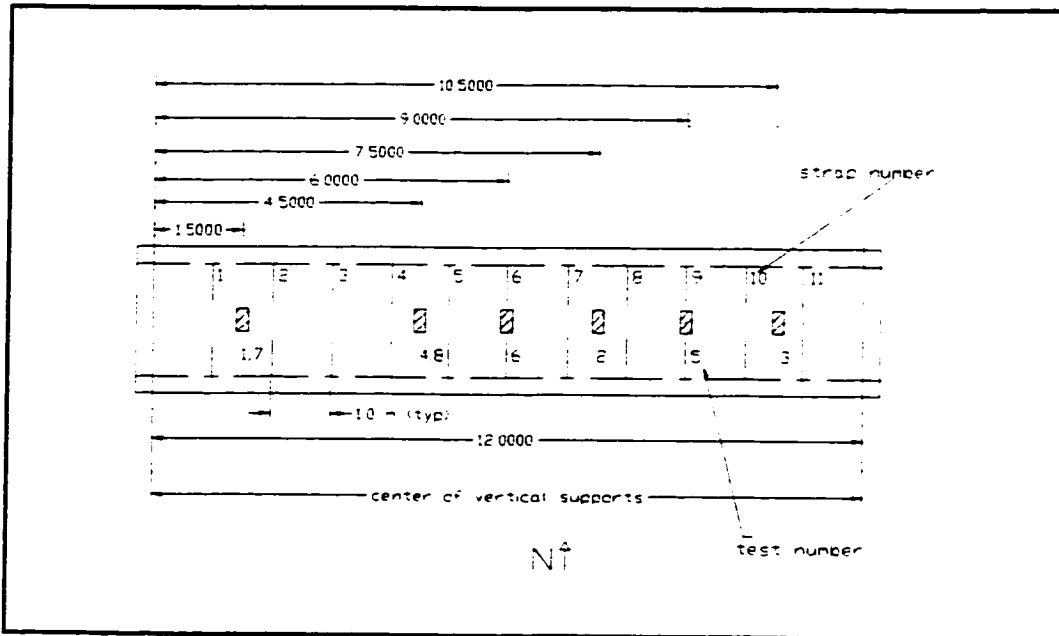


Figure 4.6: Plan of deck showing test locations

The hydraulic cylinders were controlled by a hand pump, monitored visually through a pressure dial gauge. This pump and gauge can be seen in Figure 4.7.

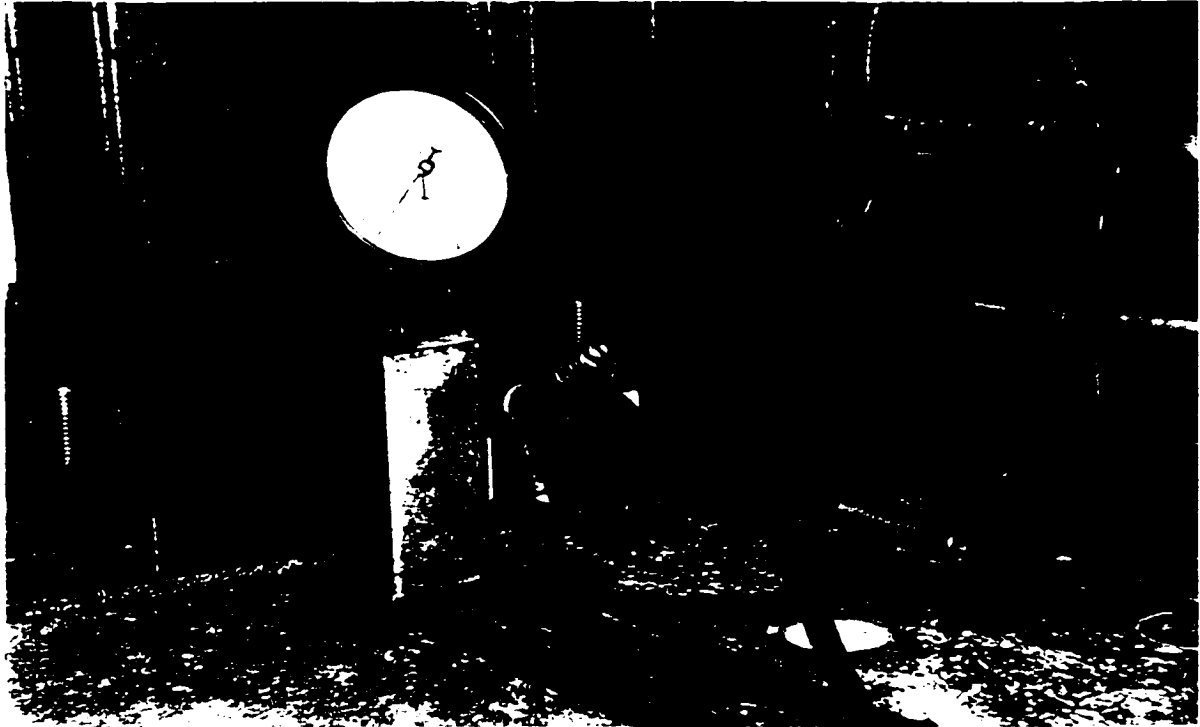


Figure 4.7: Photograph of load application set up

The arrangement of hydraulic cylinder, hand pump and pressure gauge was calibrated in a universal testing machine prior to the actual structural testing.

Deflections were monitored at each test load using a series of independently supported dial gauges mounted on an axis transverse to the deck, through the load point. The dial gauge layout is shown in the photograph included as Figure 4.8. These dial gauges could be read to an accuracy of 0.01 mm.



Figure 4.8: Photograph of deflection dial gauge layout

Strain gauges were mounted on the transverse steel straps. These gauges were electrical resistance gauges mounted normal to the member axis. All straps had gauges at the bottom extreme fibre and half of the straps also had gauges at mid-thickness. These additional gauges were used to establish the stress distribution through the depth of the strap; a constant stress would verify the assumption of axial stress in the strap. At each load step the strap strains were monitored.

The developing concrete crack pattern was also recorded as the magnitude of the concentrated load was increased. A typical pattern of cracking will be presented and discussed in a later chapter.

4.4.2 Experimental Procedure

Three series of destructive tests were performed on the full-scale structural model. Each series of tests consisted of the application of a single concentrated load applied centrally to the concrete slab between the longitudinal girders. An increasing load was applied to the deck in increments of approximately 8 kN. Constant pressure was maintained at each load step and the load was increased uniformly between these steps to simulate a static load with increasing magnitude. The load was increased until the ultimate capacity was reached. Ultimate load carrying capacity was characterized in each test by a localized punching fracture of the concrete deck slab.

The first test series consisted of four tests, referred to as tests 1 through 4. In each test in this series, a single concentrated load was applied to a slab midway between two adjacent transverse strap locations. In each of these test locations, the concrete was initially undisturbed; i.e. the concrete had no load-induced cracks in the vicinity. The tests in this first series differed with respect to the degree of external restraint provided by the transverse straps at the given test location. These test locations are shown as 1, 2, 3, and 4 on the plan of the deck in Figure 4.6.

The second series of tests were performed on areas of the slab where the

concrete had experienced some cracking as a result of tests 1 through 4. Tests 5 and 6, positioned as shown in Figure 4.6 make up the second test series.

The testing procedure was repeated for a third test series. This last series consisted of tests at locations 7 and 8, which are also indicated in Figure 4.6. In this final series, the influence of repaired deck concrete was investigated. The slab was retested at the same locations where punch outs had occurred at the culmination of tests 1 and 4 after local repairs had been made.

4.4.3 Structural Modifications Made During the Experimental Program

The size of the transverse straps was modified twice during the experimental program. Based on the results of tests 1, 2, and 3, the degree of external transverse slab restraint was reduced prior to performing test 4. A further reduction was made subsequent to test 4 before the remainder of the experimental program was carried out. These reductions were made by selective replacement of some of the transverse steel straps with thinner straps. The variation in strap cross-sectional area with location and test number is summarized in Table 4.1.

5.0 RESULTS OF EXPERIMENTAL PROGRAM

5.1 Material Testing

5.1.1 Material Tests Performed on Fresh Concrete

The compressive strength of the fibre-reinforced concrete mix was determined from cylinder tests made in accordance with CSA standard A23.2-3C, Making and Curing Concrete Compression and Flexural Test Specimens, [CSA, (1994)]. Compressive strength of the plain concrete, before the addition of the polypropylene fibres and the superplasticizer, was also measured for comparison. The results of these compressive tests are reported in Table 5.1. In this table the entries designated by a cylinder reference "NF-X" correspond to the plain concrete samples and a "F-X" designates a fibrous mix. The mean 28 day compressive strengths were calculated to be 42.8 MPa and 26.5 MPa, for the plain concrete and the FRC, respectively. This shows that there was a loss of strength for the fibre reinforced concrete, when compared to the plain concrete of more than 16 MPa.

An air content analysis was not performed on the plain concrete, before the addition of the polypropylene fibres, as the concrete specification called for 6% air and it there was no indication that it was otherwise. However, after the fibre addition and mixing in the agitator truck, during preparation of the cylinders for the fibrous mix, air bubbles were obvious in the mix. An air content analysis was performed on samples of the fresh fibrous concrete in accordance with the CSA standard A23.2-4C, entitled Air Content of Plastic Concrete by the Pressure Method, [CSA (1994)]. The results showed the air content of the fresh FRC to

be 10.5%. Subsequent to load testing, additional material tests were performed as described in the following section in an attempt to assess the effect of the fibre addition on the air content.

Table 5.1: Concrete compressive strength results

Cylinder reference	f_c MPa	Age days	Cylinder reference	f_c MPa	Age days
NF-4	30.3	7	F-3	20.4	8
NF-3	30.9	7	F-8	20.2	8
NF-2	34.1	14	F-5	20.6	14
NF-7	37.1	28	F-6	23.8	28
NF-9	42.5	64	F-1	25.3	64
NF-8	44.4	64	F-9	26.9	64
NF-5	47.3	146	F-2	27.3	146
			F-7	29.2	146
Mean (of ≥ 28 day) = 42.8		Mean (of ≥ 28 day) = 26.5			
Standard deviation = 4.3		Standard deviation = 2.0			
Coeff. of variation = 10.0		Coeff. of variation = 7.7			

5.1.2 Core Sampling of Cured FRC Deck

Core samples were taken from the cured concrete deck subsequent to the destructive testing program. Sixteen cores were extracted at regularly spaced along the exterior edges of the deck, outside the girder line, from the slab "overhang". The cores were taken from this location in order to sample virgin material that had not been affected by the applied loads. The core longitudinal spacing was approximately 2 m centre to centre, with the exact spacing adjusted to avoid local irregularities such as load-induced cracks. The cores, thus obtained were felt to be representative of the quality of the FRC along the length of the structure.

Eight of the samples were tested under compressive loading to measure the ultimate compressive capacity of the aged (223 days old) FRC concrete. The mean concrete compressive strength and standard deviation based on this data are 22.0 MPa and 2.8 MPa, respectively. Strength evaluation of the cores was made in conjunction with the method prescribed by ASTM C42-90, Standard Test Method for Obtaining and Testing Drilled Cores and Sawed Beams of Concrete, [ASTM, (1990)]. Corrected tests results are presented in Table 5.2.

Table 5.2: Compressive strength results of deck core samples

Core Sample Reference Number	Compressive Strength (MPa)
9	22.3
10	21.1
11	17.4
12	19.2
13	20.6
14	23.9
15	24.9
16	26.3

5.1.3 Air Content Analysis

A microscopic air content analysis was performed in accordance with ASTM C-457, Standard Practice for Microscopical Determination of Air-Void Content and Parameters of the Air-Void System in Hardened Concrete, [ASTM (1993)]. In accordance with the method prescribed in this standard, samples were prepared from the hardened concrete and the air void system was studied under a microscope. The FRC samples for the microscopic testing were prepared from cured concrete taken from the deck cores. Samples of plain concrete were

obtained from extra cylinders that had been prepared for compressive tests. Interpretation of the results allowed for a comparison of the air content of the plain concrete with that for the fibrous concrete. The air content of the cured fibrous concrete was also compared with the air content measurement made for the fresh fibrous mix by the pressure method, before curing.

Test results for the plain concrete, as delivered, showed the air content to be 3.2%. The air content is slightly lower than the 6% that was specified when ordering the concrete. For the laboratory testing program this difference is not expected to be significant, as only the compressive strength of the concrete had a direct bearing on the ultimate capacity of the system under load. The air content would however be important for field applications, due to its bearing on structural durability.

Air testing results of the fibrous samples show that the fibre presence has dramatically increased the percentage of entrapped air in the concrete. After the addition of the polypropylene fibres the air content was measured to be 16.3%. This value is significantly higher than the 10.5% air that was measured by the pressure method for the fresh FRC. Complete results of the microscopical testing are provided as Appendix B to this report and a summary of the results are provided below in Table 5.3. These results will be discussed in Ch.6.

Table 5.3: Summary of the results of the microscopic air testing

Mix Type	Trial No.	Specific surface mm⁻¹	Spacing factor x 10⁻⁶ m	Air Content %
FRC	1	8.5	144	16.4
	2	8.9	153	16.2
	Avg	8.7	148	16.3
Plain	1	46.9	124	3.1
	2	43.4	130	3.3
	Avg	45.2	127	3.2

The impact of the addition of the polypropylene fibres on the microstructure of the mix was evident to the naked eye. Figure 5.1 shows a photograph which compares the FRC mix to the plain concrete mix. A randomly distributed network of air bubbles can be seen in FRC mix on the left, while there are no such visible air pockets in the plain concrete on the right .

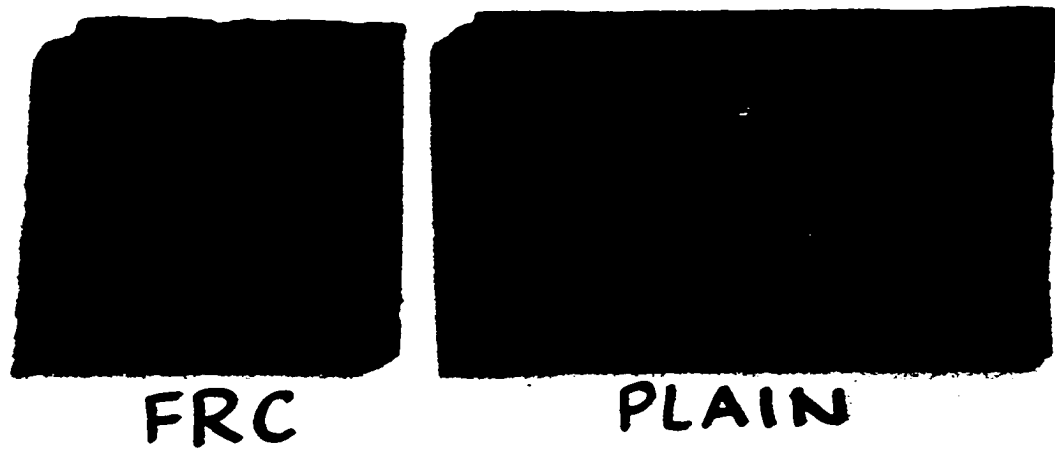


Figure 5.1: Samples of FRC and plain concrete showing visible difference in air content

Furthermore, the microscopic air testing also gave an indication of the concrete quality and the implication of the microstructure on the compressive strength.

These two aspects will be further discussed in Ch. 6.

5.2 Monitoring the Behaviour During Load Tests

The load/response history during the experiment was monitored; applying the concentrated loads incrementally to the concrete slab and measuring the strains and vertical deflections at each load step. The magnitude of the load was controlled during testing using a pressure gauge that had been calibrated prior to the test for the hand pump and the hydraulic cylinders. The accuracy of this pressure gauge was ± 45 kg; which is approximately equivalent to ± 0.634 kN for the setup having two 50 tonne cylinders and ± 0.314 kN for the one 50 tonne cylinder setup.

Strain in the steel straps were measured using electrical resistance strain gauges mounted on the steel straps. A series of straps had 3 gauges attached; two at mid-depth of the strap thickness and one on the bottom face of the strap. The strain in the remaining straps was monitored with one strain gauge located on the bottom of the strap. Using the appropriate mathematical expressions, the strains were converted to stresses and subsequently multiplied by the strap cross-sectional area to calculate the axial force in each strap at each successive load increment.

Vertical deflections of the slab and the steel girders were measured throughout the experiment using dial gauges. Typically, the deflections were sampled across a perpendicular section of the deck, taken through the load point. The load was transmitted to the deck slab through a steel plate 50 mm thick, having a contact area of 250 mm x 500 mm, representative of a loaded dual vehicle tire footprint.

5.3 Observed Cracking Behaviour During Testing

During the first testing series, destructive testing of four sections of initially uncracked concrete, the deck slab exhibited a characteristic sequence and pattern of cracking. This sequence can be described by the following progression of cracking:

- Relatively low magnitude concentrated loads caused radial cracking to begin on the underside of the slab, extending outward from the edge of the applied load.
- Also soon after the application of load, cracks appeared on the top surface of the slab adjacent to the girder flanges, generally orientated as arcs longitudinally
- As the magnitude of the applied load was increased, the radial cracks began to propagate through the slab toward its top surface.
- As the magnitude of the concentrated load was increased, a series of circumferential shear cracks began to develop on the bottom of the slab. These cracks formed on the perimeter of the loaded area.
- The shear cracks propagated along a shallow incline toward the top of the slab, moving in the direction of the loaded area.
- When the inclined shear crack intersected the radial cracks through the slab depth, the slab in the vicinity of the load was separated into a series of radial wedges, surrounding a central plug formed directly below the applied load. The top surface of this plug had approximately the shape of the load contact area and the perimeter of its underside was the lower extent of the inclined shear crack.

- Subsequent to the formation of the radial wedges, the slab sustained further load without noticeable crack development.
- Ultimately in each test, the rigid body mechanism became unstable and the centre plug of concrete punched through the deck suddenly with a release of energy.

An idealized plan view of the observed crack pattern is given in Fig. 5.2 and Fig. 5.3 contains photographs taken of cracking during load testing.

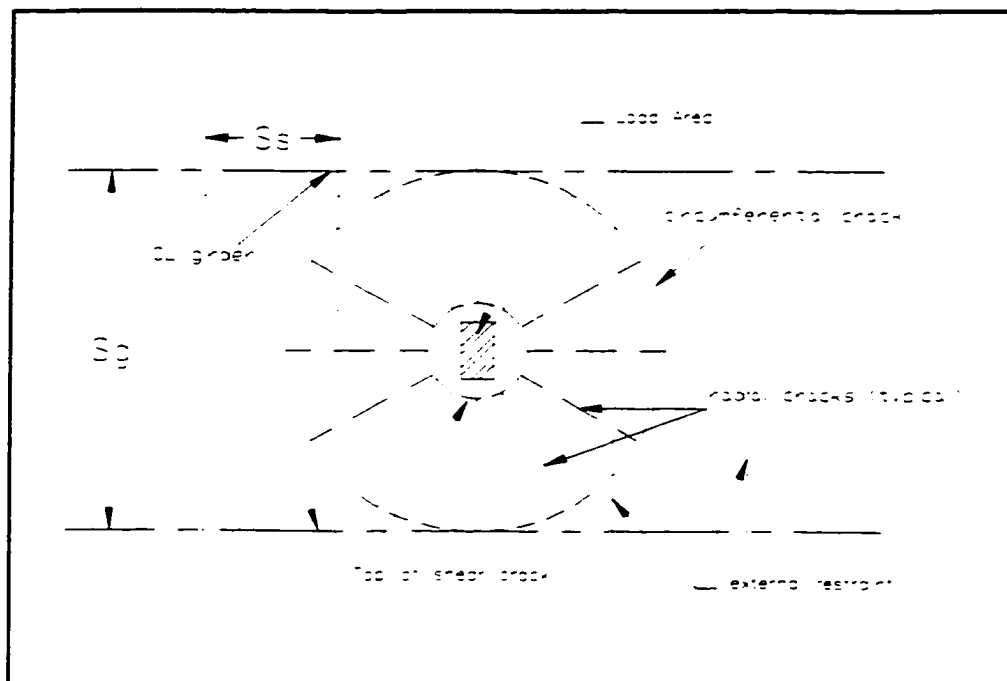


Figure 5.2: Idealized cracking pattern observed during load test

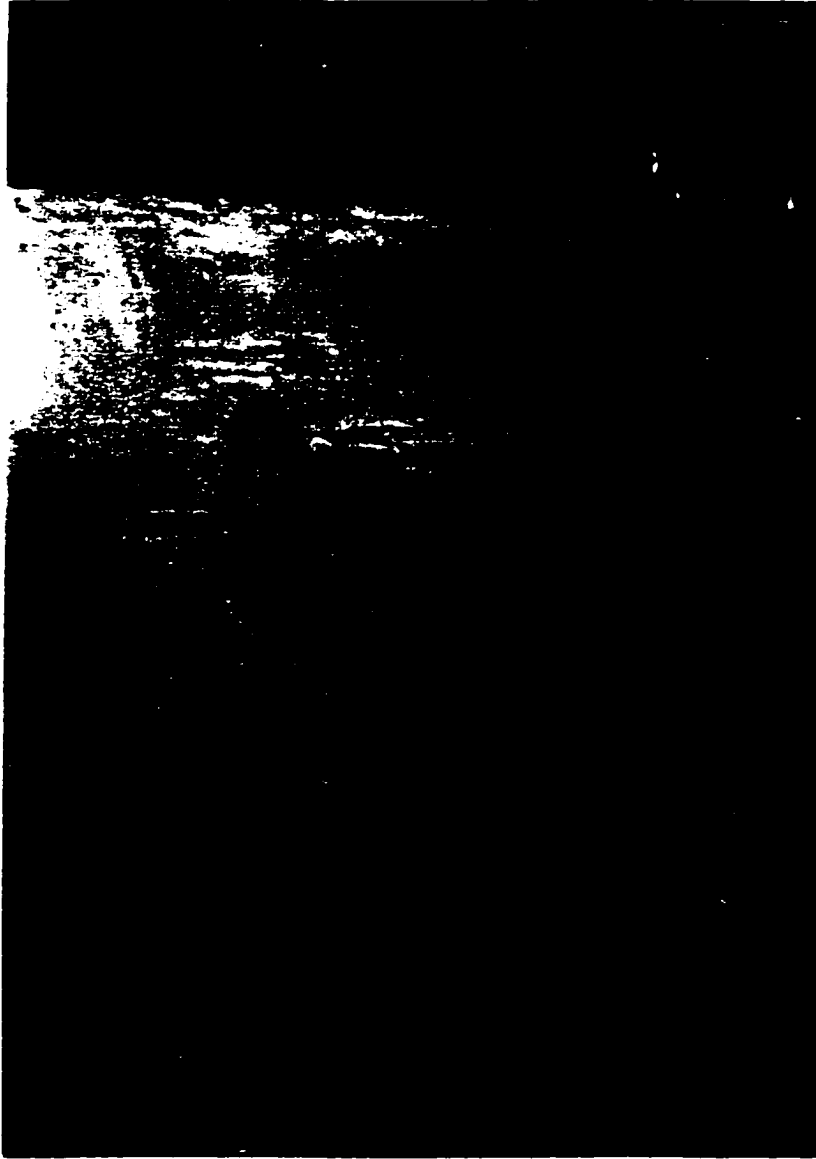


Figure 5.3 (a): Underside of slab showing formation of radial cracks



Figure 5.3 (b): Topside cracking; flexural cracks along the girder and circumferential shear cracks

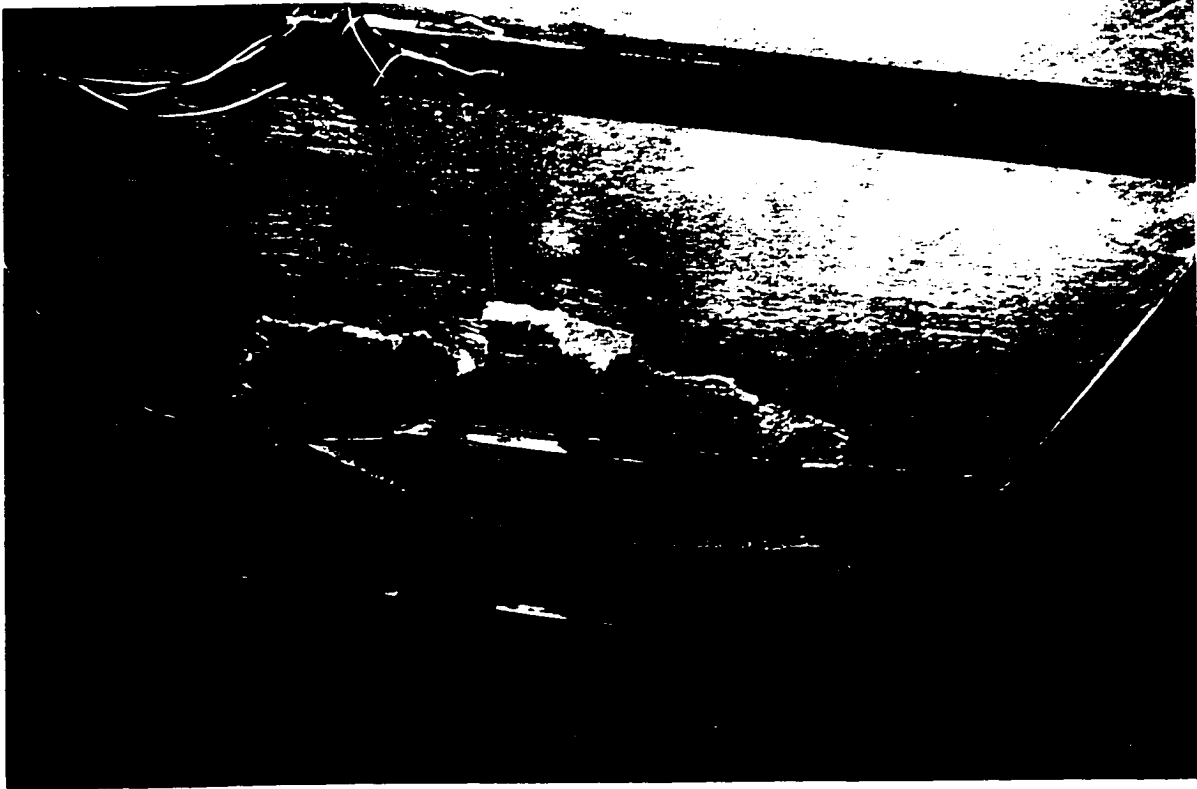


Figure 5.3 (c): Slab from below, showing radial crack development during rigid body rotation

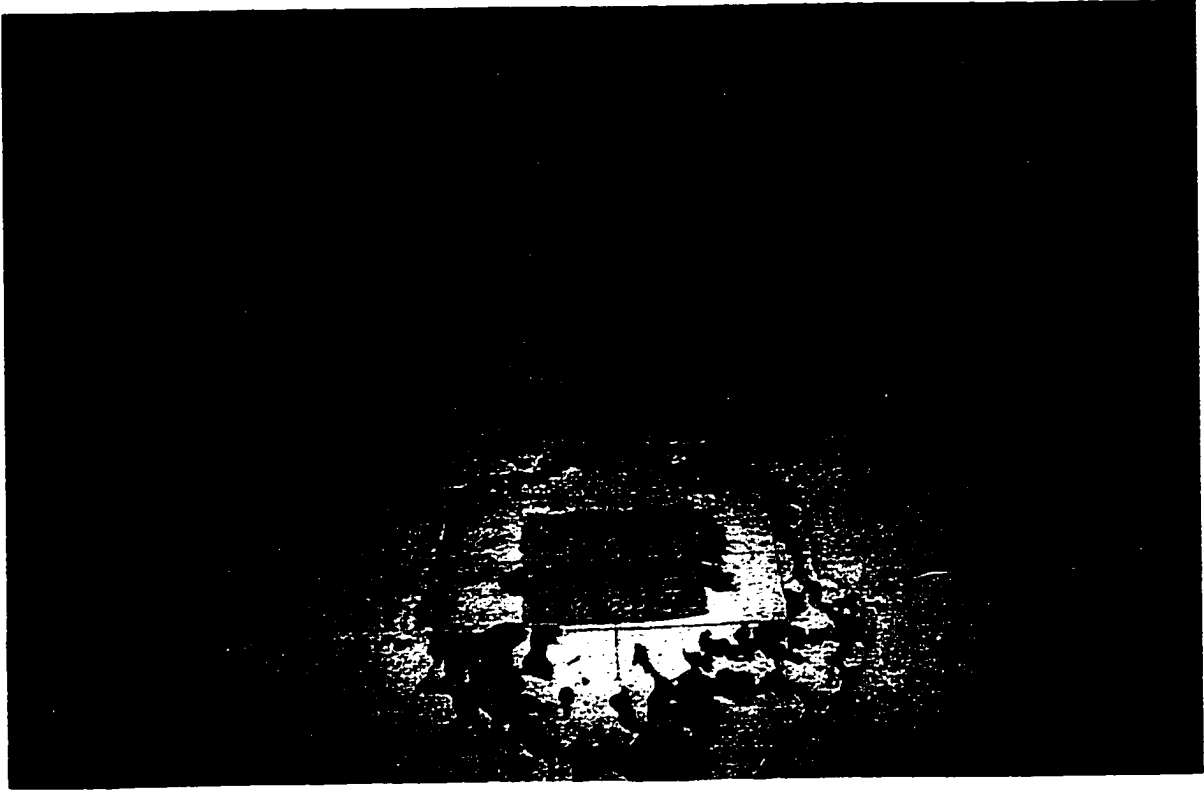


Figure 5.3 (d): Crack pattern on top surface after punching

After test 1, a transverse crack was observed at approximately midspan of the structure. This transverse crack penetrated the full-depth of the concrete slab, effectively "cutting the slab in two", transversely.

5.4 Deflection Results

The measured load-deformation histories for the first four tests is presented in Figure 5.4. It is noted that the deflections at the edge of the load were monitored until the applied load was approximately 75% of the expected ultimate load. The dial gauges were then removed from the vicinity of the load to prevent

damage to the gauges when the punching failure occurred.

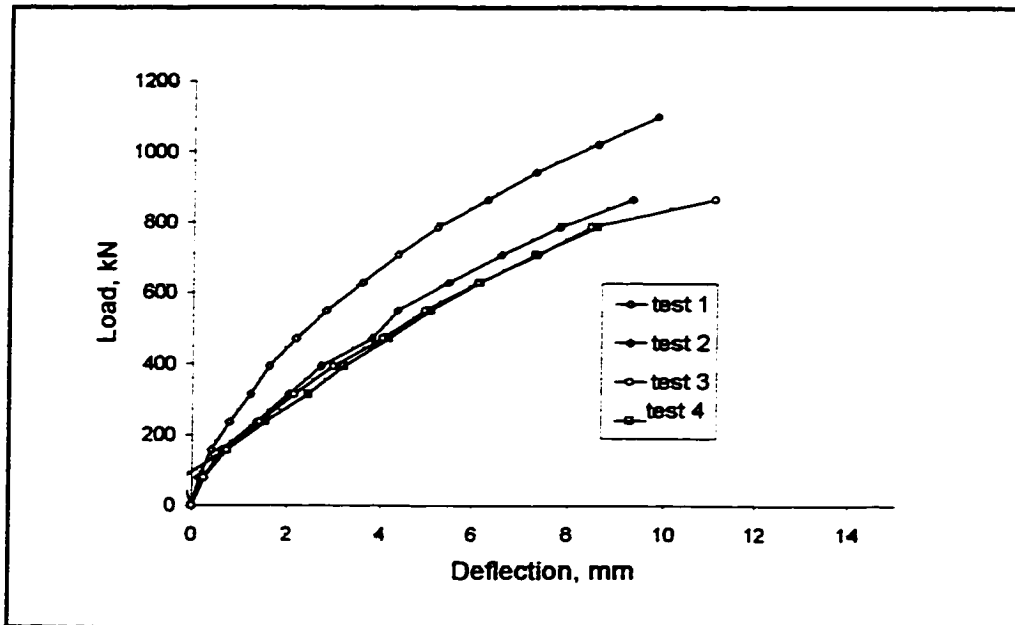


Figure 5.4: Load / deflection history measured during first test series

The graph shows the similarity of the deflection response for the test series. Each shows an initial linear portion, followed by a system that is becoming less stiff with increasing load. The initial linear portion represents the system's flexural response, prior to first concrete cracking and the subsequent nonlinear portion represents the slab arching behaviour, as cracking progresses, the series of rigid bodies develop around the load and the cracked slab responds as an arch to increased loads. It is noted that the system lateral restraint for test 1 was 2.5 times as large as that for test 4, yet the change in deflection is not as significant. For example, consider a 600 kN load. For the first test, with 25 mm straps, the maximum deflection was 3.5 mm and for the fourth test, with 6.35 mm straps, the maximum deflection was 6.1 mm.

The complete slab transverse deflection measurements for each of the 8 tests are presented in Ch. 6 in conjunction with the predicted deflections obtained from the rigid body analysis. A summary of the system lateral restraint values is provided in Table 6.4.

5.5 Strain Results

Strap strains were measured at each load increment, up to and including the load increment that preceded the punching failure. The complete strain results for the entire experimental are presented in Ch. 6, where they are discussed and compared to the strain histories predicted by an analysis.

Figure 5.5 is representative of the observed relationship between the applied load and the strap strain. (Note that the dimensions "x" as shown represent the distance from the west support.) From the strain results it can be seen that a given strap's effectiveness is directly related to its proximity to the applied load. Straps located more than 2.5 m from the applied load experienced negligible strain.

The strain measurements for those straps having three gauges show no appreciable change in strain through the depth of the bar. This confirms the assumption that the straps do indeed respond axially during arching, forming the lower tensile tie to complete the arch.

In test number 3, the strap identified as # 10 had a maximum recorded strain of

2165×10^{-6} mm/mm. The theoretical yield strain of the 300 W steel is 1500×10^{-6} mm/mm. For structural steels a recorded strain in excess of the theoretical material yield strain indicates that the member is experiencing a stress greater than that required to cause yielding. A structural quality steel would be expected to strain without further application of load and the corresponding member stress would be expected to remain at the material yield stress until "sufficient" plastic flow had taken place to strain harden the material. The elastic, plastic and strain hardening ranges are given in Figure 5.6 for a typical structural quality steel. Strain hardening of a CSA CAN3-G40.21 300W steel could be expected at a nominal strain of 0.02 mm/mm, approximately 10 times the maximum strain recorded in strap 10.

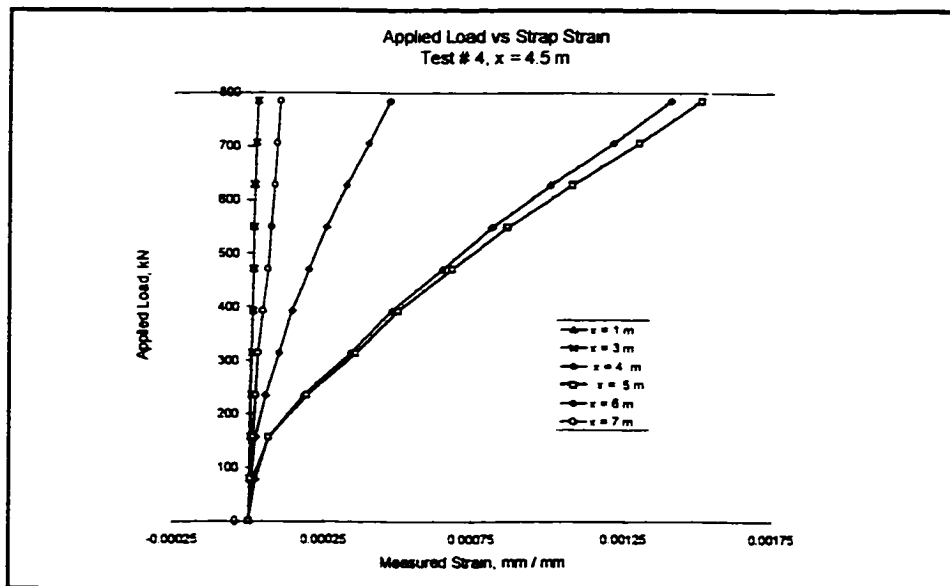


Figure 5.5: Applied load vs measured strap strain, Test # 4

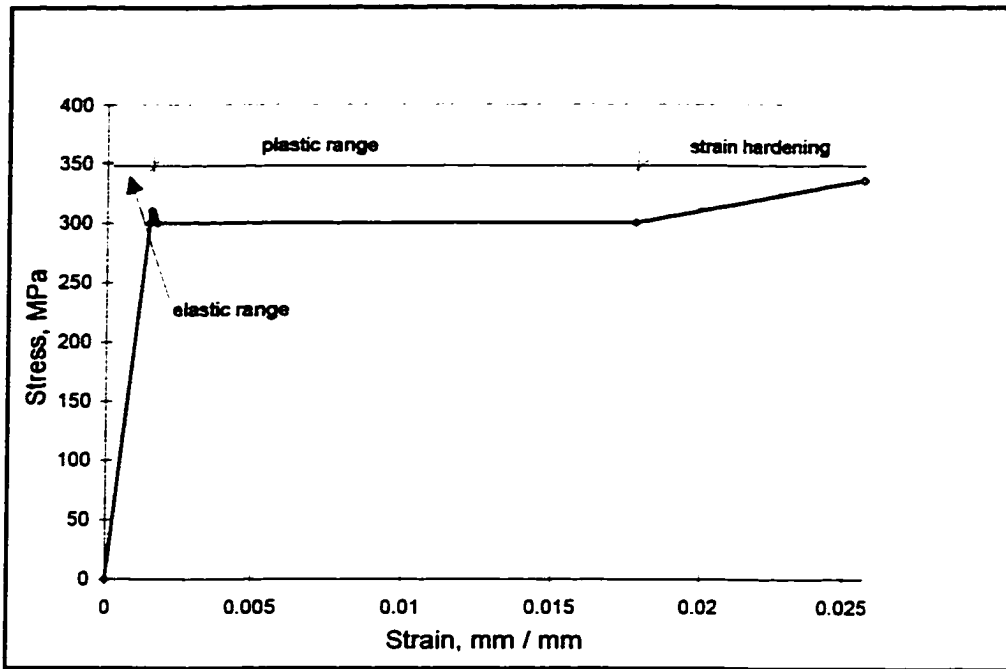


Figure 5.6: Typical stress strain diagram for structural steel,
[Salmon and Johnson, (1990)]

6.0 DISCUSSION

6.1 Comparison of Theoretical and Experimental Results

6.1.1 Comparison of Calculated Punching Load with Experimental Results

The rigid body analysis that was described in Ch.3 was used to analyze the system behaviour of the 8 slab sections that were load tested in the laboratory. The concrete compressive strength value for the analysis was taken as 22.0 MPa, based on the average of the results from the FRC core tests. For a further discussion of the compressive strength the reader is referred to section 6.2.1. The external restraint stiffness value used for the analysis varied in each test, due to the variation in strap size and the system restraint of the model at the given test location, as was described in Ch. 2 and is revisited later in this chapter.

In each case the analysis predicted that the ultimate capacity would be dictated by a punching shear failure, precipitated by concrete crushing. The ultimate punching loads obtained from the analysis and the experimental work are presented in Table 6.1, for the first four tests. The table shows that the analytical method is able to predict the ultimate load with reasonable accuracy; the mean of the ratio of the calculated punching load to the experimental punching load is 0.88, with a standard deviation of 0.05.

Table 6.1: Comparison of calculated punching load with experimental capacity

TEST No.	EXPERIMENTAL (kN)	CALCULATED (kN)	$\frac{P_{\text{calculated}}}{P_{\text{experimental}}}$
1	1128	1055	0.94
2	923	863	0.93
3	911	763	0.84
4	844	693	0.82

6.1.2 Load Deformation Behaviour

The analytical model was used to calculate the load deformation behaviour and ultimate load for each of the experimental tests. The theoretical behaviour was compared to the behaviour measured during testing and the results are presented graphically in Figures 6.1 through 6.8. The deflection plotted is that of the slab below the point of load application, midway between longitudinal girders.

For the first series of tests, Tests 1 through 4, the load was applied midway between two external steel restraints for which the surrounding concrete was intact at the commencement of each of the tests. The experimental load history

shows a nonlinear relationship between central slab deflection and the applied load throughout most of the load range. The initial response of the system, prior to flexural cracking, is expected to be linear. The measurements for the flexural portion of the system's behaviour, for deflections less than about 1 to 1.5 mm, appear linear, however the data is limited as flexural cracking begins at a low magnitude of load. Subsequent to the formation of flexural cracks, the measured response shows a system that is gradually losing stiffness as the ultimate punching load was approached. The experimental response for each of these four tests shows a stiffer system than does the predicted response obtained from the analytical model.

The second series of tests, Tests 5 and 6, were performed on areas of deteriorated concrete, which had sustained cracking during the first test series. In this second series, the point of concentrated load was applied above a transverse steel strap position.

The third test series, Tests 7 and 8, were performed on sections of repaired concrete. Two punched out portions of the deck, resulting from the first series of tests, were repaired locally and retested. The load histories shown in Figures 6.7 and 6.8 show that the system behaves less stiffly than the behaviour predicted analytically.

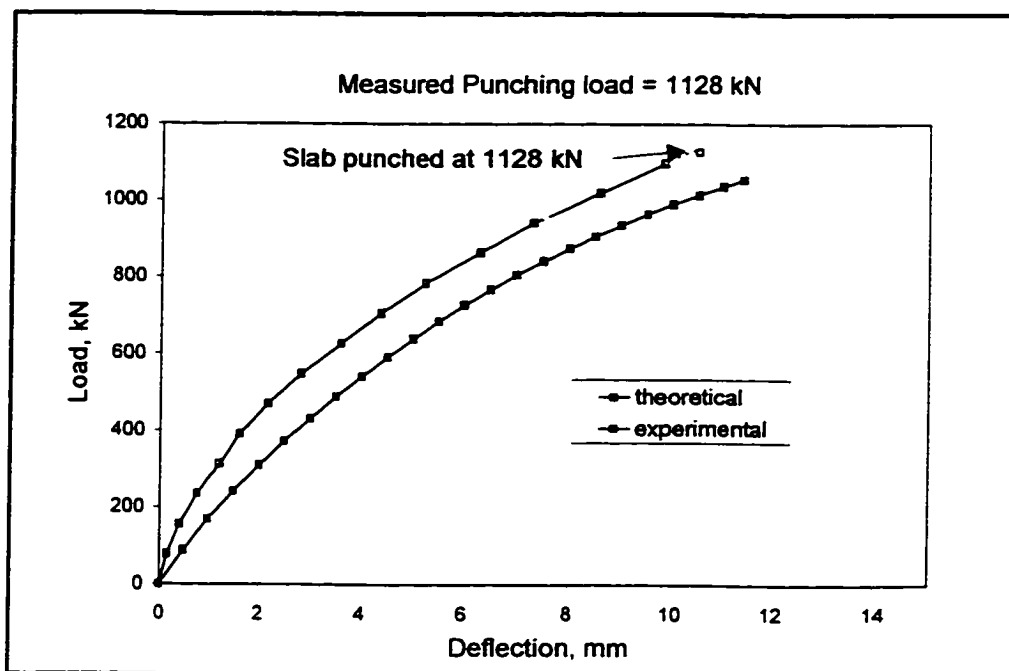


Figure 6.1: Load deformation results, Test # 1

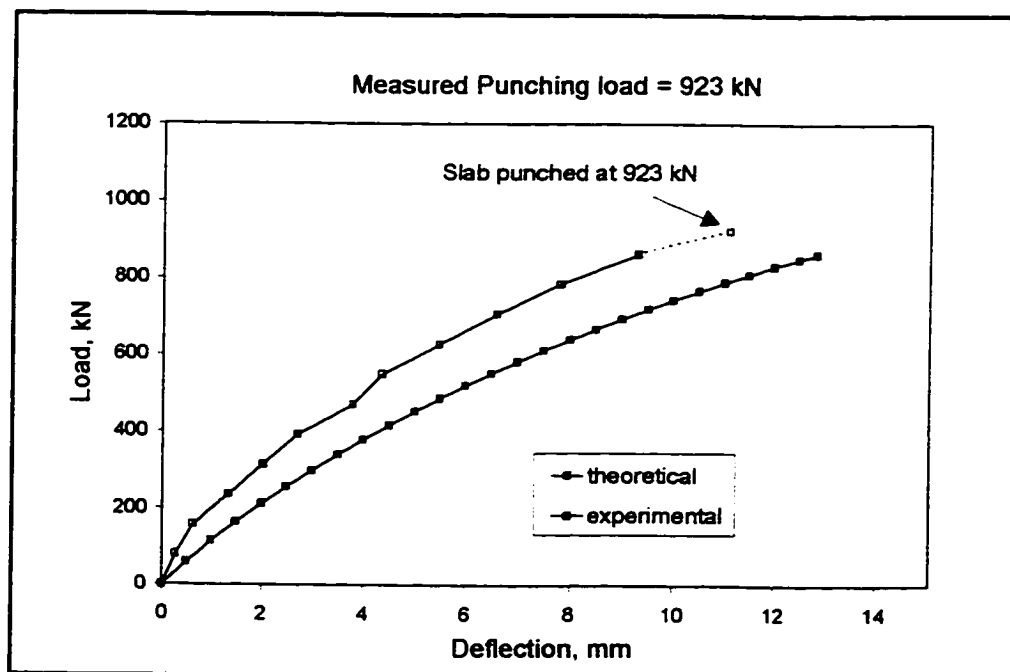


Figure 6.2: Load deformation results, Test # 2

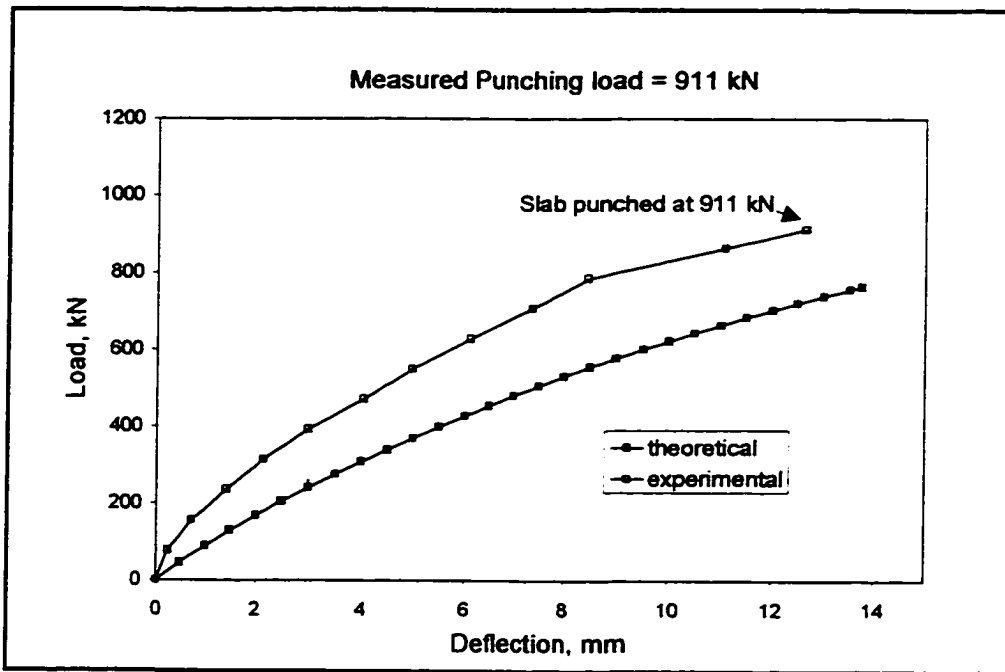


Figure 6.3: Load deformation results, Test # 3

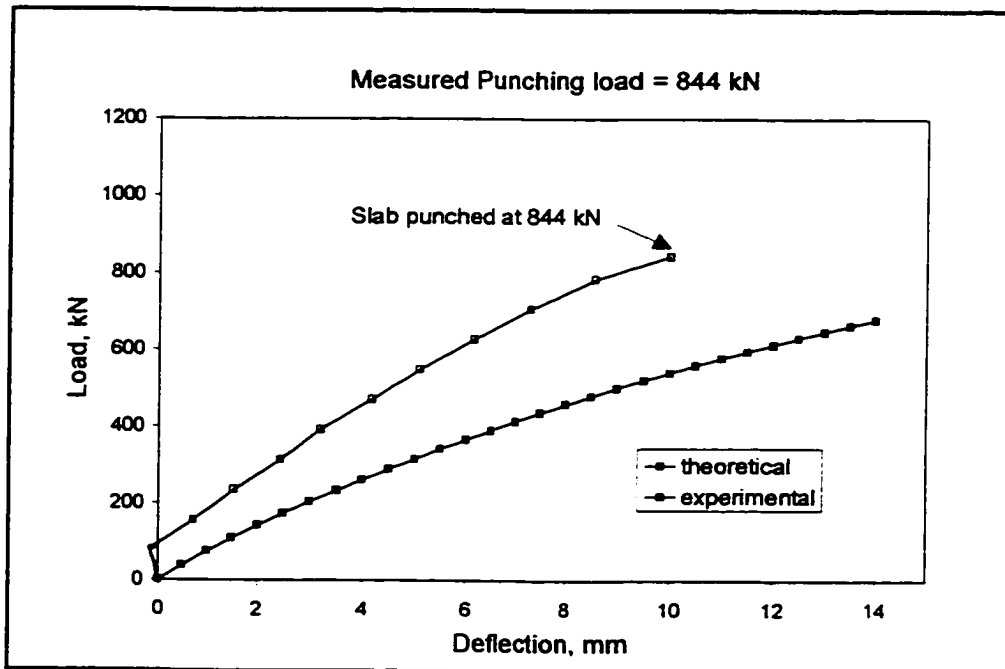


Figure 6.4: Load Deformation results, Test # 4

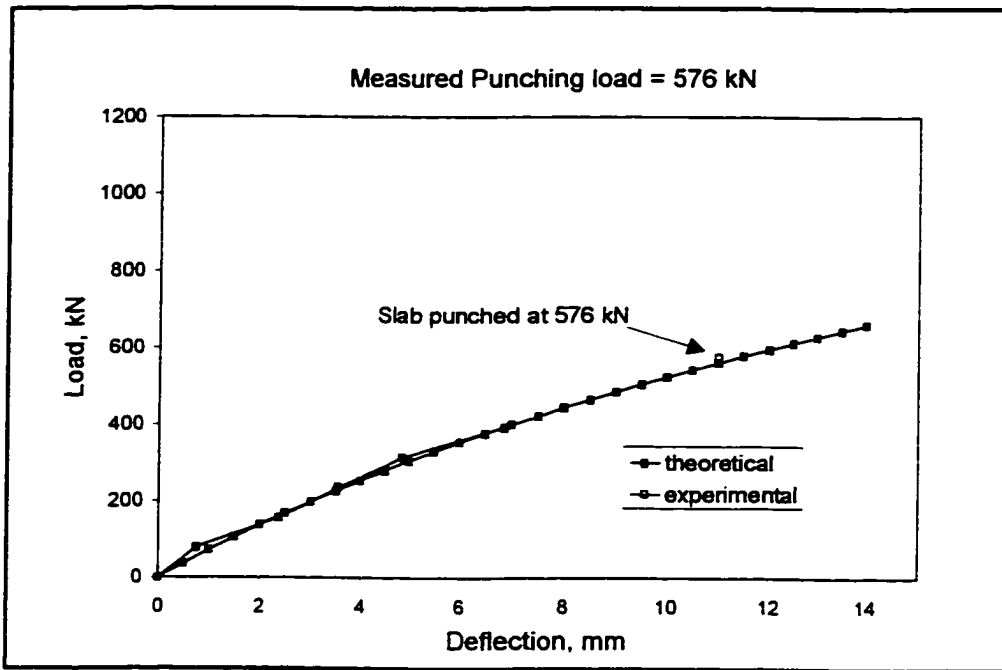


Figure 6.5: Load deformation results, Test # 5

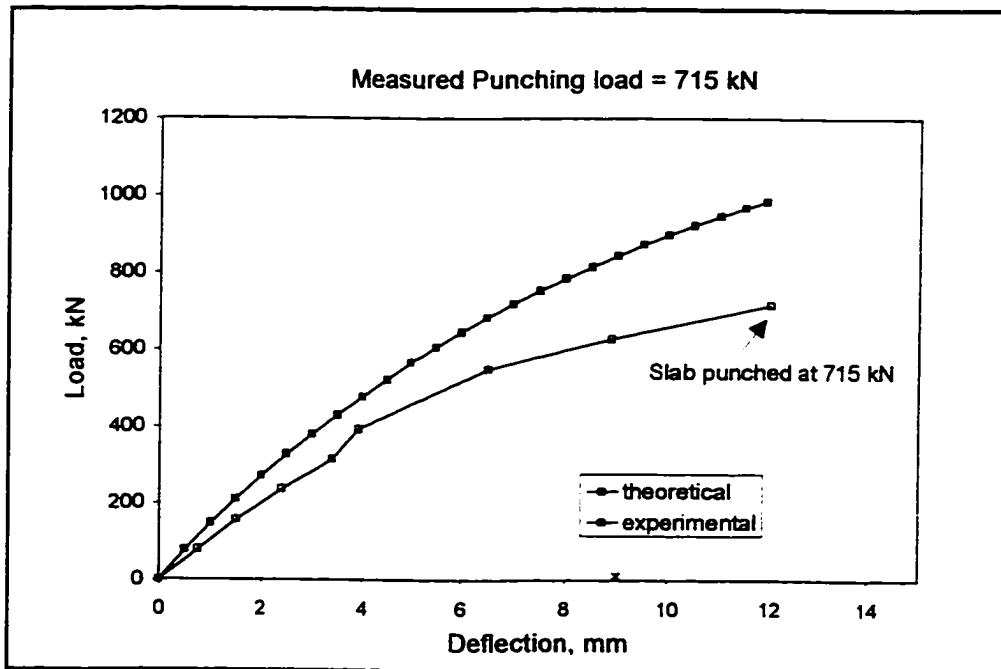


Figure 6.6: Load deformation results, Test # 6

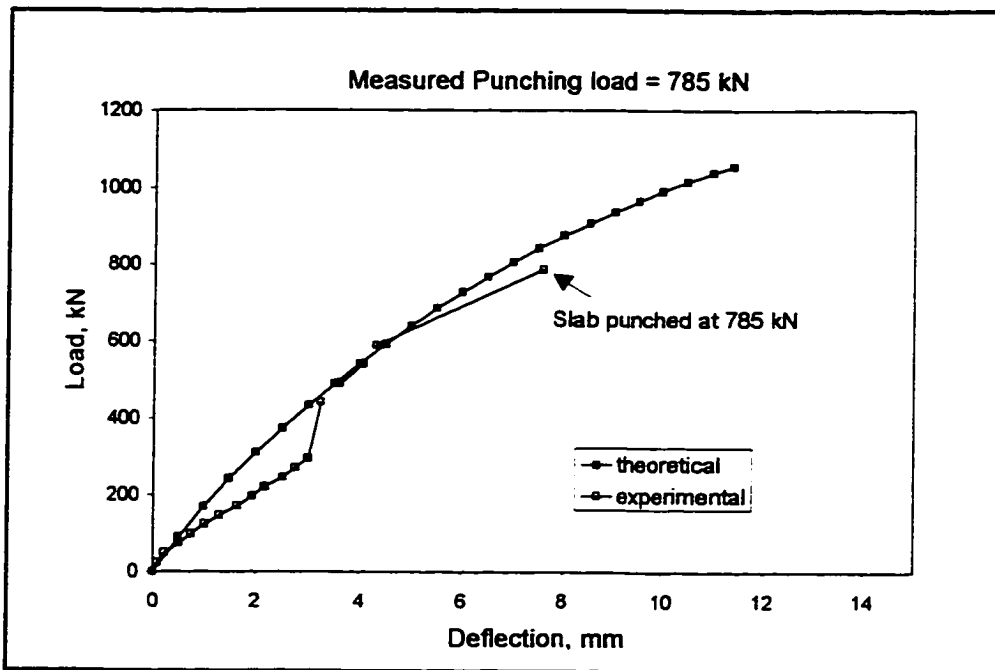


Figure 6.7: Load deformation results, Test # 7

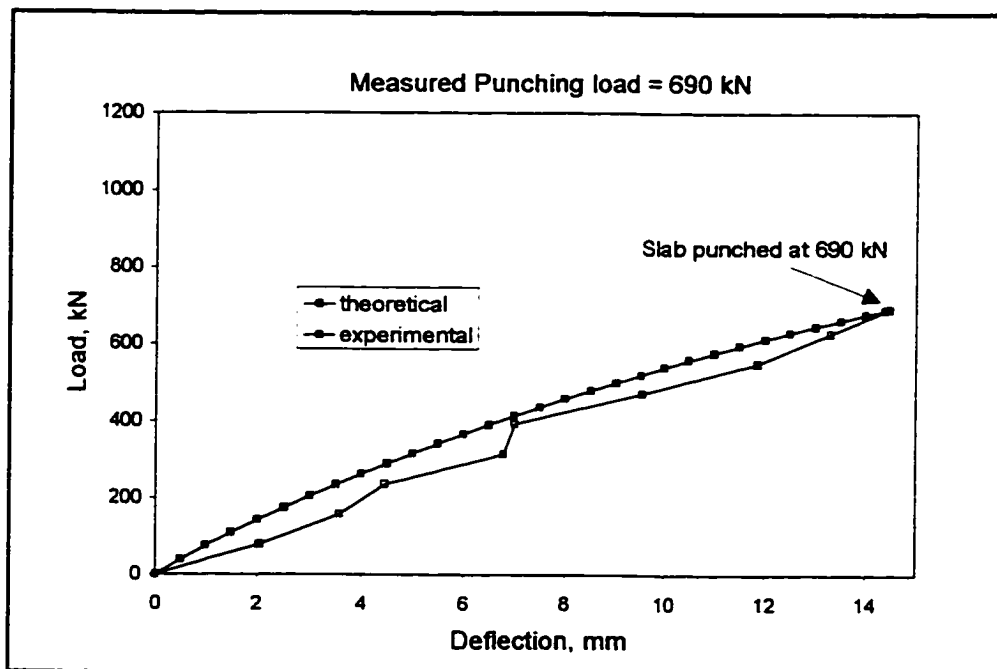


Figure 6.8: Load deformation results, Test # 8

6.1.3 Behaviour of External Restraints

6.1.3.1 Strain Behaviour

A comparison of the axial strains measured in the transverse straps in the four destructive tests of the first series is presented in Table 6.2, where strains are given for straps at four distances from the centre of the applied load; 500, 1500, 2500 and 3500 mm. The measured results, ϵ , are presented normalized by the yield strain of the steel, ϵ_y . The maximum strains are those measured in the straps closest to the applied load, or $0.5 S_s$ from the centre of the applied load. It can be seen from the tabulated values that the strap strains drop very quickly as one moves away from the load position, demonstrating that the arching behaviour is localized and that for a given load position any strap located more than 1.5 strap spaces away does not contribute significantly to the arching action.

Table 6.2: Measured strap strains

Test	Strap Thickness, mm	ϵ / ϵ_y @ 0.5 S_y	ϵ / ϵ_y @ 1.5 S_y	ϵ / ϵ_y @ 2.5 S_y	ϵ / ϵ_y @ 3.5 S_y
1	25.4	0.88	0.36	0.15	0.10
2	12.5	0.89	0.34	0.14	0.12
3	9.5	1.44	0.32	0.20	0.16
4	6.35	0.98	0.37	0.14	0.03

It can be seen that in test 3, the strap strain exceeded the nominal yield strain. The maximum strain of 1.44 times the yield strain was measured in strap number 11, positioned 1 m. from the end diaphragm, as shown in Fig. 6.9. At a strain of 1.44 times the yield strain, the structural steel could be expected to be deforming plastically, as shown in the stress strain diagram that was given in Fig. 5.3. This plastic plateau would be followed by a strain hardening range, during which even higher stresses can be attained. The strain hardening range is represented by the inclined portion of the stress strain diagram shown for strains greater than 0.0175 mm/mm. The steel can be expected to continue to behave in a ductile fashion for strains up to the ultimate strain of approximately 0.20 mm/mm. However, such plastic behaviour was not evidenced in the measured strap strain data. As shown in Figures 6.12 and 6.18, strap 11 shows a consistent linear trend between strain and load throughout the load history.

This implies that the strap material properties exceeded the rated properties, which is very common in the steel manufacturing industry, however no material tests were performed to confirm this.

Although the theoretical ultimate strain is almost 100 times greater than the maximum strap strain that was measured during the destructive testing of the full-scale model, it is felt desirable to limit the strap behaviour to the elastic range. Consequently, a strap strain of 0.0015 mm / mm (i.e. the yield strain) was established as one of the limits for the externally restrained deck.

A closer look at the strain results for test # 3 shows that the strap strain measured in the two straps straddling the load position are not symmetrical. The strain in strap 11, the end strap located above the end diaphragm, was measured to be 0.002165 mm / mm while the strap 500 mm from the load in the opposite direction, strap 10, was 0.001494 mm / mm, or approximately equal to the yield value. It can be seen that although the load was applied centrally between straps 10 and 11, the end strap resisted a greater load. The additional transverse stiffness contributed by the end diaphragm accounts for the strain pattern for the two straps. A similar trend was observed at the other end of the deck where strap 1 was strained to a maximum of $0.88 \epsilon_y$ and in strap number 2 the maximum strain was $0.80 \epsilon_y$. At this end the measured strain difference between the two straps is less than that at the opposite end of the structure. This is not surprising when one considers that the strap area at the east end of the structure is one quarter of that at the west end. Due to the difference in area, the difference in transverse stiffness between the two end straps and the end diaphragm is more pronounced at the west end of the structure, leading to a much larger difference in strains in the adjacent straps. Related to the

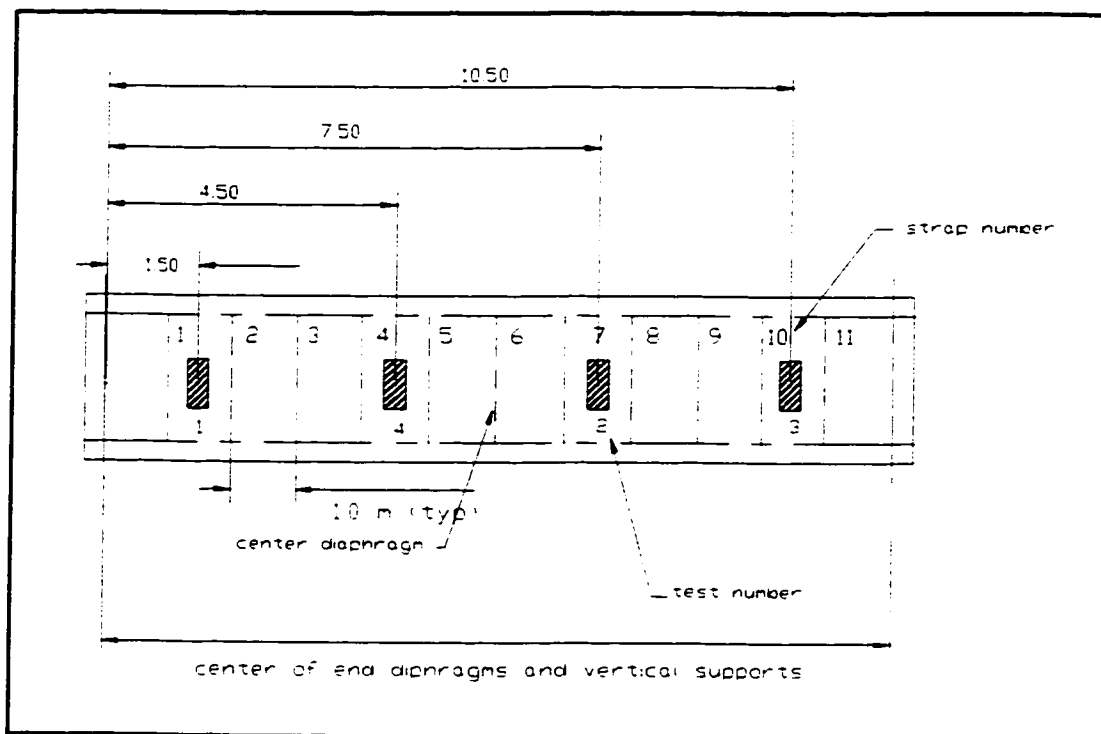


Figure 6.9: Load position for Series 1 tests

Analytically, the rigid body model was used to predict the transverse axial strain in the external restraint throughout the load history. The predicted strains are compared to the strains measured in the straps closest to the point of load application in Figures 6.10 to 6.17, which follow.

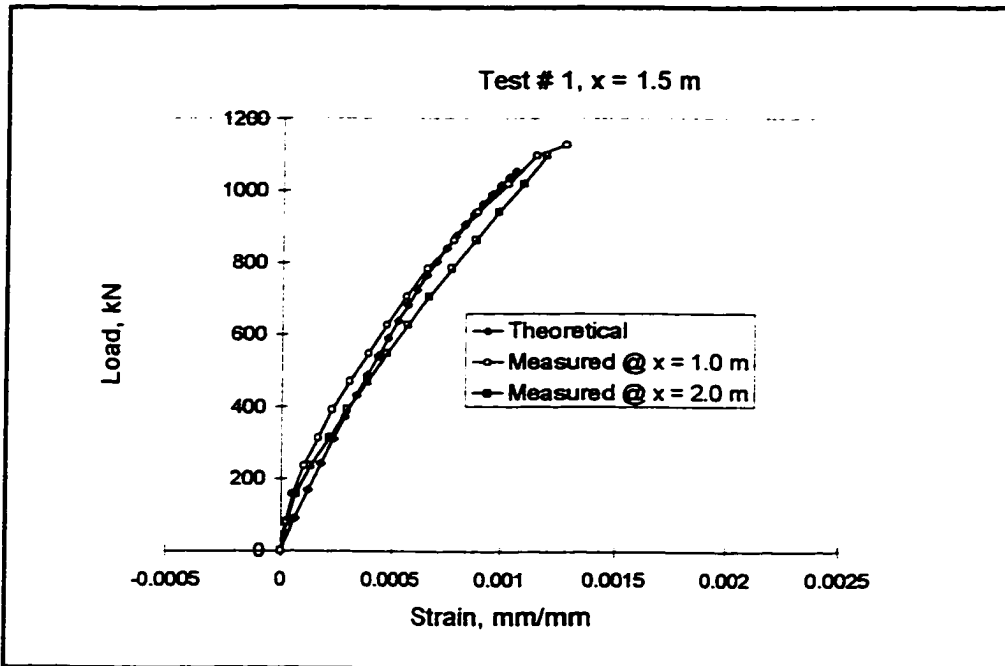


Figure 6.10: Strain in external restraints, Test # 1

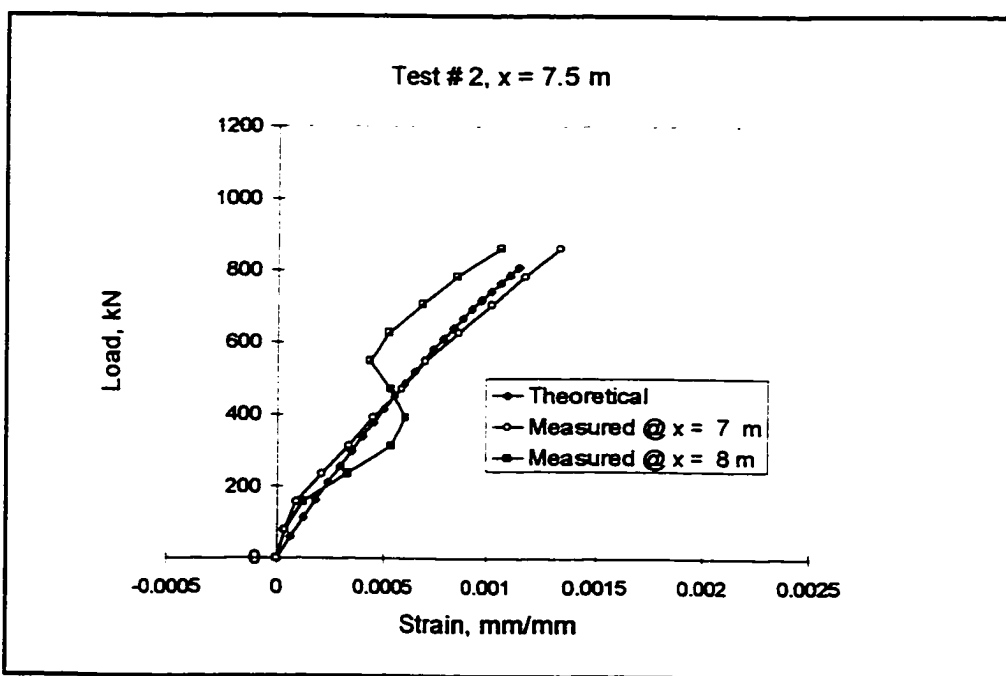


Figure 6.11: Strain in external restraints, Test # 2

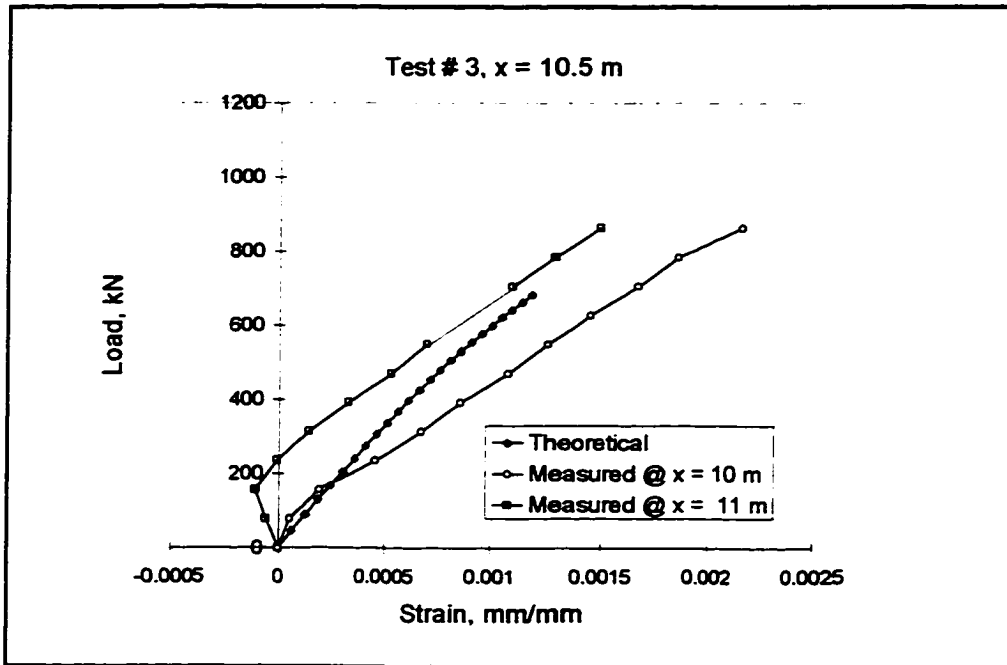


Figure 6.12: Strain in external restraints, Test # 3

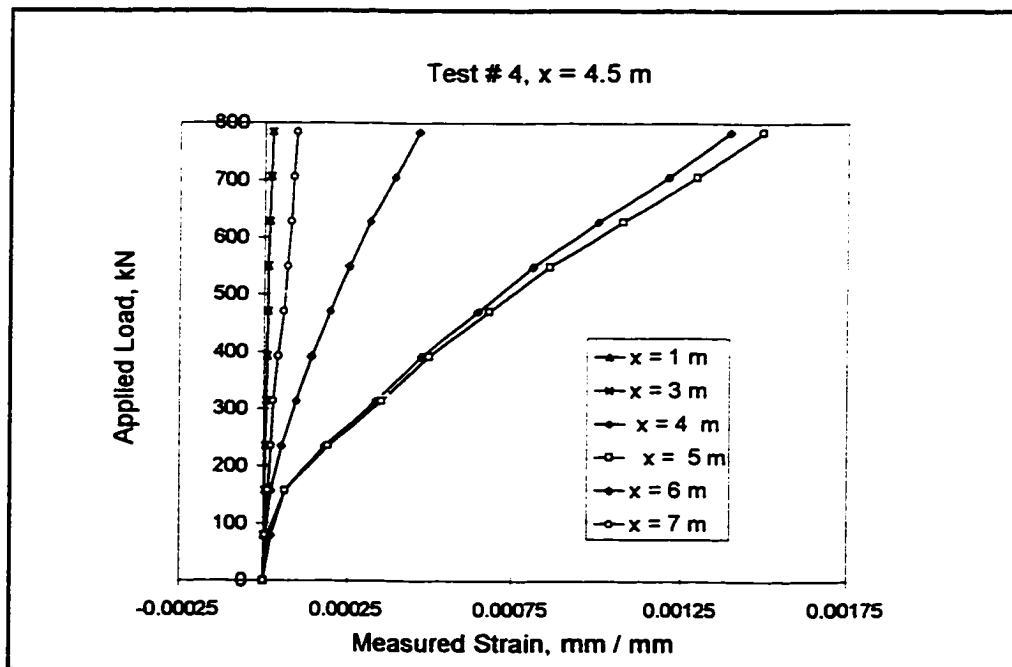


Figure 6.13: Strain in external restraints, Test # 4

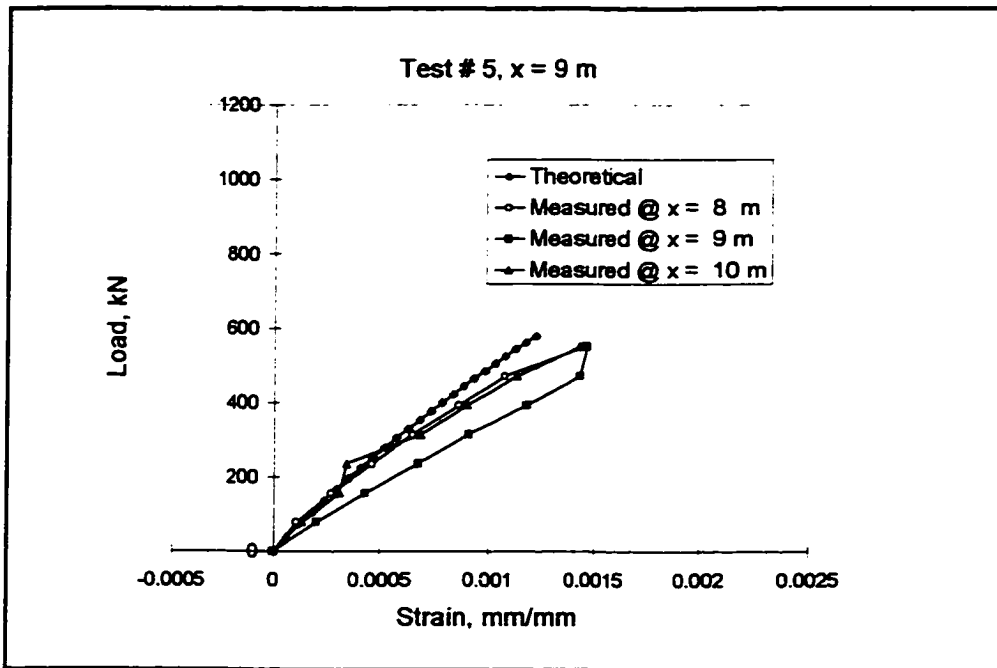


Figure 6.14: Strain in external restraint, Test # 5

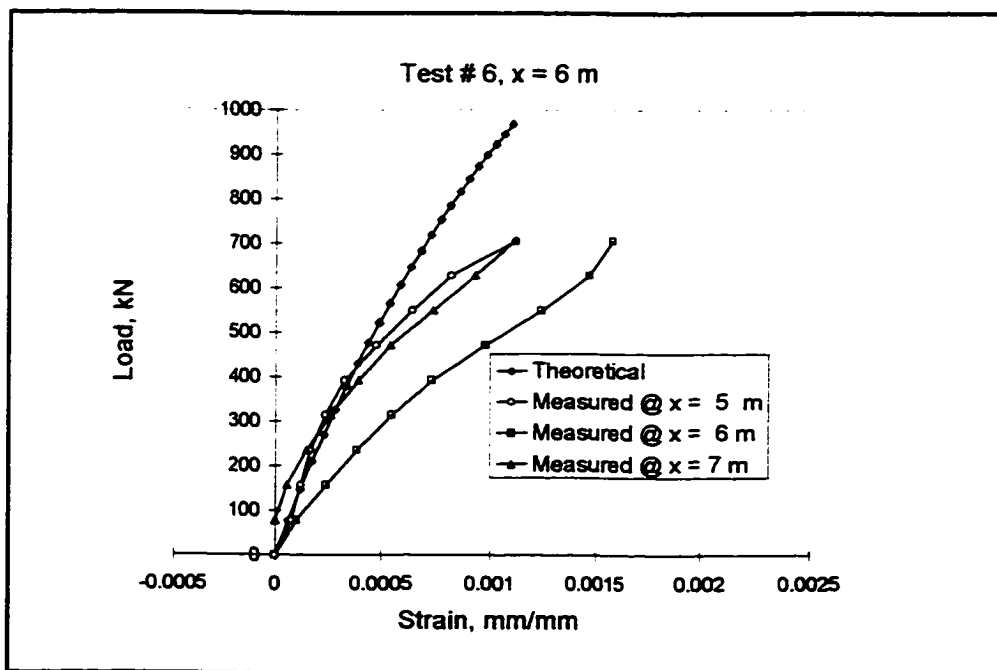


Figure 6.15: Strain in external restraint, Test # 6

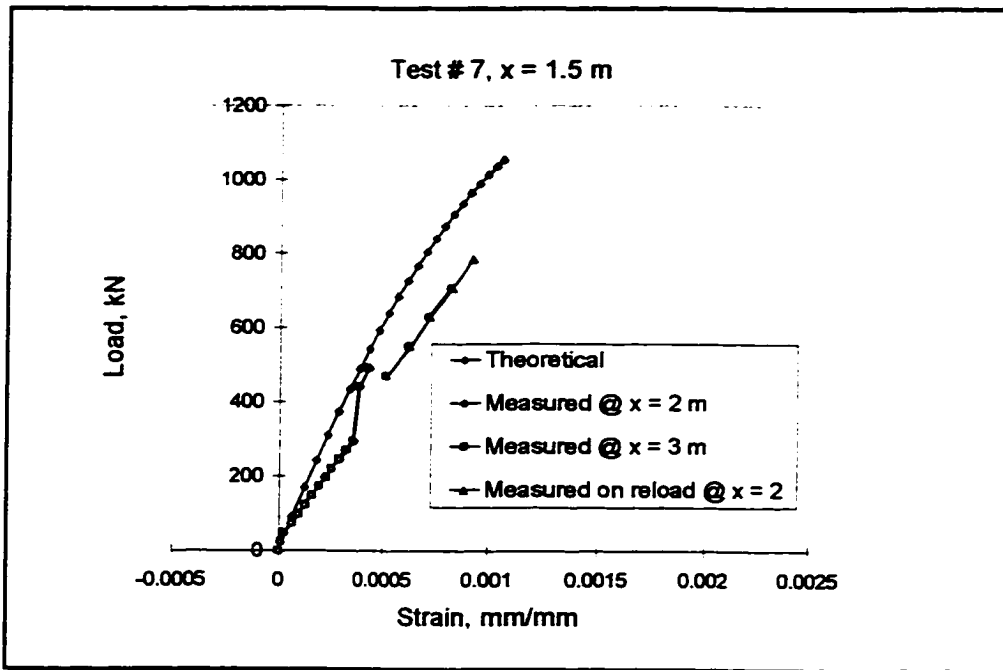


Figure 6.16: Strain in external restraints, Test # 7

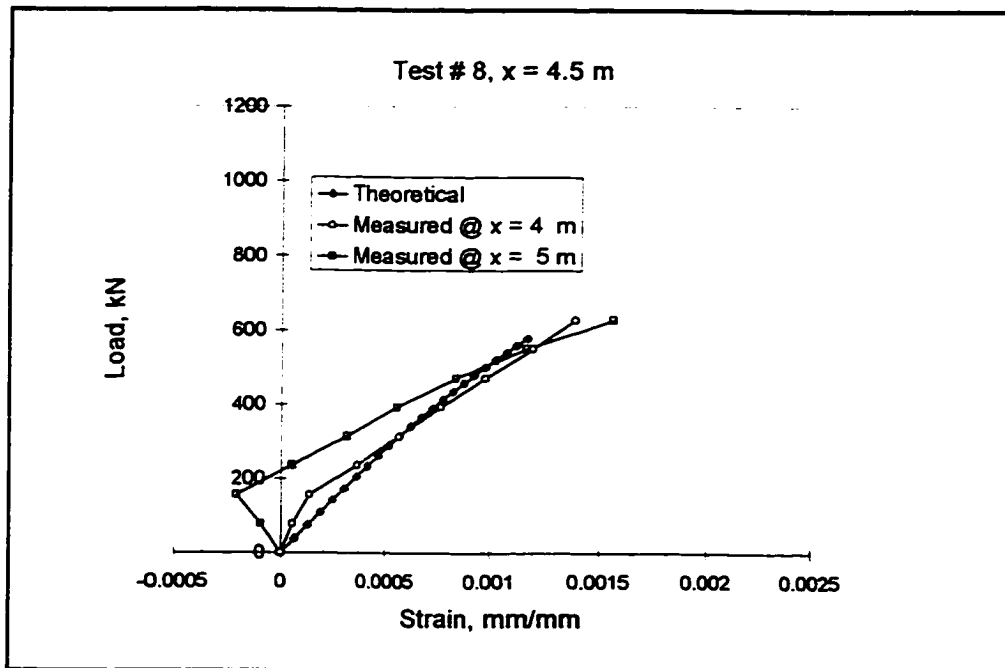


Figure 6.17: Strain in external restraints, Test # 8

The effectiveness of the steel straps dropped very quickly as the distance from the point of application of load increased. This behaviour is illustrated in Figure 6.18, where the strap number is the distance x in meters from the load application. The load was located at 10.5 m, 0.5 m from straps 10 and 11. Axial force in the straps increase fairly linearly with increasing load, with the interior strap, strap 10, being slightly more effective.

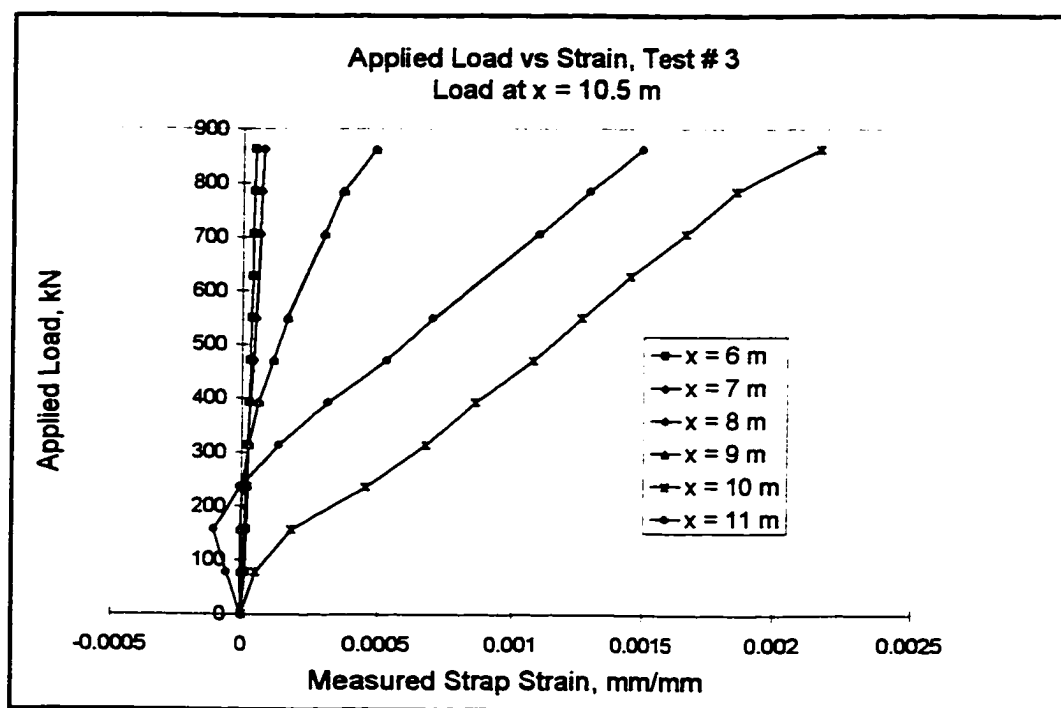


Figure 6.18: Variation in strap strain with a change in distance from the applied load

6.1.3.2 Yielding of the External Restraints

The measured strains indicated that the strap steel had not yielded in any of the 8 tests performed. It is noted that the nominal yield strain was exceeded in test # 3, yet the load/strain behaviour remained linear, as was discussed in the previous section. The measured ultimate punching load for Test # 3 was 911 kN. At a load of 863 kN, the maximum strap strain was measured to be 2165×10^{-6} mm/mm. For the structural grade of steel used in the test, yielding would theoretically occur at a strain of 1500×10^{-6} mm/mm. If this strap had undergone yielding, the steel could be expected to remain at a stress level equal to the material yield stress, in this case 300 MPa, until sufficient plastic flow had taken place to strain harden the material. Strain hardening could be expected at a strain of 0.02, or approximately 10 times the strain measured in strap # 10. It is further noted that upon unloading of the slab, had yielding occurred, there would remain a permanent residual strain in the strap which had yielded during the test. The permanent strain is expected to be less than the maximum measured strain, as the strap would unload on a line parallel to the initial elastic portion of the stress-strain curve. The expected theoretical residual strap strain is 665×10^{-6} mm/mm, or 1.33 mm extension over the length of the strap. No review of the strap condition subsequent to testing was performed to determine if the elastic limit had been exceeded.

As the strap material is reduced to optimize the system, the limit of strap yielding is expected to be the usual structural constraint. This is desirable from a safety viewpoint, as the ductility of steel through its long plastic phase would give a physical indication of distress in the system that would not exist for the more brittle limit of concrete crushing.

6.2 Polypropylene Fibre-Reinforced Concrete Properties

6.2.1 Compressive Strength

A loss of compressive strength was observed in the fibrous concrete after the laboratory addition of the superplasticizer and the polypropylene fibres. As has been reported in Ch.5, the cylinder compressive strength results had an average compressive strength of 42.8 MPa and 26.3 MPa, for the plain concrete and the FRC, respectively. This represents a compressive strength loss of 39% for the concrete mix after the addition of the polypropylene fibres. This indicates that either the FRC slab as constructed in the lab has a lower compressive strength than was planned or that the samples taken are not truly representative of the concrete in the structure. To address the latter concern, core samples from the cured concrete deck were taken and subjected to compressive testing. The compressive testing program on the core samples gave an average strength of 22.0 MPa. For the analyses undertaken to be used for comparison with the experimental work, the FRC strength was conservatively assumed to be 22.0 MPa, based on the average of the core strength results.

The OHBDC specifies a minimum allowable concrete compressive strength of 30 MPa, intended primarily as a measure to ensure adequate in service durability. The CHBDC has expanded on this durability requirement by introducing a matrix which prescribes a minimum set of concrete requirements which include a variation in prescribed compressive strength as a function of the expected use and service environment. For concrete deck slabs, according to these new criteria, the required compressive strength would vary from 30 MPa, for a dry structure not subjected to cyclic freezing and thawing, to 45 MPa, for a

slab subjected expected to be subjected to numerous cycles of freezing and thawing in a saturated state. The FRC used in the project did not attain the minimum value of 30 MPa required by both of these bridge codes.

The influence of f'_c on the ultimate punching capacity as predicted analytically is shown in Fig. 6.19. This figure shows the relationship between the predicted punch load as the compressive strength of the concrete is increased. The relationship between compressive strength and ultimate load is almost linear, though not one of direct proportionality. Consider, for example, an increase in compressive strength from 22 to 30 MPa, a 36% increase, for which the graphed relation shows an expected increase in the slab ultimate capacity of only 13%.

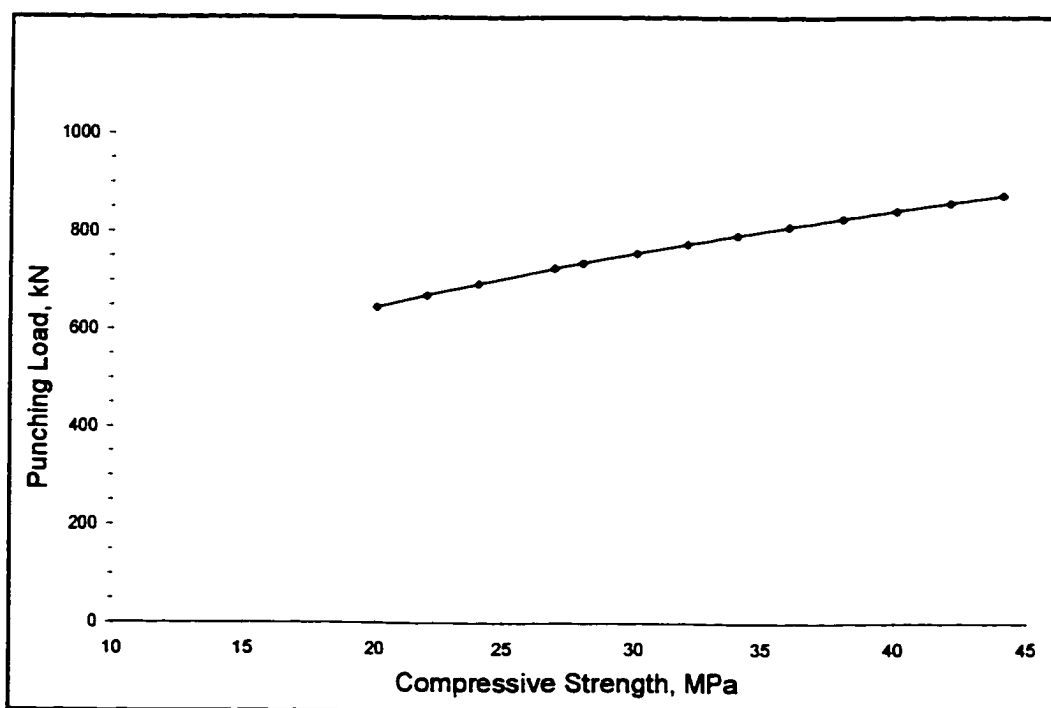


Figure 6.19: Influence of concrete compressive strength on the predicted punching load

It should be noted that for an externally reinforced bridge slab, high strength concrete is not necessarily considered to be a superior choice. Fig 6.19 shows that the ultimate capacity of such a slab system is relatively insensitive to increases in concrete compressive strength. Further, the very high cement contents required for the higher strength mixes lead to increased shrinkage, and therefore an increased cracking potential, which, in turn reduces the system durability, [Neville and Brooks, (1990)]. Therefore, although the loss of compressive strength of the FRC used for the experimental model was large, it is not seen as a significant problem for this study.

The results of a test program conducted using 57 mm fibrillated FORTA polypropylene fibres were reported in a report of the Forta Corp., [Ramakrishan and Zellers, (1989)]. This program examined the influence of fibre volume on compressive strength. The compressive strength results for a mix having a fibre volume of 0.1%, exceeded that for the plain concrete by approximately 5%. Further increasing the volume fraction to 0.2 % and 0.3%, caused reductions in the compressive strength when compared to the plain concrete mix of 3.5 % and 0.8%, respectively . And, the authors caution that fibre distribution and adequate consolidation are very important in order to achieve consistent high quality concrete. Other researchers, [Zollo et al, (1986)], have published test results which show decreased compressive strength for polypropylene mixes when compared to plain concrete mixes. Their results show compressive stress losses of 7.6%, 9.4% and 8.3% for fibre volumes of 0.1%, 0.2%, and 0.3%, respectively. Considering these results, and the higher fibre volume of the laboratory mix, 0.83 %, it seems reasonable to conclude that some of the strength loss may be attributed to the fibre presence. However, the fact that the loss is dramatically greater than the findings reported elsewhere, leads one to

believe that other factors have played a role in the compressive strength loss of the FRC. The air content, slump and fibre dispersion characteristics are discussed below in order to consider the influence of each of these parameters on the strength results.

6.2.2 Air Content

Air content analyses were performed on the plain concrete and on the FRC, as has been previously described in Ch. 5. The results show the air content of the fibre reinforced mix to be significantly higher than that of the plain concrete. Detailed results of the microscopic air evaluation tests were given in Table 5.3 and a summary of the results of all of the air tests is given in Table 6.3.

Table 6.3: Summary of air test results for plain concrete and FRC

Sample	Test Method	Air Content
Plain concrete	N / A	not tested 6% specified
FRC	Pressure method	10.5 %
Plain concrete	Microscopic Evaluation	3.2 %
FRC	Microscopic Evaluation	16.5 %

An air content of 6% had been specified to the ready-mix supplier when ordering

the concrete. The air content for the plain concrete was measured to be 3.2%, lower than that specified. However, both the pressure test and the microscopic air test show that the air content of the FRC exceeded that specified.

The CHBDC requirements specify an air content of $7.0\% \pm 1.5$ for concrete structures that will be subjected to cycles of freezing and thawing while saturated. This is the normal expected service condition for a typical Canadian bridge deck. Such an air content, generally the result of an air-entraining admixture, produces a stable network of fine, evenly spaced air bubbles. Such entrained air serves to relieve the hydraulic pressure exerted by water as it expands into ice during a freezing cycle. If left unrelieved, such pressure contributes to cracking of the concrete.

A measure of the adequacy of such entrained air is obtained from the results of the microscopic air evaluation, from which two characteristics of the air bubble system can be estimated. First is the spacing factor, an estimate of the maximum distance, in mm, of any point in the cement paste from the edge of an air void. For adequate durability in a severe freeze/thaw environment, the spacing factor is restricted to less than 0.2 mm by the CHBDC. The second quantity that can be estimated from the results of the microscopic air test is the specific surface, defined as the surface area of the air voids divided by their volume, $\text{mm}^2 / \text{mm}^3$, or mm^{-1} . This latter property gives an indication of the size of the air bubbles in the network. It is desirable that the air bubbles be as small as possible; the total void volume having a direct bearing on concrete strength, as will be discussed below. The CHBDC requirement for concrete to be subjected to numerous freeze/thaw cycles in service is that the specific surface be greater than 25 mm^{-1} .

Microscopic air test results show that the FRC and the plain concrete had spacing factors of 0.148 mm and 0.127 mm, respectively, both less than the code limit of 0.2 mm. Considering the size of the bubbles, as measured by the specific surface value, the results are not as favourable. The plain concrete mix, with a specific surface of 45.2 mm^{-1} satisfies the code requirement of that the factor exceed 25 mm^{-1} , however the FRC mix had a specific surface of 8.7 mm^{-1} , far below the requirement. [Neville and Brooks, (1990)], report that the specific surface for accidental air, or that entrapped during mixing, is usually less than 12 mm^{-1} . These test results support the conclusion that the fibre presence has dramatically increased the percentage of entrapped air in the concrete.

Entrained air is beneficial to concrete performance during freezing and thawing cycles, as it creates space for water movement under the accompanying hydraulic pressure. However, the presence of entrained air in a concrete mix negatively affects the compressive strength. Neville and Brooks show that an entrained air content of 8% results in a 42 to 47 % decrease in f_c , without other changes to the mix proportions. The following graph is reproduced from [Kosmatka et al. (1995)], showing the influence of increasing air contents for mixes with two different cement contents. An increase of air content of 9% is shown to reduce the compressive strength by 40% for a mix with $308 \text{ kg} / \text{m}^3$ of cement. An increased cement content causes further increase, of over 50%, and it is noted that the experimental FRC mix had air in excess of 10%, with a cement content of $398 \text{ kg} / \text{m}^3$.

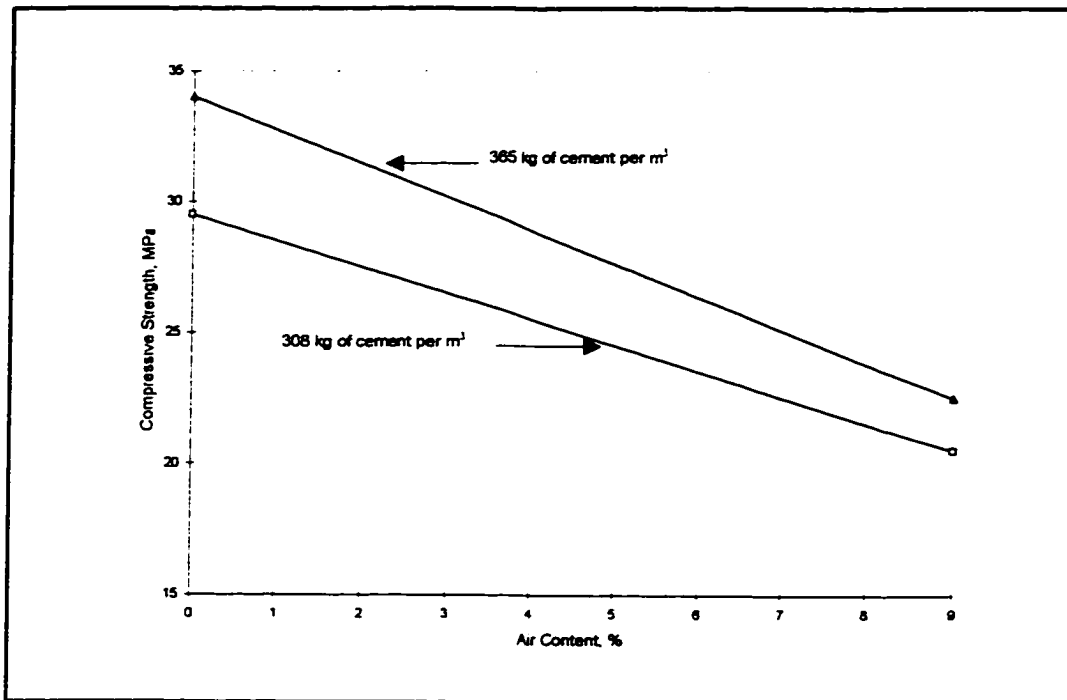


Figure 6.20: Relationship between concrete compressive strength and air content, [Kosmatka et al. (1995)]

The amount of air entrained in a concrete mix varies as a function of the volume of concrete in the mixer as a percentage of the rated capacity of the mixing drum. As the capacity of the mixer is approached, the air content increases, [Kosmatka et al. (1995)]. According to the ASTM Standard Specification for Ready-Mix Concrete, C94-90, the volume of mixed concrete is not to exceed 63% of the total drum volume to ensure proper mixing of truck mixed concrete. The drum of the agitator truck that was used to mix and deliver the ready-mix concrete to the laboratory for the experimental study was filled to almost 90% capacity. This overfilling is thought to have contributed to the large amount of air entrapped in the FRC mix.

6.2.3 Slump

The full-scale deck concrete of this study had 14 % less superplasticizer than the previous scale tests in the TUNS laboratory, but yet the slump of the fibrous concrete was measured to be 33% greater on average than that of the previous concrete mixes, [Wegner, (1992)]. The primary active ingredient in the superplasticizer used, (tradenname Rheobuild 1000), is sulphonated naphthalene formaldehyde condensate. The recommended dosage of this product by the manufacturer is 0.65 to 1.6 litres per 100 kg. of cementitious materials. The concrete for the full-scale laboratory bridge deck incorporated the superplasticizer at a rate of 1.28 litres per 100 kg. The previous test mixes were produced by the same ready-mix supplier, using the same mix design, with the same fibre volume ratio and the same brand of superplasticizer. This leads to the conclusion that the superplasticizer was not the primary contributor to the high air content of the FRC nor the degradation of the compressive strength. The presence of entrapped air would tend to increase the slump.

6.2.4 Fibre Dispersion

The formation of "fibre clumps" during mixing has given problems when high fibre contents or high aspect ratio fibres are used. [Kelly, (1975)]. The use of special mixing equipment has been suggested to alleviate the problem. For example, some suppliers recommend the addition of a chute into the hopper of the ready-mix truck. What this chute would ensure is that the fibres contact the concrete paste more quickly, rather than rotating on the drum a few times before being introduced into the paste. The latter can lead to clumping of the fibres,

less than optimum fibre distribution, and unnecessary air entrapment.

6.2.5 Steps to Improve the FRC Properties

The significant loss of compressive strength observed for the FRC mix when compared to the plain concrete is the result of a combination of factors. To explain the loss subsequent to the addition of the fibres, the construction sequence will be revisited.

The concrete used for the full-scale laboratory structure was batched at a ready-mix plant and charged into the drum of a 7 m³ agitator truck and truck-mixed before transport to the laboratory. The truck mixing speed was 16 rpm, with a mixing time of 4 to 6 minutes. After mixing, the drum speed was reduced to agitator speed (3 rpm) and the concrete was delivered to the lab. The total elapsed time between loading at the plant and arrival at the lab was 25 minutes. Upon arrival at the lab, samples of the plain concrete were taken and then the superplasticizer and the polypropylene fibres were added to the drum of the mixer. To incorporate the fibres and superplasticizer into the mix, the drum speed was increased to 16 rpm and the fibrous concrete was truck-mixed for a further 15 to 20 minutes. Placing of the deck slab took approximately 90 minutes, and complete discharge from the truck was approximately 165 minutes after initial loading at the batch plant.

From this sequence three factors are seen as contributors to the high air content and low compressive strength of the FRC mix. Firstly, the concrete was in the agitator truck for a longer period than that recommended; 2.75 hours versus 1.5

hours recommended. Secondly, the drum of the truck was overfull for optimum mixing; 89% vs 63% recommended. And, lastly, the fibre volume of the FRC mix was much higher than the recommended dosage prescribed by the manufacturer; 0.834% versus an industry standard of 0.1%.

It is felt that the overfilling of the mixing drum is very significant. Previous mixes using the same concrete mix design, similar dosages of fibrillated polypropylene fibres and superplasticizer, and a similar method of incorporating the fibres had no such loss of strength observed, [Wegner, (1993)]. It appears that over filling the drum, in combination with a high volume fraction of fibres and the addition of superplasticizer, led to excessive entrapped air, ultimately causing a significant loss of strength in the FRC.

To improve the FRC properties the following are recommended:

1. Reduce the fibre volume to the industry norm of 0.1%, utilizing the fibres at low dosages to help alleviate plastic shrinkage cracking, and to improve the ductility and toughness.
2. Observe the recommended fill volume of 63% for truck-mixed concrete offered by
3. Reduce the mixing time to ensure that the total elapsed time between charging the truck at the plant and unloading is less than 1.5 hours.

6.3 Quantifying the Slab Restraint Stiffness

In Ch. 2 a discussion of the influence of the "system" restraint and its contribution to the slab lateral restraint during arching was presented. There it was stated that the restraint stiffness value that was included in the analytical model was developed taking into account the system restraint. The system restraint was evaluated from a beam analysis, modelling the composite girder lateral bending stiffness and its torsional stiffness, as well as the axial spring stiffness of the external restraints. The beam model is represented in Fig. 6.21. In this figure, the spring stiffnesses, k_1 through k_{12} , represented the axial stiffness of the external steel restraints and the transverse diaphragms.

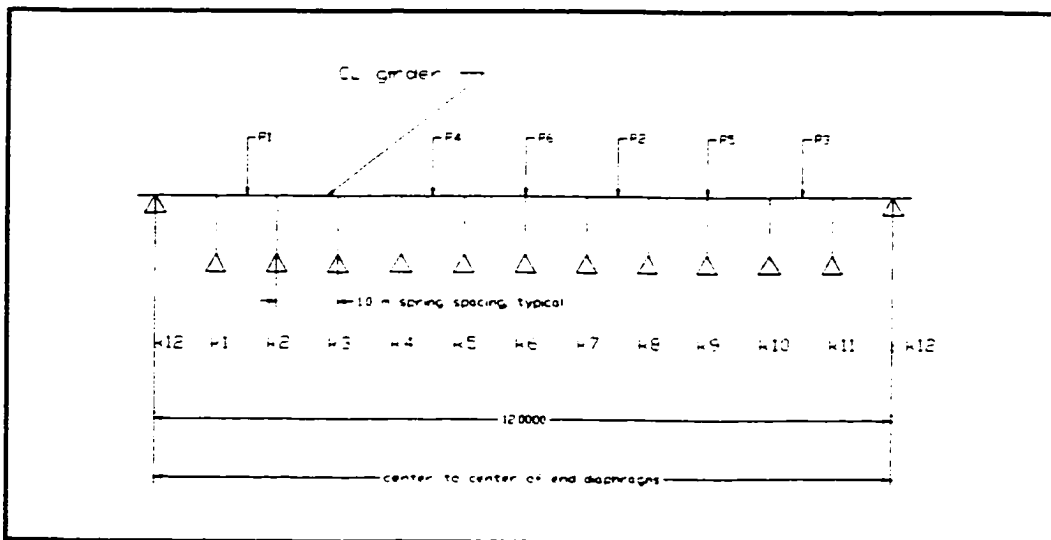


Figure 6.21: Continuous beam model used to determine the system restraint stiffness

To quantify the system restraint, a unit load was applied to the beam and the deflection at the load point calculated. The system stiffness was calculated based on the results of such an analysis from:

$$K_l = \frac{P_n}{\Delta * S_s} \quad (3)$$

where P_n is the applied unit load, N, Δ is the deflection calculated from the model, mm, and S_s is the spacing of the external restraints, mm. The stiffness thus calculated represents the total lateral stiffness of the system, K_l , in MPa.

The influence of a variation in restraint stiffness on the predicted punching load was studied, comparing analyses based on axial restraint stiffness to analyses incorporating the total restraint stiffness. A comparison of these analytical results and the experimental results are presented in Table 6.4 for the first test series. As presented here, k_s , is the axial stiffness of the external restraint as calculated from the following:

$$k_s = \frac{A_s E_s}{S_s * 0.5 * S_g} \quad (45)$$

and K_l is the system stiffness as determined from the continuous beam analysis described above. The ultimate punching loads are shown as P_{test} , indicating the punching load measured during testing, P_{k_s} , the calculated punching load assuming axial restraint, and P_{K_l} , the calculated punching load including the calculated system restraint. From this comparison, it can be seen that an improved prediction of ultimate load is achieved when one includes a measure of the total system restraint in the rigid body model. Including the girder restraint

the mean of the calculated punching load to the experimental punching load is 0.88, with a standard deviation of 0.05, whereas for a similar comparison assuming only the transverse strap axial stiffness, the mean predicted punching load is estimated as only 63% of the measured value.

Table 6.4: Comparison of the punching capacity for variations in restraint stiffness

Test No.	P_{test} (kN)	k_s (MPa)	P_{ks} (kN)	$\frac{P_{ks}}{P_{test}}$	K_1 (MPa)	P_{K1} (kN)	$\frac{P_{K1}}{P_{test}}$
1	1128	508	877	0.78	858	1055	0.94
2	923	254	613	0.66	535	863	0.93
3	911	190	523	0.57	415	763	0.84
4	844	127	417	0.49	343	693	0.82

7.0 CONCLUSIONS AND RECOMMENDATIONS

7.1 Conclusions

The full-scale experimental program that has been described is a continuation of the on-going study of externally reinforced FRC decks being performed at the Technical University of Nova Scotia. Previous half-scale tests have shown that the capacity of a composite FRC slab will be limited by the formation of a local punching-type failure if sufficient external reinforcement is provided. An analytical model was subsequently developed to predict the limiting load for such a slab. This study also established a method for optimizing the stiffness of the required external restraint. A range of values of external steel restraint has been incorporated in the full-scale test program. The behaviour of this system under concentrated loads was used to test the accuracy of the analytical model. The loading results will be used to refine the analytical representation of the system response, as required.

The following conclusions can be drawn provided that the externally restrained system conforms to the following physical characteristics:

- i. The slab span-to-depth ratio not exceed 16.
 - ii. The spacing of the external restraints not exceed one-half the spacing of the longitudinal girders.
 - iii. The system be restricted to slabs that are globally stressed in compression.
1. A full-scale slab-on-girder superstructure can be designed using a system

of external reinforcing to provide capacities exceeding the design wheel loads of Canadian bridge codes.

2. A fillet welded steel strap transversely connecting the longitudinal girder flanges is a suitable method of providing the necessary restraint to accommodate slab arching under a concentrated load representative of a highway vehicle.
3. Under full-scale testing the externally restrained FRC slab capacity reached a maximum of 1128 kN, given an external restraint having an axial stiffness of 508 N/mm/mm.
4. Ultimate capacity of the structures tested was shown to accompany a localized slab failure in which a section of the deck slab punched explosively through the deck.
5. An analytical representation of the rigid body rotation of the internal arch was shown to predict the load/response behaviour and the ultimate punching load within 11%, on average.
6. It was shown that a simple repair technique is effective in significantly restoring the slab capacity in the vicinity of a previously punched zone.
7. The system stiffness of the composite slab and girder should be accounted for when using the analytical model to establish the behaviour and ultimate punching capacity in response to a concentrated load.

7.2 Recommendations for Further Study

7.2.1 Strap attachment detail

The strap attachment detail requires further investigation. Welding the strap to the top flange of the girder induces a potential site for initiation of fatigue cracks. This is not of great concern in positive moment regions, but in negative moment regions when high tensile stresses exist in the top flange, the potential for a penalty exists.

7.2.2 FRC Mix Proportions

It is recommended that further material research be undertaken, aimed at establishing the optimum FRC mix to be used for an externally reinforced bridge slab. This work should address reducing the polypropylene fibre volume to the minimum required to control shrinkage cracking to achieve the required durability for a harsh freeze/thaw environment. Also, the mixing equipment and the mixing sequence should be the subject of further experiments to develop a reliable construction technique, practical and recommendable for field applications; a method capable of producing FRC mixes with controlled air contents and compressive strengths.

7.2.3 Material Resistance Factors

The optimization considered herein was predicated on an ultimate design load of 500 kN for slab punching and a serviceability design load of 90 kN for deflection control. It is recommended that further study be undertaken to refine the

material resistance factors for fibre reinforced concrete, on which these design load values are based.

REFERENCES

- American Association of State Highway and Transportation Officials, 1989. Standard Specifications for Highway Bridges, 14th Edition, American Association of State Highway and Transportation Officials, Washington, D.C.
- AISC Marketing Inc, 1986. Highway Structures Design Handbook, Volumes I & II, Pittsburgh, PA.
- Aitcin, P.C., Jolicoeur, C. AND MacGregor, J. G., 1994. Superplasticizers: How they Work and Why They Occasionally Don't, Concrete International, May: 45-52.
- American Society for Testing and Materials, 1990. ASTM-C42-90 Standard Test Method for Obtaining and Testing Drilled Cores and Sawed Beams of Concrete, American Society for Testing and Materials, Philadelphia, Pennsylvania.
- American Society for Testing and Materials, 1993. ASTM-C457 Practice for Microscopical Determination of Air-Void Content and Parameters of the Air-Void System in Hardened Concrete, American Society for Testing and Materials, Philadelphia, Pennsylvania.
- Bakht, B., Mufti, A.A., and Tadros, G. 1996. Providing Transverse Confinement in Deck Slabs. Proceedings of the Canadian Society for Civil Engineering Annual Conference: 443-454.
- Bakht, B. and Selvadurai, A.P.S., 1996. Performance of Steel-Free Deck Slabs under Simulated Rolling Wheel Loads, Proceedings of Second International Conference on Advanced Composite Materials in Bridges and Structures, ACMBS-II, Published by CSCE, M.M. El-Badry, editor.
- Batchelor, B. deV., Hewitt, B.E., Csagoly, P. And Holowka, M., 1978. Investigation of the Ultimate Strength of Deck Slabs of Composite Steel/Concrete Bridges, Transportation Research Record, No.66, Transportation Research Board, National Research Council, Washington, D.C.
- Bathe, K.J., 1982. Finite Element Procedures in Engineering Analysis. Prentice Hall, Inc, Englewood Cliffs, New Jersey.
- Calibration Report for OHBDC 1990, Calibration Committee, Ministry of Transportation of Ontario, Downsview, Ontario, Canada.

Canadian Standards Association, 1994. CSA Standard CAN3-A23.2-94, Methods of Test for Concrete, Canadian Standards Association, Rexdale, Ontario.

Canadian Standards Association, 1994. Canadian Highway Bridge Design Code, Draft for Committee and Public Review, (July 1994), Canadian Standards Association, Rexdale, Ontario.

Canadian Standards Association, 1988. CSA Standard CAN/CSA-S6-88, Design of Highway Bridges, Canadian Standards Association, Rexdale, Ontario.

Carmichael, David. 1993. Evaluation of the Fracture Toughness of Fiber-Reinforced Concrete using Experimental Methods and Enriched Finite Element Techniques. Master of Applied Science Thesis, Technical University of Nova Scotia.

Csagoly, Paul F., and Lybas, John M., 1989. Advanced Design Method for Concrete Bridge Deck Slabs, *Concrete International*, May: 53-63.

Demers, M. And Neale, K.W., 1994. Strengthening of Concrete Columns with Unidirectional Composite Sheets. *Developments in Short and Medium Span Bridge Engineering*, Canadian Society for Civil Engineering: 895-905.

Dubas, P., 1991. Trends in Composite Bridges. *Proceedings of the International Conference on Steel and Aluminum Structures*, ICSAS, Singapore: 1-10.

Ehlen, M.A. AND Marshall, H.E., 1996. *The Economics of New-Technology Materials: A Case Study of FRP Bridge Decking*, U.S. Department of Commerce, Technology Administration, National Institute of Standards and Technology, Gaithersburg, Maryland.

Dorton, R.A., 1976. *The Conestogo River Bridge Design and Testing*, Canadian Structural Engineering Conference, Montreal, Quebec, CISC, Toronto, Ont.

Goldfein, S., 1965. Fibrous Reinforcement for Portland Cement, *Modern Plastics*, Vol. 42, No. 8, 156-160.

Hewitt, B.E., 1972. An Investigation of the Punching Strength of Restrained Slabs with Particular Reference to the Deck Slabs of Composite I-Beam Bridges. Phd Thesis, Queen's University, Kingston, Ontario.

- Hewitt, B.E., AND Batchelor, B. deV., 1975. Punching Shear Strength of Restrained Slabs. *Journal of the Structural Division*. ASCE **101**(ST9): 1837-1853.
- Jaeger, L.G., Jategaonkar, R. AND Cheung, M.S., 1989. Effectiveness of Intermediate Diaphragms in Distributing Live Loads in Beam-and -Slab Bridges, CSCE Monograph No. 1, University of Saskatchewan Printing Services, Saskatoon, Canada.
- Kelly, A., 1975. Prospects and Problems of Fibre Reinforced Concrete, Proceedings of the Rilem Symposium, 1975, The Construction Press, Ltd., University of Leeds, U.K.
- Kinnunen, S. AND Nylander, H., 1960. Punching of Concrete Slabs Without Shear Reinforcement. Transactions, Royal Institute of Technology, Stockholm, Sweden. No 158.
- Kosmatka, Steven H., Panarese, William C., Gissing, Kathleen D., AND MacLeod, Norman, F., 1995. Design and Control of Concrete Mixes, Sixth Edition, Canadian Portland Cement Association, Ottawa, Ontario.
- Ministry of Transportation of Ontario, 1991. Ontario Highway Bridge Design Code, Third Edition. 1991. Ministry of Transportation of Ontario, Downsview, Ontario.
- Mufti, A.A.. 1991. Fibre Reinforced Concrete Deck Slabs without Steel Reinforcement, Report No. 1-1991, N.S. CAD/CAM Centre, Halifax, N.S.
- Mufti, A.A., Jaeger, L.G., Bakht, B., and Wegner, L.D. 1993. Experimental Investigation of FRC Deck Slabs without Internal Steel Reinforcement. *Canadian Journal of Civil Engineering*, **20**(3):398-406.
- Neville, A.M. And Brooks, J.J., 1990. Concrete Technology, Longman Scientific and Technical, Essex, England.
- Newhook, J.P. and Mufti, A.A. 1995. Fibre Reinforced Deck Slabs Without Steel Reinforcement: Half-Scale Testing and Mathematical Formulation. Research Report No. 1-1995. Nova Scotia CAD/CAM Centre. Nova Scotia, Canada.
- Pook, L.L., 1997. Private Correspondence. Letter from Project Engineer at Cherubini Metalworks, Dec. 1997, Dartmouth, Nova Scotia.
- Portland Cement Association, 1991. Fiber Reinforced Concrete, Publication No. SP039T, Portland Cement Association, Skokie, Illinois.

- Ramakrishnan, V. AND Zellers, R.C., 1989. Evaluation and Comparison of the Physical Properties of Standard Polypropylene Fiber Reinforced Concrete, Unpublished report prepared for the Forta Corp., South Dakota School of Mines and Technology.
- Richart, F.E., Brandtzaeg, A. and Brown, R.L., 1929. The Failure of Plain and Spirally Reinforced Concrete in Compression. University of Illinois, Engineering Experimental Station, Urbana, Bulletin No 190.
- Ritchie, J.K., Wells, P., and Wong, A.F., 1991. Economic Factors in Steel Bridge Design, Fabrication and Erection, Proceedings of the Annual Conference of the Transportation Association of Canada, Winnipeg, Man.
- Salmon, Charles G. and Johnson, John E., 1990. Steel Structures: Design and Behaviour, Third Edition, Harper and Row, Publishers, Inc., New York, N.Y.
- Selvadurai, A.P.S, and Bakht, B. 1995. Simulation of Rolling Wheel Loads on an FRC Deck Slab, Proceedings, Second University-Industry Workshop, entitled Fibre Reinforced Concrete Modern Developments, edited by Banthia and Mindess, published by UBC, 1995.
- Thorburn, J., and Mufti, A.A. 1995. Full-scale Testing of Externally Reinforced FRC Bridge Decks on Steel Girders. Proceedings of the Canadian Society for Civil Engineering Annual Conference: 543-552.
- Transportation Association of Canada, 1994. Impacts of Canada's Heavy Vehicle Weights and Dimensions Research and Interprovincial Agreement, Transportation Association of Canada, Ottawa, Ontario.
- Wegner, L.D. 1993. An Experimental and Analytical Investigation of the Failure Behaviour of Fibre Reinforced Concrete Deck Slabs without Steel Reinforcement. Master of Applied Science Thesis, Technical University of Nova Scotia.
- Wegner, L.D. AND Mufti, A.A. 1994a. Finite Element Modelling of Fibre Reinforced Concrete Decks Without Internal Reinforcement. Canadian Journal of Civil Engineering, 21(2): 231-236.
- Wegner, L. and Mufti, A.A.. 1994b. Optimization of Externally-Reinforced FRC Bridge Decks on Steel Girders. Proceedings of 1994 Canadian Society for Civil Engineering Annual Conference: 551-562.

Zollo, R.F., Ilter, J.A., and Bouchacourt, G.B., 1986. Plastic and Drying Shrinkage in Concrete Containing Collated Fibrillated Polypropylene Fibre, Third International Symposium on Developments in Fibre Reinforced Cement and Concrete, RILEM Symposium FRC 86, Vol. 1, RILEM Technical Committee 49-TFR, Paris.

APPENDIX A

FORTRAN Program

PROGRAM TO CALCULATE PUNCH SHEAR AND SNAP-THROUGH LOADS
 Rec'd Nov. 1,1994 from Dr. Mufti

```

WRITE(6,*) 'START CALCULATION'
OPEN(70,FILE='FPSFST.DAT')
OPEN(80,FILE='FPSFST.RES')
OPEN(90,FILE='FPSFST.PLT')
WRITE(6,*) 'READING DATA'
READ(70,*) C,B,FPC,SK,SL,D,B1,CK,A,IU
  
```

IU=0, STRESS IN PSI ; IU=1, STRESS IN MPA

THE 'FCTF' STRESS IN 'PSI' USED IN K&N MODEL

```

IF(IU.EQ.1) FPC1=145.*FPC
IF(IU.EQ.0) FPC1=1000.*FPC
FCB=FPC1/(.75+.000025*FPC1)
FCTF=1007.+0.392*FCB
IF(IU.EQ.0) FCTF=FCTF/1000.
IF(IU.EQ.1) FCTF=FCTF/145.
IF(IU.EQ.0) WRITE(80,*) 'UNITS ENGLISH KIPS, INCHES, SECONDS'
IF(IU.EQ.1) WRITE(80,*) 'UNITS METRIC KN, MM, SECOND'
WRITE(80,*) 'Clear Span Between Girders=',C
WRITE(80,*) 'Diameter of Equivalent Circle for Load=',B
WRITE(80,*) 'Maximum Compressive Stress of Concrete=',FPC
WRITE(80,*) 'Elastic Axial Stiffness of Strap=',SK
WRITE(80,*) 'Strap to Load Spacing=',SL
WRITE(80,*) 'Depth Of Slab=',D
WRITE(80,*) 'Beta to Define Rectangular Stress Block=',B1
WRITE(80,*) 'Concrete Constant used for confinement=',CK
WRITE(80,*) 'AREA of Load Patch=',A
WRITE(80,*) ' DELTA      ASI      Y      R4      W      ALPHA      P
1  EPS      PFAIL      STRN'
WRITE(90,1000) DELTA,ASI,Y,R4,W,ALPHA,P,EPS,PFAIL,STRN
WRITE(80,1000) DELTA,ASI,Y,R4,W,ALPHA,P,EPS,PFAIL,STRN
IPFAIL=0
DELTA=0.
Y=D/100.
FACT3=.5*(C-B)
1 CONTINUE
DELTA=DELTA+D/350.
ASI=2.*DELTA/C
ITER=1
2 CONTINUE
FACT0=LOG(.5*C/(.5*B+Y))
IF(FACT0.LE.0) WRITE(80,*) 'FACT0.LT.0 PROGRAM STOPPED'
IF(FACT0.LE.0) WRITE(6,*) 'FINISH CALCULATION'
IF(FACT0.LE.0) STOP
SS=2.*SL
SSDC=SS/C
CTHS=1.-SSDC**2
STRNB=ASI*(D-Y)/(.5*C)
STRN=CTHS*STRNB
R4=0.5*(Y**2)*(0.5*B/Y+1.)*FCTF*FACT0
W1=0.5*C*SK*ASI*(D-Y)
W=W1-R4
C2=SK*ASI*(D-Y)/(.85*FPC)
FACT1=D-0.333333*Y-.5*C2
FACT2=D-.5*B1*Y-.5*C2
  
```

```

FACT4=FACT3+ASI*FACT2
FACT5=FACT2-ASI*FACT3
FACT=( (R4/W)*FACT1+FACT5)/FACT4
IF(FACT.LE.0) WRITE(80,*) 'FACT.LE.0 PROGRAM STOPPED'
IF(FACT.LE.0) WRITE(6,*) 'FINISH CALCULATION'
IF(FACT.LE.0) STOP
ALPHA=ATAN(FACT)+ASI
P=2.*3.14159*W*TAN(ALPHA-ASI)
SIGMA1=P/A

```

```

RITCHART FAILURE CRITERIA FOR 3-D STRESSES IN CONCRETE

```

```

SIGMA3C=FPC*(1.+CK*SIGMA1/FPC)

```

```

ADINA FAILURE CRITERIA FOR 3-D STRESSES IN CONCRETE

```

```

SIGMA3C=FPC*(1.+1.5*SIGMA1)

```

```

IF(IU.EQ.1) SIGMA1=.145*(P/A)

```

```

IF(IU.EQ.1) SIGMA3C=FPC*(1.+1.5*SIGMA1)

```

```

C1=P/(.85*3.14159*B*SIN(ALPHA-ASI)*SIGMA3C)

```

```

Y1=C1*COS(ALPHA-ASI)/B1

```

```

EPS=ABS(Y-Y1)

```

```

IF(EPS.EQ.0.) GO TO 3

```

```

IF(ITER.EQ.1000) WRITE(80,*) 'Y=',Y,'Y1=',Y1

```

```

IF(ITER.EQ.1000) WRITE(6,*) 'FINISH CALCULATION'

```

```

IF(ITER.EQ.1000) STOP

```

```

IF(EPS.GT..00001) Y=Y1

```

```

ITER=ITER+1

```

```

IF(EPS.GT..0001) GO TO 2

```

```

3 ESTH=Y*ASI/(.5*B+Y)

```

```

PFAIL=.002-ESTH

```

```

IF(PFAIL.LE.0.) IPFAIL=IPFAIL+1

```

```

IF(IU.EQ.1) W=W/1000.

```

```

IF(IU.EQ.1) R4=R4/1000.

```

```

IF(IU.EQ.1) P=P/1000.

```

```

DEG=180./3.14159

```

```

ASI=DEG*ASI

```

```

ALPHA=DEG*ALPHA

```

```

IF(IPFAIL.NE.1) GO TO 100

```

```

DELTAP=(DELTAP*PFAIL-DELTA*PFAILP)/(PFAIL-PFAILP)

```

```

ASIP=(ASIP*PFAIL-ASI*PFAILP)/(PFAIL-PFAILP)

```

```

YP=(YP*PFAIL-Y*PFAILP)/(PFAIL-PFAILP)

```

```

R4P=(R4P*PFAIL-R4*PFAILP)/(PFAIL-PFAILP)

```

```

WP=(WP*PFAIL-W*PFAILP)/(PFAIL-PFAILP)

```

```

ALPHAP=(ALPHAP*PFAIL-ALPHA*PFAILP)/(PFAIL-PFAILP)

```

```

PP=(PP*PFAIL-P*PFAILP)/(PFAIL-PFAILP)

```

```

EPSP=(EPSP*PFAIL-EPS*PFAILP)/(PFAIL-PFAILP)

```

```

STRNP=(STRNP*PFAIL-STRN*PFAILP)/(PFAIL-PFAILP)

```

```

PFAILP=0.

```

```

WRITE(80,1000) DELTAP,ASIP,YP,R4P,WP,ALPHAP,PP,EPSP,PFAILP,STRNP

```

```

WRITE(90,1000) DELTAP,ASIP,YP,R4P,WP,ALPHAP,PP,EPSP,PFAILP,STRNP

```

```

WRITE(80,*) '***** Punch load criterion satisfied *****'

```

```

CONTINUE

```

```

WRITE(90,1000) DELTA,ASI,Y,R4,W,ALPHA,P,EPS,PFAIL,STRN

```

```

WRITE(80,1000) DELTA,ASI,Y,R4,W,ALPHA,P,EPS,PFAIL,STRN

```

```

*6) FORMAT(1X,F5.2,1X,F5.2,1X,F5.2,2F8.2,F8.2,1X,F8.2,1X,F8.5,2(1X,F8.

```

```

DELTAP=DELTA

```

```

ASIP=ASI

```

```

YP=Y

```

```
R4P=R4
WP=W
ALPHAP=ALPHA
PP=P
EPSP=EPS
STRNP=STRN
PFAILP=PFAIL
write(6,*) ' STILL COMPUTING AT DELTA=', DELTA, ' ITERATION=', ITER
IF(DELTA.LE.D) GO TO 1
WRITE(6,*) 'FINISH CALCULATION'
STOP
END
```

155

APPENDIX B

Results of Microscopic Air Content Testing



Department of Civil Engineering
Air Voids Characteristics
ASTM C-457

Job Name: Concrete as delivered

Operator: Blair Nickerson

Date: 24-Oct-95

Measurements

Trial No.	St	N	Sv	Sp	NBB	SBB
A	1600	440	50	414	4	8
B	1600	431	53	408	2	4
Total	3200	871	103	822	6	12

Results

Trial No.	A (%)	A/P	L_avg (10 ⁻⁶ m)	D_avg (10 ⁻⁶ m)	alpha (1/mm)	L_bar (10 ⁻⁶ m)
1	3.1%	0.12	85	128	46.9	124
2	3.3%	0.13	92	138	43.4	130
Total	3.2%	0.1	89	133	45.2	127

Results without large bubbles

Trial No.	A (%)	A/P	L_avg (10 ⁻⁶ m)	D_avg (10 ⁻⁶ m)	alpha (1/mm)	L_bar (10 ⁻⁶ m)
1	2.6%	0.10	72	108	55.4	114
2	3.1%	0.12	86	128	46.7	125
Total	2.8%	0.11	79	118	51.0	119



Department of Civil Engineering
Air Voids Characteristics
ASTM C-457

Job Name: Fiber core A & B

Operator: Blair

Date: 18-Oct-95

Measurements

Trial No.	St	N	Sv	Sp	NBB	SBB
A	1600	418	263	320	45	117
B	1600	431	259	352	46	116
Total	3200	849	522	672	91	233

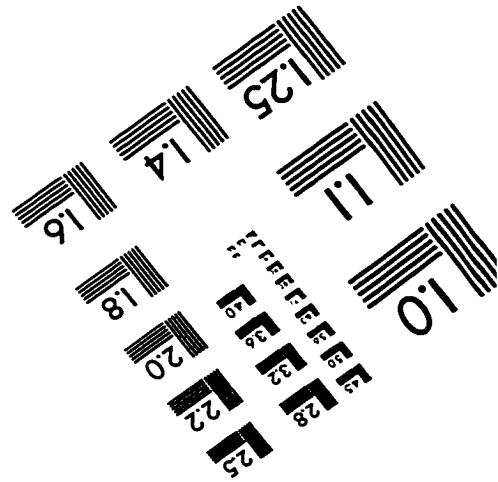
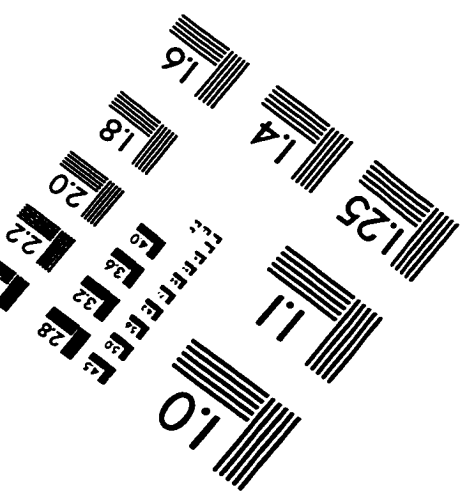
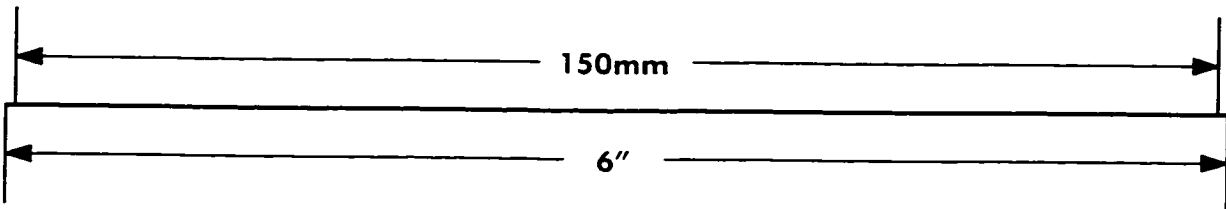
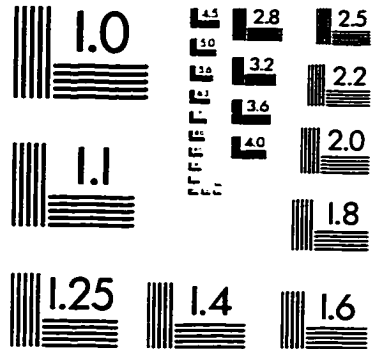
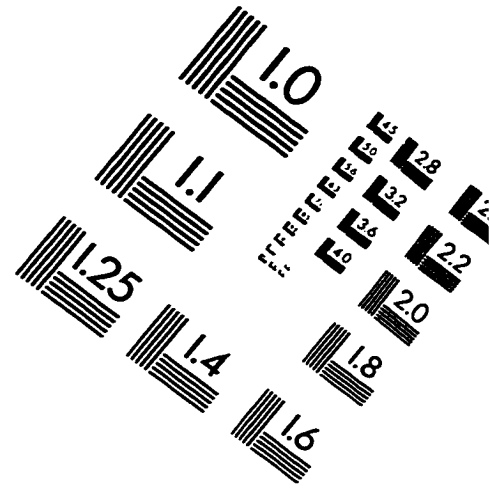
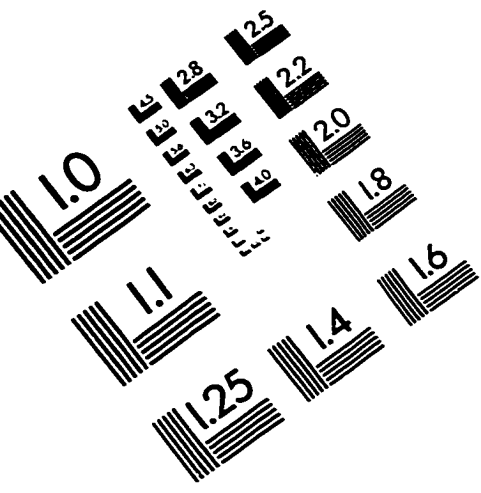
Results

Trial No.	A (%)	A/P	L_avg (10 ⁻⁶ m)	D_avg (10 ⁻⁶ m)	alpha (1/mm)	L_bar (10 ⁻⁶ m)
1	16.4%	0.82	472	708	8.5	144
2	16.2%	0.74	451	676	8.9	153
Total	16.3%	0.8	461	692	8.7	148

Results without large bubbles

Trial No.	A (%)	A/P	L_avg (10 ⁻⁶ m)	D_avg (10 ⁻⁶ m)	alpha (1/mm)	L_bar (10 ⁻⁶ m)
1	9.1%	0.46	294	440	13.6	161
2	8.9%	0.41	279	418	14.4	171
Total	9.0%	0.43	286	429	14.0	166

IMAGE EVALUATION TEST TARGET (QA-3)



APPLIED IMAGE, Inc
1653 East Main Street
Rochester, NY 14609 USA
Phone: 716/482-0300
Fax: 716/288-5989

© 1993, Applied Image, Inc., All Rights Reserved